

TALLINN UNIVERSITY OF TECHNOLOGY
DOCTORAL THESIS
38/2018

ZnO Nanostructured Layers by Wet Chemical Deposition Methods: Growth, Surface Properties, Photocatalytic Capability

INGA GROMÕKO

TALLINN UNIVERSITY OF TECHNOLOGY

School of Engineering

Department of Materials and Environmental Technology

This dissertation was accepted for the defence of the degree 28/05/2018

Supervisor: Dr. Tatjana Dedova
Department of Materials and Environmental Technology
Tallinn University of Technology, Tallinn, Estonia

Co-supervisors: Prof. Malle Krunk
Department of Materials and Environmental Technology
Tallinn University of Technology, Tallinn, Estonia

Dr. Ilona Oja Acik
Department of Materials and Environmental Technology
Tallinn University of Technology, Tallinn, Estonia

Opponents: Dr. Maxim Ganchev, Assistant Professor
Central Laboratory of Solar Energy and New Energy Sources
Bulgarian Academy of Science, Bulgaria

Dr. Aile Tamm, Senior Research Fellow in Material Science
Faculty of Science and Technology
Institute of Physics
University of Tartu, Estonia

Defence of the thesis: 28/06/2018, Tallinn

Declaration:

Hereby I declare that this doctoral thesis, my original investigation and achievement, submitted for the doctoral degree at Tallinn University of Technology has not been submitted for doctoral or equivalent academic degree.

Inga Gromõko

signature



European Union
European Regional
Development Fund



Investing
in your future

Copyright: Inga Gromõko, 2018

ISSN 2585-6898 (publication)

ISBN 978-9949-83-285-9 (publication)

ISSN 2585-6901 (PDF)

ISBN 978-9949-83-286-6 (PDF)

TALLINNA TEHNIKAÜLIKOOL
DOKTORITÖÖ
38/2018

**ZnO nanostruktuursed kihid vedeliksadestuse
meetoditel: kasvatamine, pinnaomadused,
fotokatalüütiline võimekus**

INGA GROMÕKO

Contents

List of Publications	6
Author's Contribution to the Publications	7
Introduction	8
Abbreviations, Terms and Symbols.....	10
1 Literature overview	12
1.1 Main properties of ZnO	12
1.2 Applications of ZnO	13
1.3 Synthesis of ZnO layers	15
1.3.1 Spray pyrolysis	16
1.3.2 ZnO rod layers by spray pyrolysis.....	17
1.3.3 Electrodeposition	19
1.3.4 ZnO rod layers by electrodeposition	20
1.4 Summary of literature overview and the aim of the study.....	22
2 Experimental	25
2.1 Deposition of ZnO nanostructured layers by spray pyrolysis.....	25
2.2 Deposition of ZnO nanostructured layers by electrodeposition	25
2.3 Characterisation of ZnO nanostructured layers	26
2.4 Characterisation of the photocatalytic properties of ZnO nanostructured layers....	26
3 Results and discussion.....	28
3.1 Growth of rod-shaped ZnO nanostructures by spray pyrolysis and electrodeposition ..	28
3.1.1 Influence of FTO/glass substrate morphology on the growth of ZnO rods by spray pyrolysis	28
3.1.2 Influence of metal oxide seed layer types on the growth of ZnO rods by electrodeposition	30
3.2 Bare and hierarchical ZnO nanostructures by spray pyrolysis	31
3.2.1 Growth, morphological, and structural properties of sprayed bare and hierarchical ZnO nanostructures	31
3.2.2 Photocatalytic properties of sprayed bare and hierarchical ZnO nanostructures	32
3.3 Surface properties of sprayed and electrodeposited ZnO rod layers	34
3.3.1 Wettability of sprayed and electrodeposited ZnO rod layers	35
3.3.2 Chemical composition of the surfaces of sprayed and electrodeposited ZnO rod layers...	36
3.3.3 Photocatalytic properties of sprayed and electrodeposited ZnO rod layers	39
Conclusions	42
References	44
Abstract.....	57
Lühikokkuvõte.....	60
Appendix 1	63
Appendix 2	99
Curriculum vitae.....	104
Elulookirjeldus.....	107

List of Publications

The list of author's publications, on the basis of which the thesis has been prepared:

- I T. Dedova, O. Volobujeva, M. Krunks, V. Mikli, **I. Gromyko**, A. Katerski, A. Mere. Growth of ZnO rods on FTO electrodes by spray pyrolysis. *IOP Conf. Ser.: Mater. Sci. Eng.* 49 (2013) 012001.
- II **I. Gromyko**, T. Dedova, M. Krunks, V Syritski, A. Mere, V. Mikli, T. Unt, I. Oja Acik. ZnO nanorods grown electrochemically on different metal oxide underlays. *IOP Conf. Ser.: Mater. Sci. Eng.* 77 (2015) 012012.
- III D. Klauson, **I. Gromyko**, T. Dedova, N. Pronina, M. Krichevskaya, O. Budarnaja, I. Oja Acik, O. Volobujeva, I. Sildos, K. Utt. Study of photocatalytic activity of zinc oxide nanoneedles, nanorods, pyramids and hierarchical structures obtained by spray pyrolysis. *Mater. Sci. Semicond. Process* 31 (2015) 315–324.
- IV **I. Gromyko**, M. Krunks T. Dedova, A. Katerski, D. Klauson, I. Oja Acik, Surface properties of sprayed and electrodeposited ZnO rod layers. *Appl. Surf. Sci.* 405 (2017) 521–528.

Copies of these articles are included in Appendix 1.

Author's Contribution to the Publications

Author's contribution to the papers in this thesis is:

- I Deposition of ZnO rod layers by chemical spray pyrolysis, optical properties characterisation, minor role in writing.
- II Deposition of ZnO nanostructured layers by electrochemical deposition method; deposition of ZnO and ZnS seed layers by chemical spray pyrolysis; layers characterisation, analysis of the SEM and XRD results; major role in writing.
- III Deposition of ZnO nanostructured layers by chemical spray pyrolysis, characterisation of nanostructures (XRD measurements), analysis of the results; moderate role in writing.
- IV Deposition of ZnO rod layers by chemical spray pyrolysis and electrochemical deposition methods, rod layers characterisation (water contact angle measurements, XRD and Raman measurements), analysis of the water contact angle, SEM, XRD, Raman, XPS and photocatalytic measurement results; major role in writing.

Introduction

During the last few decades, the cost-effective synthesis of low-dimensional nanostructured materials has been one of the main challenges in materials science. High surface-to-volume ratios of nanostructured layers are favourable for various applications. Today, nanostructured layers are already employed in optoelectronic devices such as solar cells, optical sensors, gas sensors, and light emitters. Among the various materials, nanostructures based on zinc oxide (ZnO) have attracted much attention. ZnO is a versatile functional material offering a variety of morphologies that is widely used in environmental, biological, electronic, and sensing applications. For environmental applications, ZnO has emerged as an outstanding photocatalyst material. Photocatalysts are commonly used in the form of powders or nanoparticles, which offer increased active surface area, thus enhancing their photocatalytic activity. However, the costs involved in the separation and recovery of the powder photocatalyst after treatment limit its potential widespread application. Therefore, an effective solution to overcome the problem could be a photocatalyst with a defined crystal structure and large surface-to-volume ratio that is attached to the substrate. A good option in this regard would be a nanorod-like morphology. Therefore, researchers have been developing synthesis strategies to prepare ZnO nanostructured layers with tailored geometry and material properties. However, obtaining a reproducible morphology by using simple inexpensive methods is still a challenge.

In this study, ZnO nanostructures were deposited by using commercially attractive, cost-effective, and relatively simple wet chemical deposition methods such as spray pyrolysis (SP) and electrodeposition (ED). The number of studies concerning the photocatalytic activity performance and controlled growth of SP ZnO rods is scarce, while information on their surface properties is absent. In comparison with SP, the ED of ZnO rods is more widely investigated; however, according to the literature, it has similar problems with respect to the controlled growth of ZnO rods on different substrates under similar deposition conditions.

Thus, the aim of this study was to extend the knowledge on the controlled growth of ZnO rods by SP and ED methods by studying the influence of substrate morphology on the resultant ZnO rod layer morphology. Another objective of the dissertation was to investigate and compare the surface properties of SP and ED rods. From an application point of view, the influence of the morphological and surface chemical properties of the SP and ED ZnO nanostructured layers on their photocatalytic activity was investigated. The results on the photocatalytic properties of the ZnO layers were obtained through a collaboration with the Laboratory of Environmental Technology at the Department of Materials and Environmental Technology in the Tallinn University of Technology.

This dissertation is based on four published articles and composed of three main chapters. Chapter 1 contains a literature overview of the main properties of ZnO in general and in the form of rods, ZnO application areas, basic principles of photocatalysis, and description of SP and ED methods. Towards the end, Chapter 1 summarizes the literature overview and formulates the aim of this study. Chapter 2 describes the experimental details of the work and the characterisation methods applied. Chapter 3 is divided into three sections and presents the obtained results and discussions on ZnO rod deposition by SP and ED on various substrates and seed layers, followed by the study on their surface properties and photocatalytic capability.

The dissertation is directly related to the research topics and the corresponding research projects in the Laboratory of Thin Film Chemical Technologies. The study has been financially supported by the Estonian Ministry of Education and Research under the project IUT 19-4, TUT base financing project B24, European Regional Development Fund through the projects TK114 (Centre of Excellence: “Mesosystems: Theory and Applications”), TK141 (Centre of Excellence: “Advanced materials and high-technology devices for sustainable energetics, sensorics and nanoelectronics”), AR12118 (Efficient plasmonic absorbers for solar cells), Archimedes Foundation (Kristjan Jaak scholarship), European Regional Development Fund (Dora plus program) and ASTRA “TUT Institutional Development Programme for 2016-2022” Graduate School of Functional Materials and Technologies (2014-2020.4.01.16-0032).

Abbreviations, Terms and Symbols

1D	One-dimensional
2D	Two-dimensional
3D	Three-dimensional
AcacH	Acetylacetone
AFM	Atomic force microscopy
c	Concentration
Δc	Decrease in the pollutant's concentration
CA	Contact angle
CE	Counter electrode
D	Diameter
DC	Doxycycline
E	Photocatalytic oxidation efficiency
e^-	Electron
E^0	Standard reduction potential
E_g	Band gap
ED	Electrodeposition
F	Faradays constant
FTO	Fluorine tin oxide
h^+	Hole
hv	Photon energy
HA	Humic acid
HF	Haze factor
ITO	Indium tin oxide
L	Length
MTBE	Methyl-tert-butylether
NBE	Near-band-edge emission
NHE	Normal hydrogen electrode
PNL	Prednisolone
R	Universal gas constant
RE	Reference electrode
RMS	Root mean square roughness
RNO	N,N-dimethyl p-nitrosoaniline
SA	Self-activated emission
Sa	Average roughness
SCE	Saturated calomel electrode
SEM	Scanning electron microscopy
SP	Spray pyrolysis
T_s	Temperature of the substrate surface
TT	Total transmittance
TTIP	Titanium tetraisopropoxide

UV-VIS	Ultraviolet-Visible light spectroscopy
WE	Working electrode
XPS	X-ray photoelectron spectroscopy
XRD	X-ray diffraction

1 Literature overview

1.1 Main properties of ZnO

ZnO is an inorganic compound of the II-VI semiconductor group. It naturally occurs as the mineral zincite [1]. ZnO is a direct wide bandgap semiconductor [$E_g(0\text{ K}) = 3.44\text{ eV}$; $E_g(300\text{ K}) = 3.37\text{ eV}$] with n-type properties that are related to its native defects such as zinc interstitials or oxygen vacancies [2-6]. Obtaining reproducible and reliable p-type ZnO still remains a challenge for the scientific community [1, 6, 7]. ZnO exhibits strong polar binding and a large exciton binding energy of 60 meV. It is a multifunctional material with piezo- and pyroelectric properties, a wide range of UV absorption, biocompatibility, and biodegradability [2–5].

ZnO may crystallize in three forms: hexagonal wurtzite, cubic zinc blende, and rocksalt (Fig. 1.1). Under general conditions, it exhibits a hexagonal wurtzite structure [8–10], where the Zn^{2+} ion is surrounded tetrahedrally by four O^{2-} ions, and vice-versa; the ions are stacked alternately along the common c-axis [8, 11]. Wurtzite ZnO has a positively charged Zn-polar surface (0001) and a negatively charged O-polar surface ($000\bar{1}$), which are terminated by the Zn^{2+} and O^{2-} ions, respectively. The planes $\{01\bar{1}0\}$ and $\{2\bar{1}\bar{1}0\}$ are non-polar and have lower surface energies, compared to the polar $\{0001\}$ facets [8, 12]. As a result, wurtzite ZnO usually tends to grow along the c-axis, maximizing the areas of the $\{01\bar{1}0\}$ and $\{2\bar{1}\bar{1}0\}$ facets due to their low surface energy [13], forming an elongated crystal. The relative surface energy of the facets is an important factor determining crystal growth and the final morphology [11].

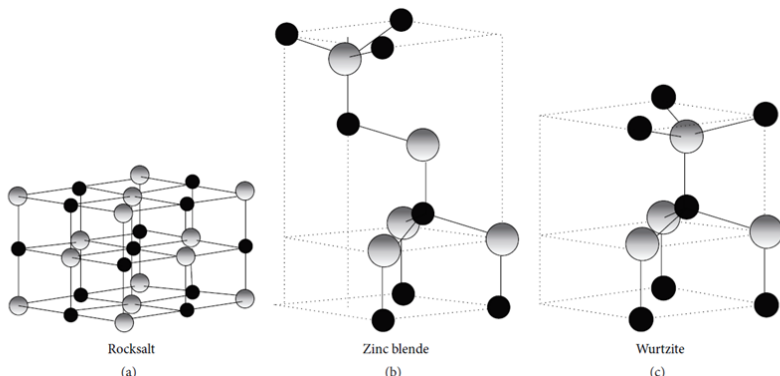


Figure 1.1 Crystal structures of ZnO (a) Rocksalt, (b) Zinc Blende, (c) Wurtzite. Black spheres refer to the O atoms, grey spheres refer to the Zn atoms [10, 14, 15].

ZnO offers a marvellous variety of morphologies among all the known materials. ZnO is commonly used in the form of powders, films, and different nano- or microstructures. All the structures can be classified into three major groups: one- (1D), two- (2D), and three-dimensional (3D). The 1D structures represent the largest group and are usually characteristic of small area (0001) facets with a high surface energy, e.g., nanorods [16–18], nanoneedles [19], nanowires [20–22], nanosprings [13, 23], nanorings [24], nanotubes [17, 25], nanobelts [13], and nanocombs [26]. The 2D structures include structures like nanoplatelets [22, 27] and nanosheets [28] that are characteristic of large area (0001) facets. Examples of 3D structures are flower-like [29–31], dandelion-like [32],

tetrapods [33], and different hierarchical structures [5, 34–37]. Schematic illustrations of the main representatives of the 1D, 2D, and 3D nanostructures are presented in Fig. 1.2.

Morphology is one of the most important parameters that has to be controlled before proceeding with the application [38].

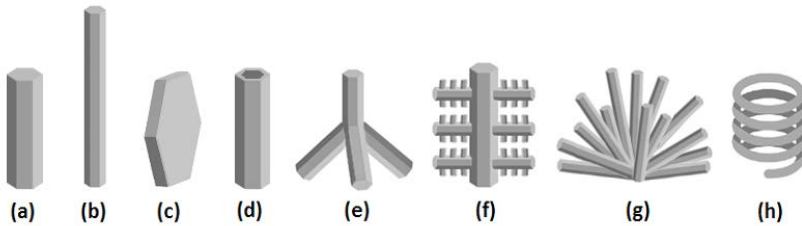


Figure 1.2 Different ZnO nanostructures: (a) rod, (b) wire, (c) plate, (d) tube, (e) tetrapod, (f) hierarchical nanostructure, (g) flower-like nanostructure, (h) spring.

1.2 Applications of ZnO

For many years, ZnO has been used as an additive in concrete, rubbers of tyres, and ceramic industries, as a white pigment (zinc white) in painting and colouring, and as an UV blocker in sunscreen crèmes [3, 5, 8]. The progress of nanoscience has expanded the field of ZnO application [4, 7, 14, 40]. A wide band gap of 3.37 eV at room temperature, high exciton binding energy of 60 meV, high thermal and mechanical stability make ZnO films attractive for potential use in electronics and optoelectronics, such as in field-emitters, light-emitting diodes, photodetectors, and lasers [40–42]. Additionally, ZnO layers can be used as a sensors [2, 4]. The high transparency of the ZnO films to visible light combined with their tuneable electrical conductivities enable their use as transparent conductive layers in thin film transistors and as optical window layers in solar cells [42, 43]. Very recently, 1D ZnO layers, mainly in form of rods, were actively applied in solar cells in order to increase the surface area of the p-n junction to provide a direct path for the electrons from the point of photogeneration to the conducting substrate, decreasing charge recombination and thus increasing the overall efficiency of the device [7, 10, 44].

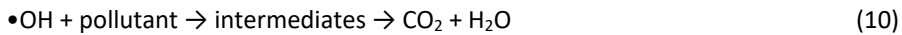
Owing to their controllable wetting properties, the potential application of ZnO layers as antifogging and self-cleaning coatings has been demonstrated [45]. Biocompatibility, biodegradability, and low toxicity make ZnO attractive for biomedicine and environmental applications [5, 46].

Among environmental applications, the use of ZnO as a photocatalyst in hydrogen production and for water cleaning from organic pollutants are worth considering [47]. As reported within the framework of this thesis, ZnO nanostructured layers have been tested as photocatalysts, and the subsequent subsections will describe this topic in more detail.

Mechanism of photocatalytic degradation of pollutants in water

Heterogeneous photocatalysis is one of the advanced oxidation processes developed to remove persistent organic pollutants from water and wastewaters. Recently, heterogeneous photocatalysis with semiconductors as photocatalysts has been an area of intense research due to the rapid degradation rate and mineralisation of pollutants to green products, etc. [48–50].

Generally, photocatalysis is a light-induced catalytic process based on the *in situ* generation of a highly reactive oxidising agents, hydroxyl radicals ($\bullet\text{OH}$), obtained at a sufficient concentration to effectively degrade the pollutants adsorbed on catalyst surface. The basic principle of the photocatalytic process is presented in reactions 1-10 below [47, 51–54].



Choice of photocatalyst materials

The suitable photocatalyst material for the degradation of the organic pollutants present in water and wastewater must be inexpensive, easily producible, efficient under light irradiation, stable during photocatalytic reactions, and not harmful to the environment. Since 1972, TiO_2 has been the most widely used and studied material for photocatalytic applications [50, 55]. However, the need to make the photocatalytic process more efficient and cheaper has reawakened the search for suitable alternatives to TiO_2 . During the last few decades, ZnO has emerged as an outstanding alternative photocatalyst material [47, 49, 56]. The number of studies investigating the photocatalytic properties of ZnO has been increasing annually, especially in the last five years (2010 – 2014), wherein ca. 1115 publications have been reported from a total amount of ca. 1500 publications for the last 15 years (2000 – 2014), according to the Web of Science database. In contrast to TiO_2 , ZnO is relatively cheaper and more efficiently generates hydroxyl ions, thus promoting the photocatalytic efficiency [47, 56–57]. Several comparative studies on photocatalytic degradation efficiency between P25 TiO_2 and ZnO commercial powders indicated ZnO as a more efficient catalyst for the degradation of organic pollutants like Remazol Black B, Remazol Brilliant Blue R [58], Reactive Blue 19 [59], Acid Brown 14 [60], Rhodamine 6G, Methyl Orange [61], etc. [62–64].

Highly dispersed powder nanoparticles have a large surface area and are therefore generally considered as the most effective photocatalysts. However, a number of problems, including the recovery of the powder photocatalyst, high aggregation tendency, and difficulties in distributing the particles uniformly, limit their practical application and have forced scientists to search for an alternative [68]. One of the good options is a photocatalyst in the form of nanostructures (rods, wires, hierarchical structures) attached to a steady substrate. Although nanostructured layers typically reveal lower surface-to-volume ratios compared to the powders, several studies have demonstrated that ZnO nanostructured layers (composed of tetrapods or hierarchical

structures) could achieve comparable or even higher photocatalytic activity than the powders [33, 34]. Examples of the photocatalytic performances of the ZnO photocatalyst in the forms of powder, films, and nanostructured layers for different preparation methods, and types of pollutants are summarised in Table 1.1 in Appendix 2 [29, 30, 36, 37, 62–64, 66–77].

Analysis of the photocatalytic results on the degradation of pollutants in water

The lack of a general agreement in the photocatalysis experiments, as well as the manner of comparing the photocatalytic efficiencies of different nanostructures complicate the comparison between the results, since very few studies have been carried out in comparable conditions (Table 1.1 in Appendix 2) [29, 30, 36, 37, 62–64, 66–77]. Nevertheless, it was observed that the photocatalytic activity of ZnO significantly varies depending on the preparation technique (hydrothermal growth, electrodeposition, spray pyrolysis, chemical bath deposition, etc.) and type of morphology (rod-, sphere-, flower layers) [72]. Differences in photocatalytic activity among the nanostructured layers could be caused by the variation of several parameters in complex, especially specific area and chemical composition of the surface. Surface properties play a determinative role during photocatalysis, since the molecules of the pollutant are adsorbed on the surface. It is generally accepted that the presence of hydroxyl groups (OH) on a surface is advantageous for photocatalytic efficiency [77, 78], since the (OH) groups are believed to react with the photogenerated holes, leading to the formation of $\bullet\text{OH}$, which mediates the degradation of the pollutants on the surface of ZnO [77]. Special attention in the literature has also been paid to the presence of surface defects (in terms of concentration and type), since they can serve as active sites and enhance the photocatalytic activity [34, 71, 79–83]. However, only a limited number of studies evaluate the changes in the photocatalytic performance by considering several variables of the surface properties. The changes in the photocatalytic activity of the aged ZnO nanostructures have also not been extensively studied [31].

Thus, nanostructured ZnO layers fixed on a steady substrate with sufficiently high effective surface areas are expected to be an efficient photocatalyst. The chemical surface properties of the ZnO nanostructures (amount of hydroxyl group and defect type and concentration) vary depending on the structure type or deposition method used, and that consequently affects the photocatalytic behaviour of the ZnO nanostructured layers. According to the literature review, spray-deposited ZnO nanostructured layers are one of the least studied samples from the photocatalytic application point of view [35, 74]. Unexpectedly, the photocatalytic efficiency of electrodeposited ZnO nanostructured layers and its correlation with surface properties have also not been extensively studied [72, 92].

1.3 Synthesis of ZnO layers

Generally, the preparation methods for ZnO layers can be divided into two basic categories: physical and chemical. The physical methods are physical vapor deposition [84], magnetron sputtering [85], pulsed laser deposition [86], and vapor-liquid-solid growth [87]. The chemical processes can be split to gas-phase (chemical vapor deposition [88], atomic layer deposition [42]) or liquid-phase (sol-gel [89], spray pyrolysis [16], electrodeposition [72], chemical bath deposition [90], spin-coating [91], hydrothermal growth [92]) methods.

Nowadays, synthesis of ZnO layers (films and nanostructures) by using wet chemical deposition methods is becoming increasingly attractive due to the relative simplicity and low cost of such techniques. According to the literature, rod-like crystals (including nanoarrays and nanowires) are the most common representatives of the ZnO nanostructures used for increasing the active surface area of the layers.

In this thesis, ZnO rod layers were deposited by means of chemical SP and ED. In addition to the main advantages of wet chemical methods, both these methods are technologically attractive, being fast and capable of being scaled up for producing large-area coatings.

1.3.1 Spray pyrolysis

Spray pyrolysis is based on the distribution of a pulverised precursor solution (aqueous or alcoholic) in the form of fine droplets onto a hot substrate where the precursor decomposes thermally [92]. The first introduction of the SP technique for thin film deposition was given in 1966 by Chamberlin and Skarman for CdS [93]. Thereafter, SP has been used to obtain a variety of other materials such as oxide layers (ZnO, In_2O_3 , SnO_x , ZrO_2 , PbO), sulfide layers (ZnS, SnS, In_2S_3 , CdS), binary, ternary, and quaternary chalcogenides [95, 96]. Nowadays, the SP technique is extensively used for the deposition of various powders, thin films, and structured materials. The relevance of the SP method is also supported by the number of publications: 7239 in the last ten years (2005-2014), of which 4495 were in the recent five years (2010-2014), based on the Web of Science database.

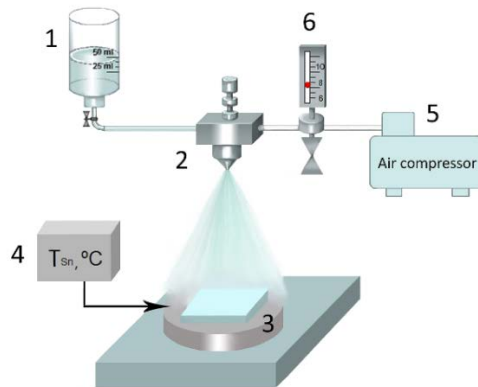


Figure 1.3 General scheme of the spray pyrolysis set-up.

A typical SP set-up is shown in Fig. 1.3 and consists of a (1) precursor solution container, (2) atomiser (including a spray nozzle) that generates fine droplets, (3) substrate heater, (4) temperature controller, (5) air compressor to deliver carrier gas to the system and (6) rotameter [93, 94, 96, 97]. The substrate, on which the desired layer is expected to be grown, is mounted on a hot plate and heated by direct contact with the heater. Among the various heating methods, liquid metal baths (like tin bath) provide good thermal contact and also make the cleaning procedure easier as the thin tin layer used can be scratched off with a scalpel [96, 98]. A variety of different atomisation techniques can be applied to control the droplet size and distribution over the substrate; pneumatic, ultrasonic, or electrostatic techniques are commonly used [5, 95, 99]. By using these techniques, droplet dimensions can be changed from micrometre to nanometre range, being the largest for the pneumatic system and smallest for the

ultrasonic and electrostatic techniques [96, 98]. The ultrasonic atomization technique, where a high-frequency sound vibration generates a fine mist of solution, is usually favoured over pneumatic spray pyrolysis for the deposition of thin films or compact layers owing to the lower velocity and highly uniform distribution of smaller droplet sizes. In this work, we used the most basic pneumatic spray set-up because practically nanostructured layers of ZnO were mainly grown using this set-up.

The properties of the final layer synthesized by the SP method are highly influenced by the deposition parameters such as a substrate temperature, precursor solution and its properties, precursor solution concentration, substrate type, droplet size, solvent, solution volume, solution spray rate, carrier gas flow rate, and distance between the nozzle and substrate [16, 35, 100–111].

In general, SP has a number of advantages. The main advantage is the use of low-cost equipment that does not require vacuum or highly priced supplements. SP methods are suited for mass production, and are capable of being scaled up over large areas and permit rapid growth rates (up to 100 nm/s) [95]. The SP method also allows to grow various coatings with complex geometries. The easy control over the desired layer properties by changing the spray parameters may be considered as an advantage of this technique. On the other hand, such sensitive dependence on each parameter necessitates high precision during experiments, since the different parameters can influence each other. For instance, the usage of certain precursors may lead to the nozzle becoming cluttered, which changes the droplet sizes and their distribution and, as a result, the layer properties. The main difficulties of the SP process are the determination and control of the substrate temperature. The choice of the substrate is also limited by the temperature. For instance, some polymeric substrates cannot be used for depositions above 400 °C. To summarise, the SP technique is a promising, effective, and versatile method for the deposition of metal oxide and metal sulphide layers with precise composition, stoichiometry, and crystallinity.

1.3.2 ZnO rod layers by spray pyrolysis

The possibility to grow elongated ZnO rod-shaped crystals by pneumatic SP method was firstly achieved in 2006 at Tallinn University of Technology, in the Laboratory of Thin Films Chemical Technologies [100]. After that, much effort has been devoted to study the SP ZnO crystals formation and its properties [16, 22, 35, 100–119]. Temperature, substrate, solvent, precursor type and concentration along with pH are key parameters that influence the final shape, dimensions, density and distribution of ZnO crystals on the substrate, subsequently their physical and chemical properties.

Influence of precursor type and concentration, growth temperature, solvent type, and solution pH

According to numerous reports on SP of ZnO rods, only the use of zinc chloride (ZnCl₂) or zinc acetate (Zn(ac)₂) as a precursor yielded the rod-like structures [16, 100, 104, 105]. Other salts such as zinc nitrate did not produce the ZnO rod-like structures [105]. The ZnCl₂ precursor yielded rods with larger diameters and lengths than those grown from a Zn(ac)₂ solution. An increase in solution concentration (ZnCl₂) from 0.05 mol/l to 0.2 mol/l leads to increasing rod dimensions. High concentrations ($c \geq 0.2$ mol/l) not only increase the dimensions of the crystals but also change their rod-shape to the tripod-shape bent down to the substrate surface [100]. Another important deposition parameter that influences ZnO rod formation is temperature. To grow separated and elongated c-axis-

oriented hexagonal ZnO rod-like crystals, temperatures higher than 490 °C are required [16]. It was established that with increasing temperature in the range 490 – 550 °C, the length and diameter of the rods deposited on glass substrates also increase [100]. By changing the solvent from water to alcohol (ethanol, isopropanol), rods could be grown using lower substrate temperatures (ca. 480 °C). The dimensions of the ZnO rods obtained from an alcoholic solution are much lower compared to those produced from aqueous media [116, 119]. An effect of the pH of the spray solution on the morphology of the ZnO rod layers was observed. The use of acidic ZnCl₂ solution (pH ~ 2) yielded separately standing ZnO rod-like crystals, whereas a less acidic solution (pH ~ 5) induced coalescence of the initial grains, and consequently, produced thicker rods with significantly lower aspect ratios [118].

Influence of the substrate

Considering that ZnO rod layers are widely used in solar cells, ZnO is commonly deposited on transparent conductive substrates such as ITO/glass and SnO₂/glass. It has been previously reported that the substrate morphology has a strong effect on the morphology of the ZnO rods synthesized by SP [100, 110, 120]. Specifically, the growth of SP ZnO rods on a substrate is controlled by the amount of nucleation centres (grain boundaries, intersections) on it [110]. The ITO/glass and SnO₂/glass substrates generally have high amounts of nuclei centres on their surfaces (markedly higher than those on soda-lime glass). Therefore, the ZnO rods grown by SP on ITO/glass and SnO₂/glass have more uniform sizes and are more densely distributed than when they are deposited on a glass substrate. However, a possible drawback of the high amount of nucleation centres is the coalescence of crystals located too close to each other. To avoid this, the precursor solution should not be concentrated (ZnCl₂ c = 0.05 – 0.1 mol/l when ITO/glass is used; c = 0.05 mol/l when FTO/glass is used) [120]. An alternative option is the adjustment of the amount of nucleation centres by chemical etching of the substrate. According to the study by Dedova et al., treatment of the ITO/glass substrate with concentrated H₂SO₄ decreased the density of the nucleation centres and, as a result, well-shaped vertically aligned ZnO rods (L = 500 nm, D = 150 nm) were formed [110]. Another morphological parameter that could also affect the resultant shape and dimensions of the ZnO crystal during SP is the substrate grain size. Several studies indicated that ITO/glass with higher grain sizes was more advantageous for the growth of elongated ZnO rods than ITO/glass with lower grain sizes [16, 120].

Thus, substrate morphology, namely, the density of nucleation centres and grain size, are important morphological parameters which affect the final morphology of the ZnO crystals grown by the SP method. However, the influence of surface roughness on ZnO rod formation by SP was not studied in detail.

Optical and surface properties of sprayed ZnO rods

Optical transparency of the ZnO rods in the visible region of the spectrum is ca. 20–65 %. Low optical transparency of the rod layers is caused by the light scattering from crystal's planes [100, 113]. Photoluminescence spectrum of SP ZnO rods generally possess weak self-activated (SA) emission band centred at ca. 500 nm and intense near band-edge (NBE) band centred at ca. 380 nm, ($I_{\text{NBE}}/I_{\text{SA}} = 30$) [116]. Thus, the high crystalline quality of the SP ZnO rods is superior compared to other solution-based methods in the sense of photoluminescence properties.

Investigations on the surface properties of SP ZnO rods are very scarce. Study on wetting properties of the SP rods grown from $\text{Zn}(\text{ac})_2$ water-alcohol solution revealed that after thermal treatment at $450\text{ }^\circ\text{C}$ SP ZnO rods are highly hydrophilic ($\text{CA} \sim 11^\circ$), but might be easily modified to hydrophobic ($\text{CA} \sim 125 - 132^\circ$) by using stearic acid or ageing during 2 months. Hydrophobic SP ZnO changed to hydrophilic ($\text{CA} \sim 21^\circ$) after UV-illumination [104]. Studies on surface chemical composition of SP ZnO rods are missing in the literature.

1.3.3 Electrodeposition

Another attractive solution-based deposition technique is ED method. ED is a process in which a redox reaction occurs upon passing an electric current between electrodes separated by an electrolyte. Layer deposition takes place at the electrode-electrolyte interface, which is called the electrical double layer [121]. Oxidation reaction occurs at the anode and reduction at the cathode. ED is a versatile technique and can be applied for depositing metals, metal alloys, and metal oxides [122].

The ED process is typically carried out in an electrolytic cell. The simplest form of an electrochemical cell is a two-electrode system. However, the most commonly used setup for ED is the three-electrode cell, consisting of a counter electrode (CE), working electrode (WE), and reference electrode (RE). The set-up shown in Fig. 1.4 has been used in our study to produce ZnO layers by ED. In order to provide an electrically conducting path between the electrodes, an electrolyte solution is needed in the cell. In addition to the reacting electrolyte, a support electrolyte can be added. The most often used support electrolyte is KCl. The electrolyte solution can be in different forms: aqueous, non-aqueous, inorganic, organic, and ionic liquids [122]. When the electrodes are inserted into an electrolyte solution, an electric field has to be applied.

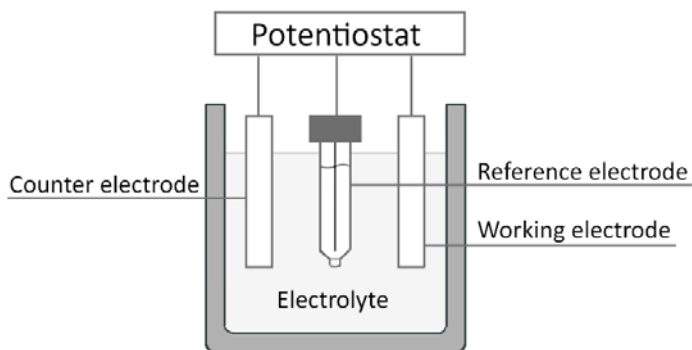


Figure 1.4 General scheme of the electrodeposition set-up.

Electrodeposition can be classified according to the nature of the electric field applied in an electrolytic cell: constant potential (potentiostatic), constant current (galvanostatic), and periodic or pulsed source [123]. In the potentiostatic mode, a desired potential is applied to the WE to supply electrons to the electrolyte during the reduction reaction. The RE has a fixed potential that is used to measure and control the potential of the WE. The RE should neither pass any current through, nor participate in the electrochemical process. Different REs have different known potentials: the normal hydrogen electrode (NHE) is defined as zero, and the Ag/AgCl (3 mol/l KCl) RE at room temperature is fixed at 0.210 V with respect to the NHE. The common substrate types

(WE) for ED are metals and conductive oxides. The CE is used to maintain the current flow needed for the desired reaction to take place on the WE.

Since different reactions will dominate at different potentials, the deposition of the desired material can be achieved by applying a specific potential. The theoretical potential needed for the desired electrochemical reaction can be calculated using the Nernst equation (11):

$$E = E^0 + \frac{RT}{nF} \ln \frac{[Ox]}{[Red]} \quad (11)$$

Where E_0 – standard reduction potential, R – universal gas constant ($8.314 \text{ J}\cdot\text{K}^{-1}\cdot\text{mol}^{-1}$), T – temperature in Kelvin ($^{\circ}\text{C} + 273$), F – Faradays constant ($96.487 \text{ C}\cdot\text{mol}^{-1}$), $[Ox]/[Red]$ – the ratio of oxidised to reduced molecules.

The properties of the ED layers can be controlled by various deposition variables such as the applied potential, precursor type, concentration, electrolyte, pH, temperature, deposition time, and substrate type [124–162].

The main advantage of the ED technique is its low cost. Deposition takes place at low temperatures and under ambient pressures. Another benefit of the method is a good reproducibility of the films as the layer properties can be easily controlled. The ED technique is easily scalable over large areas and for surfaces with complex shapes, making it applicable for mass production. The disadvantages of this method are the restriction to conductive substrates and the need for post-deposition annealing in order to improve the stoichiometry and crystallinity of the layers grown at low temperatures.

1.3.4 ZnO rod layers by electrodeposition

The first studies on the ED of ZnO layers were reported in 1996, independently by Lincot and Peulon [146], and Izaki and Omi [147]. Numerous reports have shown that the morphology, size, and distribution of the ZnO rods can be easily controlled by varying the electrochemical parameters [124–164, 167]. There are several primary factors that influence the morphology of the ZnO nanostructures: Zn precursor type and concentration, electrolyte, applied potential or current density, bath temperature, and substrate type.

Influence of oxygen precursor, zinc precursor type and concentration, solution pH, bath temperature, and applied potential

The ED of ZnO is generally based on the formation of OH^- ions through the cathodic reduction of an oxygen precursor such as molecular oxygen (12), peroxide species (13), or nitrate ions (14), followed by the reaction with Zn^{2+} ions (15). At elevated temperatures, zinc hydroxide is dehydrated to ZnO. At the elevated temperature zinc hydroxide is dehydrated to ZnO (16) [140]. E_0 is a value of standard redox potentials, below which the reaction takes place.



ZnCl₂ and Zn(NO₃)₂ are the most commonly used zinc sources to grow ZnO rod-like crystals. Zn(NO₃)₂ acts as both a precursor of Zn²⁺ ions and a source of oxygen [128–132]. When using the ZnCl₂ salt, molecular oxygen is required as an oxygen precursor. Elias et al. also reported ZnSO₄ and Zn(ac)₂ as good alternatives to ZnCl₂ [128]. It was shown that counter anions significantly tune the diameter and length of the ZnO rods. In particular, the highest aspect ratio (length/diameter = 60) has been obtained in the case of Zn(ac)₂, compared to ZnCl₂, where the aspect ratio was ca. 9 [128]. However, in some other studies, high aspect ratio (ca. 30) ED ZnO nanowires have also been grown from ZnCl₂ [132].

Various studies showed that the final morphology of the ZnO layer can be precisely controlled by adjusting the solution concentration. El Belghiti et al. explained that the concentration of Zn²⁺ ions influences the interfacial pH at the electrode surface, which in turn controls the speciation of the zinc ions and their ability to react with the growing layer [133]. When the Zn²⁺ concentration is in excess, every electro-generated OH⁻ ion is consumed by Zn²⁺ to form zinc hydroxide; the pH is neutral, which supports both lateral and longitudinal (c-axis) crystal growth. In spite of the fact that the c-axis growth rate is ca. four times higher than the lateral growth rate, when deposition under neutral pH is performed for a long duration, a continuous film instead of crystals could be obtained. When the Zn²⁺ concentration is low, OH⁻ ions are generated in excess, which increases the pH to the alkaline range (≥ 9), and the most stable forms of Zn²⁺ are the hydroxide complexes Zn(OH)₃⁻ and Zn(OH)₄²⁻. This leads to predominant growth along the c-axis direction [133, 134]. In particular, when the concentration of ZnCl₂ is ca. 5 mmol/l, the obtained ZnO crystals are thick and have low aspect ratios. By decreasing the precursor concentration to 0.2 mmol/l, the average diameter of the ZnO rods decreases [124]. Badre et al. also report that when a low concentration (2 × 10⁻² mmol/l) is used, elongated well-aligned hexagonal zinc oxide rods perpendicular to the substrate are formed [167].

According to numerous papers, the suitable temperature for the ED of elongated ED ZnO rods is in the region 70 – 90 °C [139, 142]. By increasing the deposition temperature from 70 to 90 °C, the length of the rods increased ca. two times, while the diameter decreased [132]. Changes in the applied potential also influence the final shape of the ZnO rods [124, 125]. Jangfeng et al. reported that the average diameter of the ZnO rods decreased as the applied potential changed from -0.7 to -1 V/SCE [124]. A similar tendency was observed by Xu et al. [125].

Influence of the substrate

In the ED method, the substrate not only acts as the cathode but similarly to SP deposition also plays a significant role in the nucleation and growth of ZnO rods. ZnO has been electrodeposited onto a variety of substrates such as gold, steel, copper, zinc, etc. [146–148]. The influence of the substrate can be observed by comparing the results of several groups (Canava et al., Cembrero et al., and et al. Peulon), where except for the substrate, the deposition parameters used were similar [146, 148, 149]. Owing to their potential optoelectronic application, ZnO rods are often electrodeposited onto transparent conductive oxide substrates like ITO/glass and FTO/glass [137].

As in the case of SP deposition, the amount of nucleation centres and grain sizes greatly influence the shape and distribution of the resultant rods. A wide dispersion of the substrate grain sizes leads to a wider diameter dispersion of the ZnO rods [150]; additionally, conductivity plays a role. Kim et al. reported that the distribution of the rods on high-resistivity (not measurable) substrates yielded low coverage density of the crystals [151].

On the basis of the observed literature, it should be noted that the morphology of commercial ITO/glass varies in its microstructure, and as a result, ZnO rods with different dimensions, uniformities, and ordering are obtained [16]. As a result, the obtained ZnO nanostructures have different sizes, homogeneities, and densities. Sun et al. proposed a modification of the ITO/glass surface by etching it with 6 % HCl [152]. As a result, ZnO rods uniformly covered the substrate, but decreased in dimensions. When the desired rod morphology cannot be achieved using a commercial substrate or after its modification, the common solution is to use an additional layer (seed layer or underlay) [150, 153–156]. The underlay acts as nucleation centres for the growth of ZnO nanostructures. It is reported that the coverage density of the ZnO rods grown on the substrates covered with ZnO underlay is significantly better than that of the rods grown on bare ITO/glass [150, 156]. The seed layer can be obtained by a controlled method and recipe in the home lab. The common methods used for the synthesis of the ZnO seed layer are chemical techniques like SP, spin coating, and ED [150, 157–160]. For SP and spin-coating, zinc acetate alcoholic solutions are generally used.

To the best of the author's knowledge, for the ED of ZnO rods using ZnCl_2 as the precursor, sprayed seed layers were used only by J. Elias et al. [150, 161]. In both studies, Elias et al. used ZnO layers deposited at 350 °C from $\text{Zn}(\text{ac})_2$ with the concentration of 0.1 M. The ZnO rods grown on the SP seed layer were highly oriented along the c-axis compared to the rods grown on ED seed layers.

Optical and surface properties of electrodeposited ZnO rods

Optical transparency of the ED ZnO rod layers varies in a range of 20 – 60 % [162, 163]. With increasing nanorod length (from 0.5 to 2.0 μm , respectively) total reflectance (maximum of scattering) increased from 8.6 % to 20.4 % [137]. The photoluminescence spectrum of ED ZnO rods at room temperature usually shows a NBE UV emission peak centred at ca. 380 nm and at least one broad SA emission band between 400 nm and 750 nm ($I_{\text{NBE}}/I_{\text{SA}} \sim 2$) [125]. The broad visible band (SA) is usually ascribed to defects in ZnO, such as zinc or oxygen vacancies and interstitials.

As-deposited ED ZnO rods deposited from ZnCl_2 solution, as well as annealed at 400 °C, showed highly hydrophilic nature ($\text{CA} \sim 0^\circ$) [132, 165]. Further studies observed the interdependency between the density of the nanowires and the water contact angle value, indicating that the higher the density of the nanowires is, the higher the measured contact angle [132]. The highest observed ($\text{CA} \sim 176^\circ$) superhydrophobic properties obtained for ED ZnO rods were presented by Badre et al. [166]. Superhydrophobic surfaces can be achieved by modification of ZnO rod surface with fatty acid molecules such as stearic acid [165–167]. Studies made on the characterisation of the surface chemical composition of the ED ZnO rods, indicated that the higher is amount of hydroxyls on a surface, the more hydrophilic the surface is [168].

1.4 Summary of literature overview and the aim of the study

One of the characteristic features of modern science and technology is the increasing focus on application-related aspects. Apart from the numerous applications listed in the introduction section, the ZnO rod-shaped morphology has gained enormous attention among the researchers as a promising photocatalytic material. A number of studies revealed that the photocatalytic performance of ZnO can exceed that of a well-established TiO_2 catalyst. Nanostructured ZnO layers showed photocatalytic efficiencies comparable or exceeding those of the powders, which due to their higher surface areas

typically yield the highest photocatalytic performance. Producing a reproducible and controlled ZnO rod-shaped morphology by using simple inexpensive methods is highly challenging and a desirable task in the material science community nowadays.

Among others wet chemical methods, SP and ED techniques are technologically attractive, being simple, low cost methods for growing nanostructured ZnO. The influence of the main growth parameters such as temperature and precursor type and concentration on the formation of ZnO rods has been properly studied and reported in the literature for both the methods. The most widely used deposition parameters for the growth of the elongated SP ZnO rods are: precursor ZnCl_2 or $\text{Zn}(\text{ac})_2$; $c = 0.05 - 0.1$ mol/l (ZnCl_2); $T_s = 490 - 550$ °C, and spray rate 2.4 – 2.5 ml/min. For the ED ZnO rods: the precursor is ZnCl_2 or $\text{Zn}(\text{NO}_3)_2$; $c = 0.2 - 0.02$ mmol/l (ZnCl_2); $T_s = 70 - 90$ °C, and applied potential varies from -0.7 to -1 V/SCE. The morphology of the substrate is another integral factor influencing ZnO nanorod-like crystal formation by both SP and ED methods. On the basis of a few papers, the morphologies of commercial substrates (generally transparent conductive oxide coated glass) may vary in terms of their microstructures, depending on the batch or supplier, and as a result, ZnO rods with different dimensions and morphologies are obtained. Not all the substrates resulted in the nanorod-like morphology. In some cases, the usage of a special seed layer prior the deposition (usually flat ZnO films) may support the formation of well-shaped ZnO rod layers. Still there is a gap in the literature on the relationship between certain morphological parameters of the substrate or seed layer and ZnO rod-like crystal formation. Therefore, the understanding of how exactly the substrate morphology is connected to the resultant morphology of the ZnO crystals in order to achieve reproducible growth is highly important.

A majority of studies have focused on the influence of the main technological parameters on the morphological properties (e.g., rods dimensions, density of the crystals on the substrate) of the ZnO rods, leaving behind the other properties of the crystals. However, for certain applications like photocatalysis, the surface properties (wettability, chemical composition: number of hydroxyl groups, surface defect concentration and type) of the crystals are highly important. Until now, there have been no systematic studies on the surface properties of ZnO rods obtained by both ED and SP methods. Studies on how the surface properties of the ZnO crystals influence their photocatalytic activity are also highly scarce. According to numerous papers, the photocatalytic activity of ZnO nanostructures differs from study to study, mostly depending on either the morphology or the deposition method used. A detailed study on the photocatalytic properties of spray-deposited ZnO nanostructures has not been reported in the literature.

Based on the literature overview on ZnO rod layers and from an application point of view, the objectives of the present doctoral thesis were:

1. To study the influence of the substrate and seed layer properties on the morphologies of ZnO rods deposited by chemical spray pyrolysis and electrochemical deposition methods;
2. To evaluate the photocatalytic activity of the sprayed ZnO nanostructures for different morphologies (bare rods, hierarchical structures) in relation to various organic pollutants and compare the photocatalytic activity performance of ZnO with that of the commercial catalyst P25 TiO_2 ;

3. To perform a systematic study on the surface properties (chemical composition, wettability) of sprayed and electrodeposited ZnO rod layers with similar morphologies and surface areas, obtained by adjusting the deposition parameters; To define the interdependency between the surface properties of the rods and their photocatalytic activity for as-grown, plastic-box-stored, and heat-treated samples.

2 Experimental

Prior the deposition all the substrates were washed thoroughly with soap, ethanol, sulphuric acid and rinsed with deionised water after each cleaning step.

2.1 Deposition of ZnO nanostructured layers by spray pyrolysis

In all experiments compressed air carrier gas had a flow rate of 8 l/min [I, III, IV].

Deposition of ZnO rod layers

The ZnO rods-shaped layers were prepared using the aqueous solutions of zinc chloride (ZnCl_2 , Aldrich, 98% purity). The concentration of ZnCl_2 was 0.05 [I, IV] and 0.1 mol/l [III]. Deposition temperatures on the substrate surface (T_s) were in the region from 520 to 550 °C. The solution volume was 50 ml, spray rate was maintained as 2.4 – 2.5 ml/min [I, III, IV]. Three types of commercial transparent conductive oxide layers were used as substrates: FTO/glass [I], SnO_2 /glass ($10 \times 25 \times 1 \text{ mm}^3$) [III] and ITO/glass ($10 \times 25 \times 1 \text{ mm}^3$) [III], ($25 \times 25 \times 1 \text{ mm}^3$) [IV]. Under the same deposition conditions, usage of large grain ITO/glass substrate yielded in truncated pyramid-shaped ZnO crystals [III].

Deposition of ZnO needle layers

The ZnO needle layers were synthesised by spraying the solution consisted of 0.2 mol/l zinc acetate dihydrate ($\text{Zn}(\text{ac})_2 \cdot 2\text{H}_2\text{O}$, Aldrich, 99 % purity) in water:isopropanol mixture (2:3) on glass substrate ($10 \times 25 \times 1 \text{ mm}^3$) at $T_s = 330 \text{ °C}$. The solution volume was 75 ml, spray rate was maintained as 1.5 ml/min [III].

Deposition of ZnO hierarchically structured layers

In order to deposit hierarchical structures, two-step spray depositions were performed. At first, bare rod- and pyramid-shaped crystals were grown on SnO_2 /glass and ITO/glass substrates ($10 \times 25 \times 1 \text{ mm}^3$), respectively as described earlier. Then, 40 ml of $\text{Zn}(\text{ac})_2$ aqueous solution with $c = 0.1 \text{ mol/l}$ was pulverised over those rods or pyramid-like layers at $T_s = 330 \text{ °C}$ with spray rate maintained as 4 ml/min [III].

2.2 Deposition of ZnO nanostructured layers by electrodeposition

The electrodeposition of ZnO rod-like layers was performed potentiostatically in a three-electrode electrochemical cell (Fig. 1.4). Platinum (Pt) wire was used as a counter electrode and silver/silver chloride (Ag/AgCl) 3 mol/l KCl was used as a reference electrode. ITO/glass ($10 \times 25 \times 1 \text{ mm}^3$ and $25 \times 25 \times 1 \text{ mm}^3$) substrates [III] and ITO/glass covered with ZnO or TiO_2 thin films (seed layers) were employed as working electrodes [II, IV]. The deposition solution consisted of 0.2 mmol/l ZnCl_2 (Aldrich, 98% purity) and 0.1 mol/l KCl electrolyte aqueous solutions. The solution volume was set to 50 ml. The deposition took place at steady potential of -1.0 V . Radiometer Analytical potentiostat PGP201 has been used to drive the electrodeposition system. The deposition temperature was kept at 80 °C using a temperature controlled circulator bath. Deposition time varied in a time interval of 45 – 60 min [II, IV].

Deposition of ZnO and TiO_2 seed layers

Seed layers used in paper [II] were deposited on ITO/glass substrate by spray pyrolysis technique. Technological parameters are described in Table 2.1.

Table 2.1 Technological parameters for ZnO and TiO₂ seed layers deposition.

Seed layer type	T _s , °C	Precursor	c, mol/l	Deposition time
ZnO	420	Zn(ac) ₂	0.1	29 min
	440	Zn(ac) ₂ +3 at.% InCl ₃	0.2	20 min
TiO ₂	450	TTIP + acacH	0.2 0.9	40 cycles × (1s spraying + 30s pause)

2.3 Characterisation of ZnO nanostructured layers

Methods used for the characterisation of ZnO nanostructured layers are summarised in the Table 2.2. Detailed description of each method used in this study can be found in the experimental sections of [I–IV].

Table 2.2 Methods used for the characterisation of ZnO nanostructured layers.

Properties	Characterisation method	Apparatus	Ref.
morphology; layer thickness (cross-sectional images)	SEM	Zeiss EVO-MA15, Zeiss HR FESEM Ultra 55	[I-IV]
surface roughness	AFM	NT-MDT Solver 47 Pro	[I]
phase composition, crystallites orientation, crystallite size	XRD	Rigaku Ultima IV	[I-IV]
phase composition	Raman	Horiba's LabRam HR800	[IV]
optical transmittance, reflectance, absorbance, haze factor	UV-VIS spectroscopy	Jasco V-670	[I]
wettability	Water CA measurement	DSA 25 (KRÜSS Instrument)	[IV]
chemical composition of the surface	XPS	Kratos Analytical AXIS Ultra DLD	[IV]

SEM surface and cross-sectional images were taken by Dr. Valdek Mikli and Dr. Olga Volobujeva. AFM measurements were made by Dr. Valdek Mikli. XPS spectra were recorded by Dr. Mati Danilson. All the measurements were performed in the Tallinn University of Technology.

2.4 Characterisation of the photocatalytic properties of ZnO nanostructured layers

ZnO nanostructured layers, as well as powders, generally show a good performance in degradation of organic pollutants such as dyes, in mg/l scale under UV-irradiation (Table 1.1 in Appendix 2). However, there are many various pollutant substances with different chemical structure that might have different approach for degradation. For the evaluation of the photocatalytic activity of ZnO samples in this work, different types of

micropollutants not so widely studied in presence of ZnO photocatalyst were purposely have been chosen: methyl-tert-butyl ether (MTBE), humic acid (HA), N, N-dimethyl p-nitrosoaniline (RNO), prednisolone (PNL), and doxycycline (DC). The brief review of each compound is presented in Table 2.3 in Appendix 2.

In paper [III] photocatalytic activity of sprayed ZnO nanostructured layers was measured through the photocatalytic oxidation of MTBE, HA, RNO and PNL. Experiments were carried out in a thermostatted (20 °C) 200-ml batch reactor under UV-lamps (Philips Actinic 15 W mercury low-pressure lamps, with emission at 365 nm, irradiance intensity 1.2 mW/cm²) equipped with reflectors. The experimental time was chosen to be 2h for MTBE (initial concentration 100 mg/l) and PNL (initial concentration 10 mg/l), 6 h in case of RNO (initial concentration 50 mg/l), and 24 h with HA (initial concentration 25 mg/l).

Photocatalytic performance of sprayed ZnO nanostructured layers was expressed by photocatalytic oxidation efficiency (17), showing the amount of pollutant degraded per 1 Wh of energy reaching the treated solution surface.

$$E = \frac{\Delta c \times V \times 10000}{I \times S \times t} \quad (17)$$

where E - the photocatalytic oxidation efficiency (mg/Wh); Δc - the decrease in the pollutant's concentration (mg/l), or chemical oxygen demand (mg O₂/l) ; V - the volume of the treated sample/pollutant (l); I - the irradiance, (mW/cm²); S - the irradiated area (cm²); t - the treatment time (h).

In paper [IV] photocatalytic activity of sprayed and electrodeposited ZnO rod layers was measured through the photocatalytic oxidation of DC. Experiments were carried out in a thermostatted (20 °C) 20-ml batch reactor under UVA-LED lamp (LZ1-UV00, LED Engin Inc. with emission at 365 nm, irradiance intensity 7.5 mW/cm²). The experimental time was 4 h. DC initial concentration was 25 mg/l. Photocatalytic performance of sprayed and electrodeposited ZnO rod layers was expressed as the decrease of normalised concentration (C/C₀) during the treatment time.

Measurements were performed in The Laboratory of Environmental Technology in the Tallinn University of Technology by Dr. Deniss Klauson.

3 Results and discussion

The following sections summarise the results of the studies on the deposition and properties of SP and ED ZnO rod layers. The results have been published in papers [I], [II], [III], and [IV].

3.1 Growth of rod-shaped ZnO nanostructures by spray pyrolysis and electrodeposition

3.1.1 Influence of FTO/glass substrate morphology on the growth of ZnO rods by spray pyrolysis

In practice, commercial transparent conductive oxide substrates such as ITO/glass or SnO₂/glass differ in morphology depending on the batch or supplier. Taking into account the influence of the substrate on rod formation and owing to the number of FTO/glass substrates with different morphologies, a systematic investigation on the influence of the FTO/glass substrate type on the resultant SP ZnO rod-layer morphology has been performed and published in a paper [I].

We investigated commercial FTO/glass substrates with five different morphologies and growth of ZnO crystals on them [I]. The AFM and SEM images of typical FTO-a, b, c substrates and the corresponding ZnO rod-like layers grown on them at similar growth conditions are presented in Fig. 3.1. The morphological parameters obtained from the SEM and AFM studies for FTO/glass substrates and the dimensions of ZnO crystals are summarised in Table 3.1.

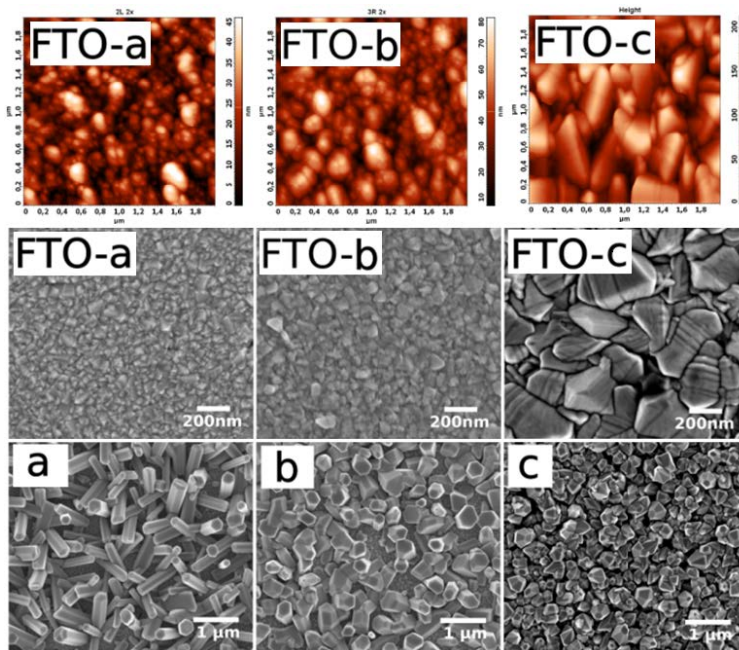


Figure 3.1 Upper row: AFM images of the substrates FTO-a, b and c; middle row: SEM images of the same substrates; bottom row: SEM images of ZnO rod-like crystals grown on corresponding substrates (a, b, c correspond to FTO-a, b and c respectively).

Table 3.1 Characteristics of FTO substrates (root mean square roughness (RMS), average roughness (Sa), average grain and crystallite size) and dimensions of the ZnO crystals grown on corresponding substrates (L – length, D – diameter).

	Properties of FTO substrates				Dimensions of ZnO crystals		
	RMS, nm (AFM)	Sa, nm (AFM)	Average grain size, nm (SEM)	Crystallite size, nm (XRD)	L, nm (SEM)	D, nm (SEM)	Aspect Ratio, L/D
FTO-a	9	7	50	13	1400	300	4.5
FTO-b	12	10	80	15	600	500	1
FTO-c	36	30	250	40	300	300	1

It can be seen from Fig. 3.1 and Table 3.1 that the FTO/glass substrates mainly differ in terms of roughness, crystallite and grain sizes. Among the studied substrates, elongated (L ~ 1400 nm) and uniformly sized ZnO rods with the highest aspect ratio value of 4.5 were grown on the FTO-a substrate. This substrate had one of the lowest roughness values (RMS = 9 nm), with grain sizes of around 50 nm. Rods grown on a FTO/glass substrate with a lower roughness (RMS = 7 nm) were also elongated, however, they revealed smaller dimensions (L ~ 800 nm) and an aspect ratio of 3 (presented in Table 1 in [1]). On FTO/glass substrates with roughness ≥ 12 nm (FTO-b and FTO-c), the obtained ZnO rods had smaller lengths and the lowest aspect ratios (Table 3.1). These results are in good agreement with that reported for the ZnO rods grown on a GaN substrate by the metalorganic chemical vapour deposition method and the ZnO seed layers obtained by solution growth, where growth of elongated ZnO rods was favoured by using relatively smooth substrates. Thus, for the spray deposition of the elongated ZnO rods with aspect ratios value 3 or higher, apart from a specific amount of nucleation centres, a roughness of the substrate around 9 nm or less than 12 nm is required.

According to the XRD study, a relationship between the orientation of the crystallites of the FTO and the morphology of the ZnO rods was not observed.

Haze factor (HF) measurements were used as an additional method to estimate the surface roughness of the FTO/glass substrates. HF spectra were calculated from optical transmittance spectral measurements as the ratio of the diffuse transmittance to the total transmittance and show the light scattering ability of the sample. It is assumed that difference in light scattering behaviour depends on the surface morphology [169]. The HF spectra of the FTO-a, b and c substrates are presented in Fig. 3.2. The rougher the FTO

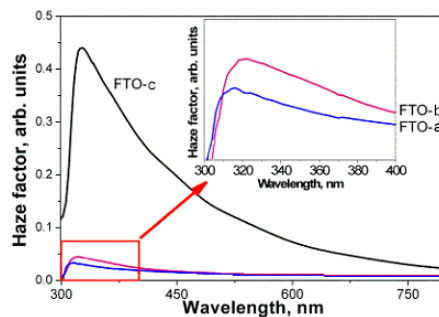


Figure 3.2 Haze factor spectra of FTO-a, b and c substrates.

layer on the glass substrate, the higher is the HF. The observed results correspond well with the AFM results on surface roughness. Thus, HF measurements could be used as an additional fast tool to evaluate the surface roughness of the substrate, and consequently, its suitability for the growth of elongated ZnO rods.

Several studies on SP reported that the growth of rod-like structures on a FTO/glass substrate without a seeding layer yielded non-uniform or randomly orientated ZnO rods, without providing detailed information on the substrate morphology [170]. This study clarifies that commercial FTO/glass substrates differ from one another and that their grain sizes may vary over a wide range (in our study, from 30 to 250 nm), therefore, an individual approach for each specific substrate is highly recommended.

In summary, the relationship between substrate grain sizes, surface roughness, and rod formation was established. The FTO/glass substrates with high roughnesses (> 12 nm) and grain sizes (> 80 nm) are not suitable for the growth of ZnO rod-like crystals. FTO/glass substrates with lower RMS and grain size values are advantageous for the growth of elongated ZnO rod-like crystals.

3.1.2 Influence of metal oxide seed layer types on the growth of ZnO rods by electrodeposition

Since the formation of ZnO rod-like crystals is very sensitive to the substrate, attention must be paid to obtain substrates with controlled and repeatable properties in order to reproduce ZnO nanorods with similar morphologies. Herein, various types of seed layers (ZnO, ZnO:In, TiO₂) with easily reproducible morphologies were grown on an ITO/glass substrate by SP. The influence of the seed layers on the formation of the ED ZnO rods is investigated in paper [II].

The SEM images of the ZnO seed layer substrates grown by SP and ZnO crystals grown by ED on those ZnO seed layers are shown in Fig. 3.3.

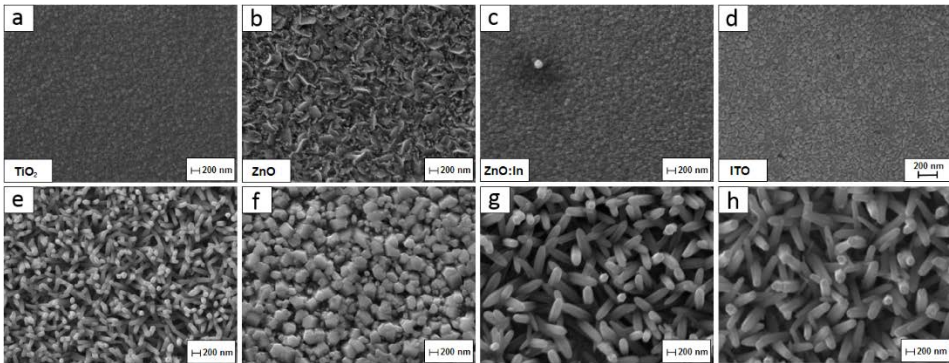


Figure 3.3 Upper row: SEM images of a) TiO₂ seed layer grown at $T_s = 450$ °C; b) ZnO seed layer grown from Zn(ac)₂ solution with $c = 0.1$ mol/l at $T_s = 420$ °C; c) ZnO seed layer grown from Zn(ac)₂ solution with $c = 0.2$ mol/l doped with In (3 at.%) at $T_s = 440$ °C; d) ITO layer without seed layer; bottom row: SEM images ED ZnO rod-like crystals (e, f, g, h) grown on seed layers a, b, c, and ITO layer, respectively.

As can be seen from Fig. 3.3a, b, and c, the sprayed seed layers vary in their morphology, which influenced the morphology of the resultant ZnO crystals. According to the SEM study, the TiO₂ seed layer, presented in Fig. 3.3a, is compact, flat, and composed of densely packed fine grains. As a result, the ZnO rods grown on the TiO₂ seed layer showed uniformly dense coverage, having a diameter of ca. 60 nm and length

ca. 370 nm (Fig. 3.3e). In contrast, the ZnO seed layer has a highly structured surface composed of grains with different shapes, including platelets and nanoneedles (Fig. 3.3b). The ZnO structures grown on the ZnO seed layer were composed of a mixture of fat and thin compactly standing ZnO crystals ($D \sim 150 - 300$ nm, $L \sim 150$ nm) (Fig. 3.4f). The surface of the ZnO seed layer doped with indium (ZnO:In) is dense and flat. The ZnO rods deposited onto the ZnO:In seed layer have uniform dimensions ($D \sim 200$ nm, $L \sim 700$ nm) (Fig. 3.3g) and are comparable to those grown on bare ITO/glass without a seed layer ($D \sim 170$ nm, $L \sim 700$ nm) (Fig. 3.3h).

It should be noted that the ZnO rods grown on ITO/glass, FTO/glass (Fig. 1d in [III]) substrates and on the ZnO:In seed layer are markedly larger than the ZnO crystals grown on TiO_2 and undoped ZnO seed layers. This could be explained by the differences in the electrical conductivity of the films. The ITO, FTO, and ZnO:In films are several times more conductive than the TiO_2 and undoped ZnO layers.

The XRD patterns of the ZnO crystals are presented in Fig. 4 in [II]. According to XRD analysis, the ED crystals are of ZnO and the orientation of the crystallites in the seed layer has no effect on the orientation of the ZnO crystals.

Thus, the dimensions, shape, and density of the ZnO rods depend strongly on the properties of the substrate or seed layer used. Well-shaped hexagonal ZnO crystals were grown on the seed layers with smooth, flat, fine-grained, and uniform morphologies, while the seed layers whose surfaces were composed of grains of different sizes induced the growth of ZnO crystals with different sizes and shapes. Electrically more conductive substrates such as ITO/glass, $\text{SnO}_2/\text{glass}$, and indium-doped ZnO seed layer induce the growth of ZnO rods with larger dimensions ($D \sim 200$ nm, $L \sim 700$ nm). ZnO rods with smaller dimensions were grown on less conductive seed layers like TiO_2 and undoped ZnO ($D \sim 60$ nm, $L \sim 350$ nm).

3.2 Bare and hierarchical ZnO nanostructures by spray pyrolysis

Results on deposition of ZnO nanostructures with different morphologies (bare- and hierarchical structures) by SP and evaluation of their photocatalytic activity in relation to various organic pollutants are published in paper [III].

3.2.1 Growth, morphological, and structural properties of sprayed bare and hierarchical ZnO nanostructures

By adjustment the SP deposition parameters such as the type and concentration of the Zn precursor, temperature of the substrate, substrate type ($\text{SnO}_2/\text{glass}$ or ITO/glass), spraying rate, and solution volume, ZnO was deposited in the form of various nanostructures [III]. Bare ZnO structures, like needles (S-1), rods (S-2), and pyramid-shaped crystals (S-4), were obtained by one-step spray pyrolysis. For the deposition of hierarchical structures (S-3 and S-4), two-step spray depositions were performed, where the $\text{Zn}(\text{ac})_2$ solution (2nd step) was pulverised over the bare crystal structure (1st step)s. The detailed experimental description is presented in section 2.1. The SEM images and schematic illustrations of the obtained SP ZnO nanostructured layers are presented in Fig. 3.4. According to the SEM study, sample S-1 is composed of two types of structures:

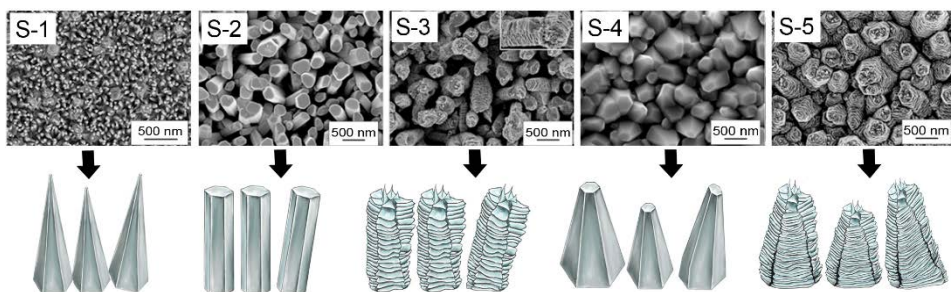


Figure 3.4 SEM images and of ZnO layers composed of: (S-1) nanoneedles, (S-2) rods, (S-3) hierarchical structures grown on the rods, (S-4) pyramid-shaped crystals and (S-5) hierarchical structures grown on pyramids and their schematic illustrations, respectively.

mainly nanoneedles with diameter of ca. 20 nm and length ca. 100 nm and random individual large crystals ($D = 170$ nm) between the needles. The needle-like morphology is specific for the SP ZnO layers produced from the $\text{Zn}(\text{ac})_2$ solution at deposition temperatures in the range 400 – 450 °C [104]. Sample S-2 is composed of elongated vertically aligned ZnO rods with diameter of ca. 250 nm and length ca. 1 μm . Sample S-3, obtained by two-step spray deposition, exhibits hierarchical structures, where dense networks of platelets wounded the rod-like pillars with nanoneedles on top. The formation of the nanoneedles on the top (002) plane has been shown in earlier studies using $\text{Zn}(\text{ac})_2$ as a branching solution and could be explained by the high surface energy of the (002) plane [35]. Sample S-4 was composed of truncated pyramid-shaped crystals deposited in similar deposition conditions as the rod-like sample S-2. By using the large grained ITO/glass substrate (S-4), instead of the SnO_2 /glass substrate (S-2), the truncated pyramid-shaped crystals were obtained. Sample S-5 is composed of hierarchical truncated pyramid-shaped crystals, and the morphology is similar to that of the surface of S-3; it is mainly composed of densely packed platelets and some needles on the top plane of the crystal.

According to the XRD study (Fig.4 in [III]), the layers showed reflections at 2θ values of 31.73°, 34.36°, 36.21°, 47.47°, 62.75°, and 67.85° corresponding to the (100), (002), (101), (102), (103), and (112) planes of ZnO, respectively, confirming the formation of the hexagonal wurtzite structure of ZnO, according to PDF 01-080-0074. In comparison with the standard powder diffraction data (PDF 01-080-0074), the (002) reflection in all the samples is predominant (the intensity ratios of $I_{(002)}/I_{(103)}$ have the highest values compared to other ratios), which indicates that all the ZnO nanostructured samples are preferred oriented in the direction of the c-axis.

3.2.2 Photocatalytic properties of sprayed bare and hierarchical ZnO nanostructures

The photocatalytic activity of the ZnO nanostructured layers was evaluated by means of the photocatalytic oxidation activity of several organic pollutants, namely, methyl-tert-butyl ether (MTBE), humic acid (HA), N, N-dimethyl p-nitrosoaniline (RNO), and prednisolone (PNL). The photocatalytic activity of the studied ZnO nanostructured layers was compared to the photocatalytic oxidation performance of the commercial photocatalyst P25 TiO_2 (Evonik). The outstanding photocatalytic performance achieved for the MTBE pollutant is presented in Fig. 3.5.

Independent of the morphology, the ZnO nanostructured layers showed higher MTBE photocatalytic degradation than the P25 TiO_2 slurry (170 $\text{mg O}_2 \text{ W}^{-1} \text{ h}^{-1}$). It can be seen from Fig. 3.5 that the MTBE photocatalytic oxidation efficiency of sample S-5 (hierarchical

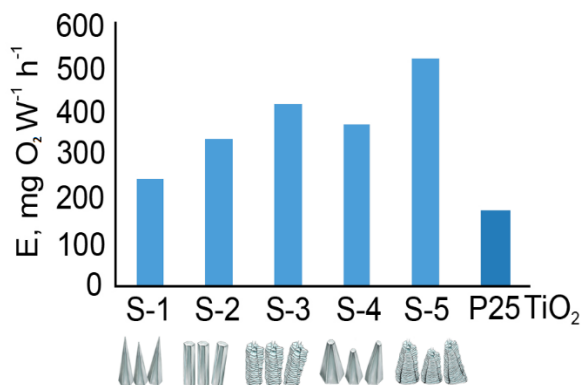


Figure 3.5 Results of MTBE (100 mg/l) photocatalytic oxidation by ZnO layers compared to P25 Evonik TiO₂ in form of slurry (1 g/l); the experimental time 2h.

structure grown on pyramids) was the highest, 518 mg O₂ W⁻¹ h⁻¹, after 2 h, exceeding the TiO₂ performance by three times. Numerous reports support the fact that hierarchical structures having increased surface area compared to bare 1D structures are more beneficial for photocatalytic performance [35, 36]. The results of MTBE photocatalytic oxidation by the hierarchical ZnO nanostructures (S-3 and S-5), obtained from this study, confirm these assumptions.

According to the investigations on the surface properties of SP and ED ZnO rods [IV], it can be assumed that the chemical composition of the surfaces of the ZnO nanostructures obtained in this study may also influence the photocatalytic performance. Since ZnO nanoneedles (S-1), bare rod- and pyramid-shaped structures (S-2, S-4), and hierarchical structures (S-3, S-5) were obtained at different deposition conditions, different chemical compositions of the surface were expected for these samples. Fig. 3.5 confirms that the photocatalytic oxidation activity towards MTBE of S-2 and S-4 samples, sprayed in similar conditions, showed nearly similar results, being 320 and 330 mg O₂ W⁻¹ h⁻¹ after 2 h, respectively. On the other hand, the hierarchical ZnO nanostructures of both S-3 and S-5 showed higher photocatalytic efficiencies in comparison with the bare structures S-2 and S-4.

A different trend in the photocatalytic degradation was observed for the RNO pollutant (Fig. 6 in [III]), where the highest photocatalytic performance was achieved after 6 h for the S-2 sample (rods), indicating that not only the surface area of the ZnO nanostructure affects the photocatalytic behaviour. A similar tendency was observed by Guo et al. and Tong et al., where ZnO layers composed of tetrapods or hierarchical nanostructures showed significantly higher photocatalytic degradation efficiencies of organic dyes such as methyl orange and methylene blue in comparison to ZnO nanoparticles with much higher surface areas [33, 34]. The observed difference in the photocatalytic degradation for the RNO pollutant can be explained by the different characters of the oxidising species produced by the ZnO nanostructures and their different interactions with the pollutants. ZnO nanostructures were not efficient in degrading the HA and PLN pollutants (Fig. 6 in [III]).

In summary, all the studied ZnO nanostructures were effective for the photocatalytic oxidation of the MTBE pollutant. It was found that the photocatalytic efficiency varies depending on the type of ZnO nanostructure. The highest photocatalytic oxidation efficiency of the MTBE pollutant was achieved by the hierarchical pyramid-shaped SP

ZnO nanostructures, indicating that a ZnO structure with increased surface area is beneficial for the degradation of such types of pollutants. Different trends were observed in the photocatalytic efficiency of other pollutants (RNO, HA, and PNL). Therefore, it can be concluded that the photocatalytic activity of the nanostructured ZnO depends on a combination of several factors including morphological and probably surface chemical properties, but varies individually for the different types of pollutants. For a deeper understanding of the role of surface properties on photocatalytic activity, ZnO samples with similar morphologies and specific surface areas should be compared through a more detailed study.

3.3 Surface properties of sprayed and electrodeposited ZnO rod layers

For this study, two types of ZnO rod layers deposited on ITO/glass substrates were investigated in parallel: SP and ED. The results have been published in a paper [IV].

By adjusting the deposition parameters during the SP and ED processes and choosing a suitable type of ITO/glass substrate, ZnO rods with relatively similar morphologies and specific surface areas were deposited (Fig. 3.6).

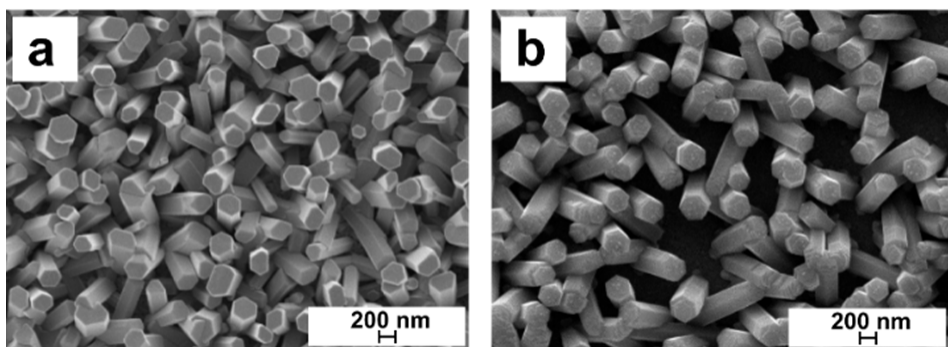


Figure 3.6 SEM micrographs of (a) SP ZnO rods on ITO/glass substrate, (b) ED ZnO rods on ITO/glass substrate.

The dimensions (length and diameter), number of crystals per cm^2 , and specific surface area of the deposited ZnO rods are summarized in Table 3.2. According to the calculations, both SP and ED samples have nearly similar specific surface areas of ca. $4 \text{ cm}^2/\text{cm}^2$.

Table 3.2 Summary of ZnO rods dimensional parameters (L – length, D – diameter), density of crystals and specific surface area of ZnO rods.

Sample	Dimensions		Number of crystals, pcs/ cm^2	Specific surface area, cm^2/cm^2
	L , nm	D , nm		
SP	750	300	6 E+08	~4
ED	950	350	3 E+08	~4

According to the XRD study (Fig. 2 in [IV]), both SP and ED ZnO rod layers are composed of hexagonal (wurtzite) ZnO. The most intense (002) reflection peak at the 2θ value of 34.39° for the SP and ED rods reveals the strong c-axis orientation of the crystallites in both the samples. The results of this study correspond well with the SEM observations, where it is shown that the SP and ED rods are only slightly tilted and positioned almost vertically on the substrate.

3.3.1 Wettability of sprayed and electrodeposited ZnO rod layers

Surface wettability of the ZnO rod layers was investigated by measuring the static water contact angle (CA). Table 3.3 summarises the average water CA values, together with the droplet photographs of the as-deposited, two-month-plastic-box-aged, and annealed at 400 °C SP and ED ZnO rod layers during the 30 min.

Table 3.3 Contact angle values of as-deposited, aged (stored in plastic boxes) and heat-treated (at 400 °C during the 30 min) SP and ED ZnO rods.

Sample	As-deposited	Two-month-aged	Heat-treated
SP	CA ~ 12° 	CA ~ 50° 	CA ~ 9° 
ED	CA ~ 3° 	CA ~ 120° 	CA ~ 3° 

According to the results, the as-sprayed ZnO rods are hydrophilic (CA < 90°) in nature, with CAs of ca. 12°. These values are close to those earlier reported for as-deposited ZnO nanostructured layers (CA of 11 – 13°) produced by SP from zinc acetate solutions [104]. An electrochemically as-grown ZnO rod sample is superhydrophilic (CA ≤ 5 – 10° [171]), showing CA values of 3°. These data are in good agreement with the studies of Barde et al., where superhydrophilic behaviour of electrodeposited ZnO rods (CA of ca. 2° or less) was reported [167].

After keeping the samples in a plastic box for two weeks, the difference in the wetting behaviour of the ED and SP deposited rods becomes pronounced. The ED and SP ZnO rod layers showed CA values of 112° and 40°, respectively (Table 2 in [IV]). A longer storage time (two months) in a plastic box did not change the wetting behaviour of the SP and ED rods significantly. The CA of the SP rods has increased up to 50°, while that of the ED rods has also increased slightly, up to 120°. Thus, the SP rods remained hydrophilic even after two months of storage. Similar to the ED rods, the wettability of hydrothermally grown rods has been reported to change from superhydrophilic (CA ~ 0°) to superhydrophobic (CA ~ 150°) upon storage for 20 days in the dark [172].

Reverse hydrophilic behaviour for all the types of rods studied was detected after heat treatment of the samples at 400 °C for 30 min in air (Table 3.3). The water CAs decreased so remarkably that the ZnO rod surfaces again became hydrophilic, with CA values close to that of the as-deposited samples. The CA of the SP rods has shown slightly higher values (CA ~ 9°) compared to the ED ZnO rods (CA ~ 3°). The reversibility of the wetting properties from the hydrophobic to the hydrophilic state after heating is a very common feature of the ZnO rods obtained by solution methods [171]. However, to the best knowledge of the author, there has been no precise study on the influence of the chemical composition of the ZnO rod surface on the wetting behaviour observed in the literature.

Wettability behaviour is governed and explained by both chemical composition and geometrical feature of the crystals. The ZnO rods deposited for this study have relatively similar morphology (crystals orientation, shape, “exposed” planes, distribution and specific surface area), therefore all the differences in wettability behaviour of the samples probably could be attributed to the difference in surface chemical properties. Wettability results reveal that chemical composition of the SP and ED ZnO rods surfaces

is different and for that reason chemical composition of the rod layers surfaces has been investigated.

3.3.2 Chemical composition of the surfaces of sprayed and electrodeposited ZnO rod layers

XPS analysis was used to investigate the chemical composition, presence and type of defects, and degree of contamination of the surface of as-deposited, aged, and heat-treated SP and ED rods. Therefore, O1s and C1s core level spectra are of the greatest interest in this study.

O1s core level spectra

According to the XPS survey, the asymmetric O1s core level peaks of the ZnO SP and ED rod samples can be deconvoluted by using Lorentzian-Gaussian (function pseudo-Voigt) fitting analysis into two, three or four peaks, as shown in Fig 3.7. The peaks centred at 530.4 ± 0.3 eV, 531.9 ± 0.1 eV, 531.1 eV and 533.2 ± 0.4 eV are attributed to the (Me-O) bond [173], surface hydroxyl (OH⁻) groups [174], oxygen vacancies (V_o) [79] and oxygen bonds with carbon (C-O and C=O) or H₂O [175, 176], respectively (Fig. 3.7).

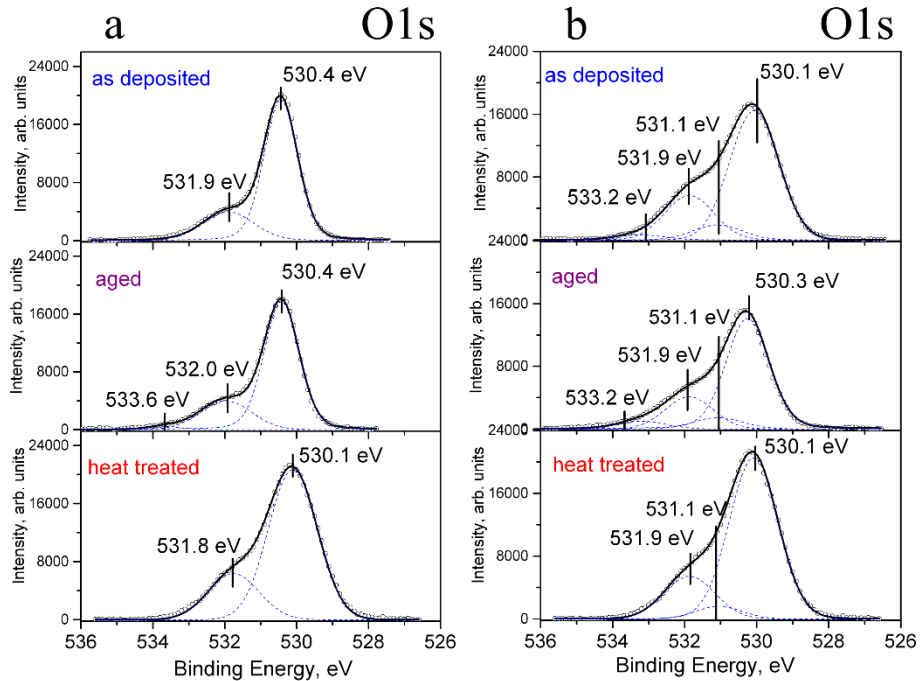


Figure 3.7 XPS spectra of as-deposited, aged and heat-treated 30 min at 400 °C in air ZnO rod samples in the binding energy region of O1s: (a) SP rods and (b) ED rods.

The atomic concentrations of all the detected components (Zn-O, V_o, OH⁻, H₂O or C-O or C=O) were calculated from the integrated areas of the O1s spectra of the SP and ED ZnO rod samples using Scofield's cross-sections. Since both the SP and ED ZnO rods were grown on the ITO substrate, the Me-O bond corresponding to the binding energy (BE) of 530.4 ± 0.3 eV originates from the two oxides ZnO and In₂O₃:Sn (ITO). In order to calculate the atomic concentration of the single Zn-O component, the In-O part coming from the

ITO substrate was subtracted from the Me-O peak area. The atomic ratios of OH⁻/Zn-O and V_o/Zn-O are presented in Table 3.4.

Table 3.4 XPS analysis data (atomic ratios of the OH⁻/Zn-O and V_o/Zn-O) obtained from the O1s core level peaks.

	SP ZnO rod sample			ED ZnO rod sample		
	As-dep.	Two-month-aged	Heat-treated	As-dep.	Two-month-aged	Heat-treated
[OH ⁻]/[Zn-O], arb.units (at.%/at.%)	0.3	0.3	0.4	1.2	0.7	0.8
[V _o]/ [Zn-O] arb.units (at.%/at.%)	-	-	-	0.4	0.3	0.2

The O1s spectra of the as-deposited, aged, and heat-treated SP ZnO rod samples showed peaks at BE = 530.4 ± 0.3 eV and BE = 531.9 ± 0.1 eV, corresponding to the Zn-O bond and the (OH⁻) groups, respectively.

The relative amount of (OH⁻) groups on the surface of the SP rod sample remained almost constant after the ageing and annealing steps (Table 3.4). In contrast to the SP rods, the ED rod sample showed a higher relative amount of the hydroxyl groups. This could be explained by the fact that the Zn(OH)_n species formed in the solution adhered onto the substrate surface and was only partly dehydrated to ZnO during the ED process [173], while the SP rods are fabricated at high temperatures, and therefore, the relative amount of the (OH⁻) groups is expected to be lower. In contrast to the SP rod sample, independent of the storage or heat-treatment, the peak at the BE of 531.1 eV ascribed to the oxygen-deficient region or the V_o present on the O1s spectra of the ED rods (Fig. 3.7, Table 3.4). The presence of V_o could be explained by the defect nature of ED ZnO rods. Raman study (Fig. 4 in [IV]) additionally confirms the defects of the ED ZnO rod samples, showing the shift associated with the oxygen vacancy defect located in the region 560 – 580 cm⁻¹ of the Raman spectra of the ED rods (centred at 564 cm⁻¹). In contrast, the typically highly crystalline SP ZnO do not reveal a shift in that region. It has been reported that the V_o possess enhanced adsorption energy and subsequently high capability to bind the (OH⁻) groups [177, 178]. Such interdependency between V_o and the (OH⁻) groups was observed for the ED rods: the higher the amount of V_o, the higher is the amount of (OH⁻) groups on the sample surface (Table 3.4).

After two months of ageing in a plastic box at ambient conditions, a low-intensity peak centred at the BE of 533.2 ± 0.4 eV (Fig. 3.7), assigned to the oxygen bonds with carbon (C-O and C=O) or H₂O, was detected on the XPS spectrum of the SP and ED ZnO rod samples [175, 176]. After heat-treatment, the peak disappeared in both the cases.

The results of the XPS studies are in good correlation with the wettability results of the as-deposited ZnO rods layers, showing that a higher amount of the hydroxyl groups contributes to higher hydrophilicity of the samples: CA ~ 3° for ED rods (Table 3.3). However, such correlation disappeared for the aged samples, indicating that the wettability results cannot be directly connected to the amount of (OH⁻) groups on the surface. A CA value of 50° for the aged SP rod sample, in contrast to the CA value of 12° for the as-deposited SP rod sample (Table 3.3), indicates that in addition to the (OH⁻) groups, the presence of other species on the surface probably affects the surface wetting properties. Furthermore, the aged ED rod sample showed hydrophobic properties

(CA $\sim 120^\circ$) while having ca. two times higher amount of (OH⁻) groups than the aged SP rod sample, which remains hydrophilic (CA $\sim 50^\circ$).

It could be speculated that the (OH⁻) groups in the aged samples were inactivated by the carbon species settled on the surface due to the atmospheric contamination from the exposure of the sample to ambient conditions. Carbon is commonly recognised as a surface contaminant. Several studies on ZnO nanostructures confirmed that wettability changes from hydrophilic to hydrophobic after storage (2-4 weeks) under ambient conditions [179]. This is attributed to the replacement of the initial surface (OH⁻) groups with thermodynamically more stable oxygen atoms, which are less polar and, thus, increase the surface hydrophobicity and adsorption ability of the organic contaminants from the air. Contaminant adsorption decreases the surface energy of the substrate and increases its hydrophobicity, which is reflected in an increased CA value [180]. This assumption is also supported by the fact that the CA values of both the ED and SP samples decrease after heating, although no significant change is detected in the relative amount of the (OH⁻) groups (Table 3.4).

C1s core level spectra

According to the XPS study, the C1s core level spectra of the SP and ED rods could be resolved into four main peaks centred at 285.0 eV, 285.7 eV, 286.5 \pm 0.3 eV, and 289.0 eV, corresponding to the C=C, C-C/C-H, C-O-C/C-O, and COOH/C=O, respectively (Fig. 3.8). Furthermore, the discussion is focused on hydrocarbon species (C=C, C-C/C-H), as these are more dominant compared to oxygen-containing organics (C-O-C/C-O, COOH/C=O).

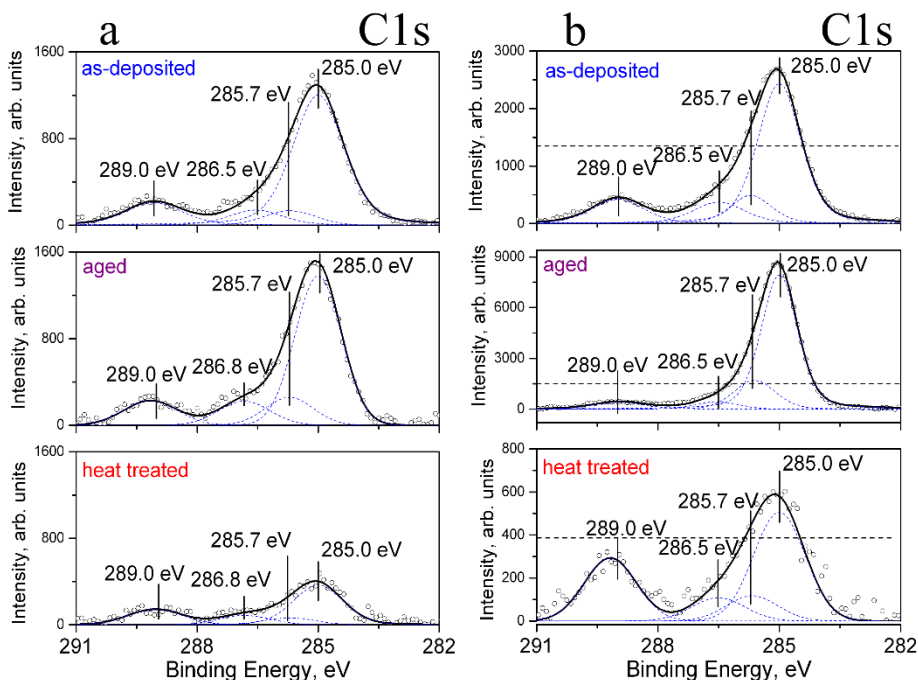


Figure 3.8 XPS spectra of as-deposited, aged, and heat-treated at 400 °C in air ZnO rod samples in the C1s binding energy region, (a) SP rods and (b) ED rods. Note: Scale is different. Horizontal Dashed lines on ED C1s spectra correspond to the peak maximum of analogue SP rods.

The intensity of the C=C peak of the as-deposited and aged SP rod samples on XPS spectra showed only a small increase compared to the as-deposited value (Table 3.5). The intensity of the C=C peak of the aged ZnO ED rod sample is about three times higher than that of the as-deposited ED sample (Table 3.5). These results are in good accordance with the CA measurements, revealing that the SP rod sample increased in CA from 12° to 50°, though it remained hydrophilic even after two months of storage, whereas the ED rods changed from superhydrophilic (CA ~ 3°) to hydrophobic (CA ~ 120°). Additionally, broad bands in the region of 1250 – 1750 cm⁻¹ (Fig. 4 in [IV]), commonly assigned to the C-C and C-H species, were observed only on the Raman spectra of the aged ED rods [181].

Table 3.5 Intensities of C=C peaks at BE=285 eV from C1s core level spectra for ZnO samples.

SP ZnO rod sample			ED ZnO rod sample		
As-dep.	Two-month-aged	Heat-treated	As-dep.	Two-month-aged	Heat-treated
1400	1500	400	2700	9000	600

After heat treatment for 30 min at 400 °C, the intensity of the C=C peak decreases ca. 15 times for the ED rod sample and ca. four times for the SP rod sample, in comparison with the aged samples (Table 3.5), being even less than those of the as-deposited samples. The Raman spectrum of the annealed ED rods after ageing demonstrates that the broadened peak in the region of 1250 – 1750 cm⁻¹, corresponding to the C-C and C-H species, present in the spectrum of the aged ED sample disappears after thermal treatment (Fig.4 in [IV]).

The CA values of the SP and ED heat-treated samples decreased back to the initial values characteristic of the as-deposited samples. Reversible wettability behaviour was observed mainly due to the efficient removal of contaminants from the sample surface during annealing.

Thus, according to the XPS, Raman, and wettability studies, the as-deposited ED rods contain higher amounts of (OH⁻) groups and V_o defects on the surface, and therefore, are more susceptible to faster and easier contamination by carbon species from air and plastic boxes, compared to the SP rods.

3.3.3 Photocatalytic properties of sprayed and electrodeposited ZnO rod layers

The photocatalytic activity of the as-deposited, aged, and heat-treated SP and ED ZnO rod samples was investigated through the photocatalytic degradation of the antibiotic doxycycline (DC). The results on the decrease in DC normalised concentration with time are presented in Fig. 3.9.

The as-deposited ED rods have shown the highest photocatalytic activity among all the studied samples; ca. 75 % of the initial amount of DC was degraded after 30 min. After the experimental time of 4 h, ca. 85 % of the initial DC was decomposed by the as-deposited ED rods. In contrast to the ED rods, the as-deposited SP rods showed a degradation efficiency of ca. 48% after 4h. Here, the photocatalytic activity of the as-deposited ED rods is ca. two times higher than that of the as-deposited SP rods. According to the wettability, XPS, and Raman studies, such a result could be explained by the higher amount of (OH⁻) groups and V_o defects on the surface of the as-deposited ED rods compared to the as-deposited SP rods, and a relatively low degree of contamination on the surface. It is well-known that V_o and (OH⁻) groups make the surface more hydrophilic and assist the trapping of photoinduced electrons and holes, thus promoting the photocatalytic degradation process [174].

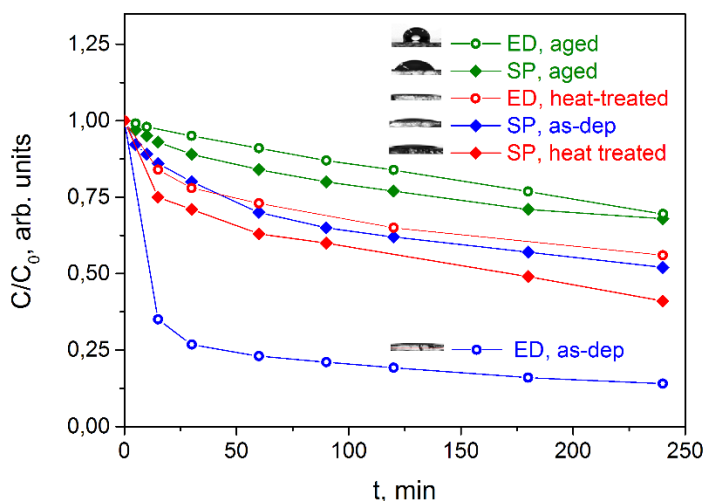


Figure 3.9 Decrease in doxycycline normalised concentration by ZnO rod layers.

Both SP and ED rods showed reduced photocatalytic activity performance after ageing: only 30 % of the initial amount of DC was degraded (after 4 h). The decreased photocatalytic activity of the aged samples is caused by surface contamination involving airborne hydrocarbon species, as confirmed by the XPS study. The contaminants settled on the ZnO rod surface decreased the DC adsorption ability, leading to worse photocatalytic performance of the rods. In contrast to the ED rods, the changes in the photocatalytic activity of the SP rods after two months of ageing are less pronounced, due to the lower amount of contaminants on the surface, indicating that the photocatalytic activity of the SP rods do not change significantly. After the experimental time of 4 h, the as-deposited SP rods decomposed ca. 48 % of DC, while the aged ones were able to decompose ca. 30 %.

In order to study the possibility of restoring the surface properties of the SP and ED rods after ageing, the samples were heat-treated. The photocatalytic activity of the heat-treated SP rods was restored and even improved (60 %/4 h) compared to that of the as-deposited SP rods (48 %/4 h). Since the amount of (OH⁻) groups on the surface of the as-deposited, aged, and annealed SP rod samples was almost the same, the improvement in photocatalytic activity can be explained by the reduced amount of contaminants in the annealed SP sample (Table 3.5).

The photocatalytic activity of the annealed ED rod samples slightly improved (45 %/4 h) compared to that of the aged ED rods (30 %/4 h), but was much below the original photocatalytic activity of the as-deposited sample (85 %/4 h). The obtained results are in correspondence with the XPS study, which showed the relative amount of (OH⁻) groups and V_o on the surface of the heat-treated ED rod sample is lower than on the as-deposited ED rods sample (Table 3.4).

A higher photocatalytic activity of the annealed SP rod samples compared to that of the annealed ED rods sample, in spite of the higher relative amount of (OH⁻) groups on the surface of the annealed ED rod sample, can be explained by the higher amount of contaminants or contaminating species on the surface of the annealed ED rods.

To summarise this section, the highest photocatalytic activity was demonstrated by the as-deposited ED rods (85 %/4 h). Ageing of the ED ZnO rods decreased their

photocatalytic performance to 30 %/4 h, which was not restored to the initial level after heat treatment. The SP rods are less photocatalytically active (as-dep. 48 %/4 h), though their photocatalytic performance is more stable (aged 30 %/4 h) compared to the ED rods. The reversibility in wettability behaviour (highly hydrophilic surface after heat treatment) was not accompanied by a reversibility in the photocatalytic activity of the ED ZnO rods.

Conclusions

The main conclusions from this dissertation can be summarised as follows:

1. Commercial FTO/glass substrates differ in FTO layer roughness and grain size values, which are important parameters in controlling the growth of ZnO rod layers by SP on those electrodes. It has been shown that FTO/glass, with the RMS values of FTO in the range 7 – 9 nm and grain sizes in the range 30 – 50 nm, yielded elongated hexagonal ZnO rod-like crystals with aspect ratios values in the range 3 to 4.5. FTO/glass substrates with higher roughness (≥ 12 nm) and grain sizes (≥ 80 nm) are not suitable for the growth of ZnO rod-like crystals.
2. The relationship between the morphology and conductivity of the seed layer and the dimensions of the ZnO rods obtained by electrodeposition was established. Hexagonal ZnO crystals were ED on the seed layers with smooth and fine-grained morphologies (TiO₂, ZnO:In seed layers, commercial ITO electrode). Underlays with a surface composed of grains of different sizes (undoped ZnO seed layers) induce the growth of short ZnO crystals with nonuniform diameters ($D \sim 150 - 300$ nm, $L \sim 150$ nm). Electrically more conductive substrates such as ITO and indium-doped ZnO seed layer induce the growth of ZnO rods with larger dimensions ($D \sim 200$ nm, $L \sim 700$ nm), but ZnO rods with smaller dimensions were grown on less conductive seed layers like TiO₂ ($D \sim 60$ nm, $L \sim 350$ nm) and undoped ZnO.
3. It has been shown that ZnO nanostructured layers grown by the fast and cost-effective SP method are efficient for the photocatalytic degradation of organic pollutants in water. ZnO layers comprising nanoneedles, rods, pyramids, or hierarchical rods or pyramids demonstrated higher photocatalytic efficiency of methyl-tert-butyl ether oxidation than the generally well known photocatalyst commercial P25 TiO₂ powder. The highest oxidation efficiency ($518 \text{ mg O}_2 \text{ W}^{-1} \text{ h}^{-1}$ after 2 h), which is three times higher compared to commercial TiO₂ powder, was obtained for the sample with the hierarchical structure grown on pyramids, which also has the highest surface area. ZnO rod layers with similar morphologies and surface areas were deposited by SP and ED. The different chemical compositions of the surfaces (amount of hydroxyl and carbon containing groups, oxygen vacancies) of the as-deposited, aged, and annealed SP and ED ZnO rods determine their wettability and photocatalytic properties:
 - The hydroxyl groups on the as-deposited ZnO rods make the surface hydrophilic (SP rods CA $\sim 12^\circ$, ED rods CA $\sim 3^\circ$) and photocatalytically active (48 % of the initial amount of doxycycline is degraded after 4 h for the SP rods and 85 % for the ED rods). According to the XPS study, the as-deposited ED ZnO rods showed the highest relative amount of hydroxyl groups on their surface ($[\text{OH}]/[\text{Zn-O}] \sim 1.2 \text{ at.\%/at.\%}$), and subsequently, the highest photocatalytic activity among the studied samples.
 - The impact of hydroxyl groups on two-months-aged-in-plastic-box ZnO rod layers is completely shaded by the increased amount of carbon groups. As a result, the CA increases (SP rods CA $\sim 50^\circ$, ED rods CA $\sim 120^\circ$), and the photocatalytic efficiency of the SP and ED rod layers drops down (30 %/4 h).

- Annealing of the ZnO rods at 400 °C for 30 min restores their initial wettability (SP rods CA \sim 9°, ED rods CA \sim 3°), however, the photocatalytic activity of the heat-treated ED rod layers shows only a moderate improvement (45 %/4 h) compared to the aged ED ZnO rod layers (30 %/4 h), not reaching the initial efficiency of the as-ED ZnO samples (85 %/4 h). The photocatalytic activity of the SP heat-treated ZnO rod layers was improved (60 %/4 h) compared to that of the aged SP rod layers (30 %/4 h) or as-deposited SP rod layers (48 %/4 h).

References

- [1] C. Klingshirn, ZnO: From basics towards applications, *Phys. Status Solidi B* 244 (2007) 3027–3073.
- [2] L. Schmidt-Mende, J. L. MacManus-Driscoll, ZnO – nanostructures, defects, and devices, *Mater. Today* 10 (2007) 40–48.
- [3] C. Klingshirn, J. Fallert, H. Zhou, J. Sartor, C. Thiele, F. Maier-Flaig, D. Schneider, and H. Kalt, 65 years of ZnO research – old and very recent results, *Phys. Status Solidi B* 247 (2010) 1424–1447.
- [4] S. Xu, Z. L. Wang, One-Dimensional ZnO Nanostructures: Solution Growth and Functional Properties, *Nano Res.* 11 (2011) 1013–1098.
- [5] A. Kołodziejczak-Radzimska, T. Jesionowski, Zinc Oxide—From Synthesis to Application: A Review, *Materials* 7 (2014) 2833-2881.
- [6] J. C. Fan, K. M. Sreekanth, Z. Xie, S. L. Chang, K. V. Rao, p-Type ZnO materials Theory, growth, properties and devices, *Prog. Mater. Sci.* 58 (2013) 874–985.
- [7] Ü. Özgür, D. Hofstetter, H. Morkoç, ZnO Devices and Applications review and future prospects, *Proceedings of the IEEE* 98 (2010) 1255–1268.
- [8] C. Jagadish, S. J. Pearton (Eds), *Zinc Oxide Bulk, Thin Films and Nanostructures: Processing, Properties, and Applications*, Amsterdam: Elsevier (2006) 1–589.
- [9] Y. Zhang, M. K. Ram, E. K. Stefanakos, D. Y. Goswami, Synthesis, Characterization, and Applications of ZnO Nanowires, *J. Nanomater.* 2012 (2012) 1–22.
- [10] H. Morkoç, Ü. Özgür, General Properties of ZnO, in *Zinc Oxide: Fundamentals, Materials and Device Technology*, Weinheim: WILEY-VCH Verlag GmbH & Co. KGaA (2009) 1–488.
- [11] A. Iglesias-Juez, A. Kubacka, G. Colón, M. Fernández-García, New and Future Developments in Catalysis: Chapter 10. Photocatalytic Nanooxides: The Case of TiO₂ and ZnO, Elsevier Inc. *Chapters* (2013) 245–266.
- [12] Z. L. Wang, Zinc oxide nanostructures: growth, properties and applications, *J. Phys.: Condens. Matter* 16 (2004) R829–R858.
- [13] X. Y. Konga, Z. L. Wang, Polar-surface dominated ZnO nanobelts and the electrostatic energy induced nanohelices, nanosprings, and nanospirals, *Appl. Phys. Lett.* 84 (2004) 1–3.
- [14] Ü. Özgür, Ya. I. Alivov, C. Liu, A. Teke, M. A. Reshchikov, S. Doğan, V. Avrutin, S.-J. Cho, H. Morkoç, A comprehensive review of ZnO materials and devices, *J. Appl. Phys.* 98 (2005) 041301.
- [15] M. A. Johar, R. A. Afzal, A. A. Alazba, U. Manzoor, Photocatalysis and Bandgap Engineering Using ZnO Nanocomposites, *Adv. Mater. Sci. Eng.* 2015 (2015) 1–22.
- [16] T. Dedova, M. Krunk, M. Grossberg, O. Volobujeva, I. Oja Acik, A novel deposition method to grow ZnO nanorods Spray pyrolysis, *Superlattices Microstruct.* 42 (2007) 444–450.

- [17] Q. Li, V. Kumar, Y. Li, H. Zhang, T. J. Marks, R. P. H. Chang, Fabrication of ZnO Nanorods and Nanotubes in Aqueous Solutions, *Chem. Mater.* 17 (2005) 1001–1006.
- [18] T. Frade, M. E. Melo Jorge, A. Gomes, One-dimensional ZnO nanostructured films: Effect of oxide nanoparticles, *Mater. Lett.* 82 (2012) 13–15.
- [19] H. J. Fan, R. Scholz, A. Dadgar, A. Krost, M. Zacharias, A low-temperature evaporation route for ZnO nanoneedles and nanosaws, *Appl. Phys. A* 80 (2005) 457–460.
- [20] K. S. Ranjith, R. Geethu, K. P. Vijayakumar, R. T. Rajendrakumar, Control of interconnected ZnO nanowires to vertically aligned ZnO nanorod arrays by tailoring the underlying spray deposited ZnO seed layer, *Mater. Res. Bull.* 60 (2014) 584–588.
- [21] L. C. Tien, S. J. Pearton, D. P. Norton, F. Ren, Synthesis and microstructure of vertically aligned ZnO nanowires grown by high-pressure-assisted pulsed-laser deposition, *J. Mater. Sci.* 43 (2008) 6925–6932.
- [22] M. T. Htay, Y. Hashimoto, K. Ito, Growth of ZnO Submicron Single-Crystalline Platelets, Wires, and Rods by Ultrasonic Spray Pyrolysis, *Jpn. J. Appl. Phys.* 46 (2007) 440–448.
- [23] H. Wang, T. Wu, Formation of complex nanostructures driven by polar surfaces, *J. Mater. Chem.* 21 (2011) 15095–15099.
- [24] X.Y. Kong, Y. Ding, R. Yang, Z. L. Wang, Single-Crystal Nanorings Formed by Epitaxial Self-Coiling of Polar Nanobelts, *Science* 303 (2004) 1348–1351.
- [25] J. Elias, R. Tena-Zaera, G.-Y. Wang, C. Lévy-Clément, Conversion of ZnO Nanowires into Nanotubes with Tailored Dimensions, *Chem. Mater.* 20 (2008) 6633–6637.
- [26] T. Xu, P. Ji, M. He, J. Li, Growth and Structure of Pure ZnO Micro/Nanocombs, *J. Nanomater.* 2012 (2012) 1–5.
- [27] J. Liu, L. Xu, B. Wei, W. Lv, H. Gao, X. Zhang, One-step hydrothermal synthesis and optical properties of aluminium doped ZnO hexagonal nanoplates on a zinc substrate, *Cryst. Eng. Comm.* 13 (2011) 1283–1286.
- [28] H. Sun, M. Luo, W. Weng, K. Cheng, P. Du, G. Shen, G. Han, Room-temperature preparation of ZnO nanosheets grown on Si substrates by a seed-layer assisted solution route, *Nanotechnology* 19 (2008) 125603.
- [29] Y. Sun, L. Wang, X. Yu, K. Chen, Facile synthesis of flower-like 3D ZnO superstructures via solution route, *Cryst. Eng. Comm.* 14 (2012) 3199–3204.
- [30] Y. Fang, Z. Li, S. Xu, D. Han, D. Lu, Optical properties and photocatalytic activities of spherical ZnO and flower-like ZnO structures synthesized by facile hydrothermal method, *J. Alloys Compd.* 575 (2013) 359–363.
- [31] S. Kuriakose, N. Bhardwaj, J. Singh, B. Satpati, S. Mohapatra, Structural, optical and photocatalytic properties of flower-like ZnO nanostructures prepared by a facile wet chemical method, *Beilstein J. Nanotechnol.* 4 (2013) 763–770.
- [32] N.-F. Hsu, M. Chang, K.-T. Hsu, Rapid synthesis of ZnO dandelion-like nanostructures and their applications in humidity sensing and photocatalysis, *Mat. Sci. Semicon. Proc.* 21 (2014) 200–205.

- [33] M. Y. Guo, A. M. C. Ng, F. Liu, A. B. Djuricic, W. K. Chan, H. Su, K. S. Wong, Effect of Native Defects on Photocatalytic Properties of ZnO, *J. Phys. Chem. C* 115 (2011) 11095–11101.
- [34] Y. Tong, J. Cheng, Y. Liu, G. Gu Siu, Enhanced photocatalytic performance of ZnO hierarchical nanostructures synthesized via a two-temperature aqueous solution route, *Scr. Mater.* 60 (2009) 1093–1096.
- [35] T. Dedova, M. Krunks, I. Oja Acik, D. Klauson, O. Volobujeva, A. Mere, Hierarchical nanostructures of ZnO obtained by spray pyrolysis, *Mater. Chem. Phys.* 141 (2013) 69–75.
- [36] H. Lu, S. Wang, L. Zhao, J. Li, B. Dong, Z. Xu, Hierarchical ZnO microarchitectures assembled by ultrathin nanosheets: hydrothermal synthesis and enhanced photocatalytic activity, *J. Mater. Chem.* 21 (2011) 4228–4234.
- [37] L. Xu, Z. Li, Q. Cai, H. Wang, H. Gao, W. Lv, J. Liu, Precursor template synthesis of three-dimensional mesoporous ZnO hierarchical structures and their photocatalytic properties, *Cryst. Eng. Comm.* 12 (2010) 2166–2172.
- [38] Z. L. Wang, Nanostructures of zinc oxide, *Materials Today*, (2004) 26–33.
- [39] C. Klingshirn, ZnO Material, Physics and Applications, *Chem. Phys. Chem.* 8 (2007) 782–803.
- [40] A. B. Djuricic, X. Chen, Y. H. Leung, A. M. C. Ng, ZnO nanostructures growth, properties and applications, *J. Mater. Chem.* 22 (2012) 6526–6535.
- [41] A. B. Djuricic, A. M. C. Ng, X. Y. Chen, ZnO nanostructures for optoelectronics Material properties and device applications, *Prog. Quantum Electron.* 34 (2010) 191–259.
- [42] T. Tynell, M. Karppinen, Atomic layer deposition of ZnO: a review, *Semicond. Sci. Technol.* 29 (2014) 1–15.
- [43] S. Agrawal, R. Rane, S. Mukherjee, ZnO Thin Film Deposition for TCO Application in Solar Cell, *Conference Papers in Energy*, 2013 (2013) 1–7.
- [44] M. Krunks, E. Kärber, A. Katerski, K. Otto, I. Oja Acik, T. Dedova, A. Mere, Extremely thin absorber layer solar cells on zinc oxide nanorods by chemical spray, *Sol. Energy Mater. Sol. Cells* 94 (2010) 1191–1195.
- [45] M. Wen, L. Wang, M. Zhang, L. Jiang, Y. Zheng, Antifogging and Icing-Delay Properties of Composite Micro- and Nanostructured Surfaces, *ACS Appl. Mater. Interfaces* 6 (2014) 3963–3968.
- [46] Y. Zhang, T. R. Nayak, H. Hong, W. Cai, Biomedical Applications of Zinc Oxide Nanomaterials, *Curr. Mol. Med.* 13 (2013) 1633–1645.
- [47] Y. Zhang, M. K. Ram, E. K. Stefanakos, D. Y. Goswami, Synthesis, Characterization, and Applications of ZnO Nanowires, *J. Nanomater.* 2012 (2012) 1–22.
- [48] H. Wang, L. Zhang, Z. Chen, J. Hu, S. Li, Z. Wang, J. Liu, X. Wang, Semiconductor heterojunction photocatalysts: design, construction, and photocatalytic performances, *Chem. Soc. Rev.* 43 (2014) 5234–5244.
- [49] F. Fresno, R. Portela, S. Suarez, J. M. Coronado, Photocatalytic materials_ recent achievements and near future trends, *J. Mater. Chem. A* 2 (2014) 2863–2884.

- [50] H. Zhou, Y. Qu, T. Zeid, X. Duan, Towards highly efficient photocatalysts using semiconductor nanoarchitectures, *Energy Environ. Sci.* 5 (2012) 6732–6743.
- [51] M. Yasmina, K. Mourad, S. H. Mohammed, C. Khaoula, Treatment heterogeneous photocatalysis; Factors influencing the photocatalytic degradation by TiO₂, *Energy Procedia* 50 (2014) 559–566.
- [52] J.-M. Herrmann, Heterogeneous photocatalysis fundamentals and applications to the removal of various types of aqueous pollutants, *Catal. Today* 53 (1999) 115–129.
- [53] A. Houas, H. Lachheb, M. Ksibi, E. Elaloui, C. Guillard, J.-M. Herrmann, Photocatalytic degradation pathway of methylene blue in water, *Appl. Catal. B* 31 (2001) 145–157.
- [54] M. Umar, H. A. Aziz, Photocatalytic Degradation of Organic Pollutants in Water, *Organic Pollutants - Monitoring, Risk and Treatment*, (2013) 196–208.
- [55] J. Schneider, M. Matsuoka, M. Takeuchi, J. Zhang, Y. Horiuchi, M. Anpo, D. W. Bahnemann, Understanding TiO₂ Photocatalysis: Mechanisms and Materials, *Chem. Rev.* 114 (2014) 9919–9986.
- [56] C. Tian, Q. Zhang, A. Wu, M. Jiang, Z. Liang, B. Jiang, H. Fu, Cost-effective large-scale synthesis of ZnO photocatalyst with excellent performance for dye photodegradation, *Chem. Commun.* 48 (2012) 2858–2860.
- [57] S. Baruah, M. A. Mahmood, M. T. Z. Myint, T. Bora, J. Dutta, Enhanced visible light photocatalysis through fast crystallization of zinc oxide nanorods, *Beilstein J. Nanotechnol.* 1 (2010) 14–20.
- [58] C. A. K. Gouvea, F. Wypych, S. G. Moraes, N. Duran, N. Nagata, P. Peralta-Zamora, Semiconductor-assisted photocatalytic degradation of reactive dyes in aqueous solution, *Chemosphere* 40 (2000) 433–440.
- [59] C. Lizama, J. Freer, J. Baeza, H. D. Mansilla, Optimized photodegradation of Reactive Blue 19 on TiO₂ and ZnO suspensions, *Cataly. Today* 76 (2002) 235–246.
- [60] S. Sakthivel, B. Neppolian, M.V. Shankar, B. Arabindoo, M. Palanichamy, V. Murugesan, Solar photocatalytic degradation of azo dye: comparison of photocatalytic efficiency of ZnO and TiO₂, *Sol. Energy Mater. Sol. Cells* 77 (2003) 65–82.
- [61] S. K. Kansal, M. Singh, D. Sud, Studies on photodegradation of two commercial dyes in aqueous phase using different photocatalysts, *J. Hazard. Mater.* 141 (2007) 581–590.
- [62] L. Lin, Y. Yang, L. Men, X. Wang, D. He, Y. Chai, B. Zhao, S. Ghoshroy, Q. Tang, A highly efficient TiO₂@ZnO n–p–n heterojunction nanorod photocatalyst, *Nanoscale* 5 (2013) 588–593.
- [63] X. Liu, Z. Li, W. Zhao, C. Zhao, J. Yang, Y. Wang, Zinc Oxide nanorod/Au composite arrays and their enhanced photocatalytic properties, *J. Colloid Interface Sci.* 432 (2014) 170–175.
- [64] Y. Zhang, M. K. Ram, E.K. Stefanakos, D. Y. Goswami, Enhanced photocatalytic activity of iron doped zinc oxide nanowires for water decontamination, *Surf. Coat. Technol.* 217 (2013) 119–123.

- [65] P. Fernandez-Ibanez, J. Blanco, S. Malato, F. J. de las Nieves, Application of the colloidal stability of TiO₂ particles for recovery and reuse in solar photocatalysis, *Water Res.* 37 (2003) 3180–3188.
- [66] J. Jiang, X. Zhang, P. Sun, L. Zhang, ZnO/BiOI Heterostructures: Photoinduced Charge-Transfer Property and Enhanced Visible-Light Photocatalytic Activity, *J. Phys. Chem. C* 115 (2011) 20555–20564.
- [67] R. Saravanan, S. Karthikeyan, V. K. Gupta, G. Sekaran, V. Narayanan, A. Stephen, Enhanced photocatalytic activity of ZnO/CuO nanocomposite for the degradation of textile dye on visible light illumination, *Mater. Sci. Eng. C* 33 (2013) 91–98.
- [68] J. Lu, H. Wang, S. Dong, F. Wang, Y. Dong, Effect of Ag shapes and surface compositions on the photocatalytic performance of Ag/ZnO nanorods, *J. Alloys Compd.* 617 (2014) 869–876.
- [69] N. Daneshvar, M. H. Rasoulifard, A. R. Khataee, F. Hosseinzadeh, Removal of C.I. Acid Orange 7 from aqueous solution by UV irradiation in the presence of ZnO nanopowder, *J. Hazard. Mater.* 143 (2007) 95–101.
- [70] N. Daneshvar, S. Aber, M. S. Seyed Dorraji, A. R. Khataee, M. H. Rasoulifard, Photocatalytic degradation of the insecticide diazinon in the presence of prepared nanocrystalline ZnO powders under irradiation of UV-C light, *Sep. Purif. Technol.* 58 (2007) 91–98.
- [71] F. Liu, M. Y. Guo, Y. H. Leung, A. B. Djuricic, A. M. C. Ng, W. K. Chan, Effect of starting properties and annealing on photocatalytic activity of ZnO nanoparticles, *Appl. Surf. Sci.* 283 (2013) 914–923.
- [72] X. Li, X. Fang, X. Chen, X. Wang, J. Li, F. Fang, Z. Wei, X. Chu, F. Wang, Enhanced Photocatalytic Activity of Mg-Doped ZnO Nanorods Prepared by Electrodeposition, *Integr. Ferroelectr.* 144 (2013) 22–28.
- [73] G. Kenanakis, N. Katsarakis, Ultrasonic spray pyrolysis growth of ZnO and ZnO:Al nanostructured films: Application to photocatalysis, *Mater. Res. Bull.* 60 (2014) 752–759.
- [74] I. Altın, I. Polat, E. Bacaksız, M. Sökmen, ZnO and ZnS microrods coated on glass and photocatalytic activity, *Appl. Surf. Sci.* 258 (2012) 4861–4865.
- [75] M. Bizarro, A. Sánchez-Arzate, I. Garduno-Wilches, J. C. Alonso, A. Ortiz, Synthesis and characterization of ZnO and ZnO:Al by spray pyrolysis with high photocatalytic properties, *Catal. Today* 166 (2011) 129–134.
- [76] X. Li, J. Wang, J. Yang, J. Lang, S. Lü, M. Wei, X. Meng, C. Kou, X. Li, Comparison of photocatalytic activity of ZnO rod arrays with various diameter sizes and orientation, *J. Alloys Compd.* 580 (2013) 205–210.
- [77] M. E. Simonsen, Z. Li, E. G. Sjøgaard, Influence of the OH groups on the photocatalytic activity and photoinduced hydrophilicity of microwave assisted sol-gel TiO₂ film, *Appl. Surf. Sci.* 255 (2009) 8054–8062.

- [78] M. E. Simonsen, H. J. Zheshen, L. Erik, G. Sjøgaard, Surface properties and photocatalytic activity of nanocrystalline titania films, *J. Photochem. Photobiol. A Chem.* 200 (2008) 192–200.
- [79] X. Zhang, J. Qin, Y. Xue, P. Yu, B. Zhang, L. Wang, R. Liu, Effect of aspect ratio and surface defects on the photocatalytic activity of ZnO nanorods, *Sci. Rep.* 4 (2014) 4596.
- [80] J. Wang, Z. Wang, B. Huang, Y. Ma, Y. Liu, X. Qin, X. Zhang, Y. Dai, Oxygen Vacancy Induced Band-Gap Narrowing and Enhanced Visible Light Photocatalytic Activity of ZnO, *ACS Appl. Mater. Interfaces* 4 (2012) 4024–4030.
- [81] D. Chen, Z. Wang, T. Ren, H. Ding, W. Yao, R. Zong, Y. Zhu, Influence of Defects on the Photocatalytic Activity of ZnO, *J. Phys. Chem. C* 118 (2014) 15300–15307.
- [82] M. Kong, Y. Li, X. Chen, T. Tian, P. Fang, F. Zheng, X. Zhao, Tuning the Relative Concentration Ratio of Bulk Defects to Surface Defects in TiO₂ Nanocrystals Leads to High Photocatalytic Efficiency, *J. Am. Chem. Soc.* 133 (2011) 16414–16417.
- [83] L. Xue, L. Jin-hua, L. Shi-Jun, F. Xuan, F. Fang, C. Xue-Ying, W. Xiao-Hua, H. Jia-Xin, Fabrication and Visible Light Photocatalytic Activity of Co-doped ZnO Nanorods, *Chem. Res. Chin. Univ.* 29 (2013) 1032–1035.
- [84] G. Jimenez-Cadena, E. Comini, M. Ferroni, A. Vomiero, G. Sberveglieri, Synthesis of different ZnO nanostructures by modified PVD process and potential use for 1dye-sensitized solar cells, *Mater. Chem. Phys.* 124 (2010) 694–698.
- [85] W. Gao, Z. Li, ZnO thin films produced by magnetron sputtering, *Ceram. Int.* 30 (2004) 1155–1159.
- [86] Y. Sun, G. M. Fuge, M. N.R. Ashfold, Growth mechanisms for ZnO nanorods formed by pulsed laser deposition, *Superlattices and Microstruct.* 39 (2006) 33–40.
- [87] Q. X. Zhao, P. Klason, M. Willander, Growth of ZnO nanostructures by vapor–liquid–solid method, *Appl. Phys. A* 88 (2007) 27–30.
- [88] J.-J. Wu, S.-C. Liu, Low-Temperature Growth of Well-Aligned ZnO Nanorods by Chemical Vapor Deposition, *Adv. Mater.* 14 (2002) 215–218.
- [89] K. L. Foo, U. Hashim, K. Muhammad, C. H. Voon, Sol–gel synthesized zinc oxide nanorods and their structural and optical investigation for optoelectronic application, *Nanoscale Res. Lett.* 9 (2014) 1–10.
- [90] S.-H. Yi, S.-K. Choi, J.-M. Jang, J.-A. Kim, W.-G. Jung, Low-temperature growth of ZnO nanorods by chemical bath deposition, *J. Colloid Interface Sci.* 313 (2007) 705–710.
- [91] N. Hasuike, T. Harada, T. Kiyohara, K. Nishio, K. Kisoda, H. Harima, Low temperature synthesis of ZnO thin films by spin-coating technique, *Phys. Status Solidi C* 8 (2011) 506–508.
- [92] Y. Lee, Y. Zhang, S. L. G. Ng, F. C. Kartawidjaja, J. Wang, Hydrothermal Growth of Vertical ZnO Nanorods, *J. Am. Ceram. Soc.* 92 (2009) 1940–1945.

- [93] L. Filipovic, S. Selberherr, G. C. Mutinati, E. Brunet, S. Steinhauer, A. Köck, J. Teva, J. Kraft, J. Siegert, F. Schrank, Modeling Spray Pyrolysis Deposition, Proceedings of the World Congress on Engineering 2013 Vol II (2013).
- [94] R. R. Chamberlin, J. S. Skarman, Chemical Spray Deposition Process for Inorganic Films, *J. Electrochem. Soc.* 113 (1966) 86–89.
- [95] P. S. Patil, Versatility of chemical spray pyrolysis technique, *Mater. Chem. Phys.* 59 (1999) 185–198.
- [96] J. B. Mooney, S. B. Radding, Spray Pyrolysis Processing, *Ann. Rev. Mater. Sci.* 12 (1982) 81–101.
- [97] D. Perendis, L. J. Gauckler, Thin film deposition using spray pyrolysis, *J. Electroceram.* 14 (2005) 103–111.
- [98] J. H. Bang, Y. T. Didenko, R. J. Helmich, K. S. Suslick, Nanostructured Materials Through Ultrasonic Spray Pyrolysis, *Material Matters* 7 15–20 [Online], Available: <http://www.sigmaaldrich.com/technical-documents/articles/material-matters/ultrasonic-spray-pyrolysis.html> [Accessed: 01-Apr-2018].
- [99] J.-H. Jeong, Y.-S. Jeon, K.-O. Jeon, K.-S. Hwang, B.-H. Kim, Preparation of zinc oxide films by an electrostatic spray deposition process, *J. Ceram. Process. Res.* 7 (2006) 70–74.
- [100] M. Krunk, T. Dedova, I. Oja Acik, Spray pyrolysis deposition of zinc oxide nanostructured layers, *Thin Solid Films*, 515 (2006) 1157–1160.
- [101] E. Arca, K. Fleischer, I. V. Shvets, Influence of the precursors and chemical composition of the solution on the properties of ZnO thin films grown by spray pyrolysis. *J. Phys. Chem. C* 113, 21074–21081 (2009).
- [102] T. Dedova, O. Volobujeva, J. Klauson, A. Mere, M. Krunk, ZnO Nanorods via Spray Deposition of Solutions Containing Zinc Chloride and Thiocarbamide, *Nanoscale Res. Lett.* 2 (2007) 391–396.
- [103] J. F. Guillemoles, D. Lincot, P. Cowache, J. Vedel, Solvent Effect on ZnO thin films prepared by spray pyrolysis. In: A. Luque, G. Sala, W. Palz, G. Santos, P. Helm, (Eds.) Tenth E.C. Photovoltaic Solar Energy Conference. Dordrecht: Springer (1991) 609–612.
- [104] T. Dedova, J. Klauson, C. Badre, T. Pauporté, R. Nisumaa, A. Mere, O. Volobujeva, M. Krunk, Chemical spray deposition of zinc oxide nanostructured layers from zinc acetate solutions, *Phys. Status Solidi A* 205 (2008) 2355–2359.
- [105] E. Bacaksiz, M. Parlak, M. Tomakin, A. Özcelik, M. Karakız, M. Altunbas, The effects of zinc nitrate, zinc acetate and zinc chloride precursors on investigation of structural and optical properties of ZnO thin films, *J. Alloys Compd.* 466 (2008) 447–450.
- [106] D. Perednis, L. J. Gauckler, Thin film deposition using spray pyrolysis, *J. Electroceram.* 14 (2005) 103–111.
- [107] H. Wagata, N. Ohashi, T. Taniguchi, K. Katsumata, K. Okada, N. Matsushita, Control of the microstructure and crystalline orientation of ZnO films on a seed-free glass substrate by using a spin-spray method, *Cryst. Growth Des.* 10 (2010) 4968–4975.

- [108] A. El Hichou, M. Addou, J. Ebothé, M. Troyon, Influence of deposition temperature (T_s), air flow rate (f) and precursors on cathodoluminescence properties of ZnO thin films prepared by spray pyrolysis. *J. Lumin.* 113 (2005) 183–190.
- [109] E. Bacaksiz, S. Aksu, S. Yılmaz, M. Parlak, M. Altunbaş, Structural, optical and electrical properties of Al-doped ZnO microrods prepared by spray pyrolysis, *Thin Solid Films* 518 (2010) 4076–4080.
- [110] T. Dedova, I. Oja Acik, M. Krunks, V. Mikli, O. Volobujeva, A. Mere, Effect of substrate morphology on the nucleation and growth of ZnO nanorods prepared by spray pyrolysis, *Thin Solid Films* 520 (2012) 4650–4653.
- [111] M. Kriisa, M. Krunks, E. Kärber, M. Kukk, V. Mikli, A. Mere, Effect of Solution Spray Rate on the Properties of Chemically Sprayed ZnO:In Thin Films, *Journal of Nanomaterials*, 2013 (2013) 1–9.
- [112] A. Nakaruk, C. C. Sorrell, Conceptual model for spray pyrolysis mechanism_ fabrication and annealing of titania thin films, *J. Coat. Technol. Res.* 7 (2010) 665–676.
- [113] U. Alver, T. Kılınc, E. Bacaksız, T. Küçükömeroğlu, S. Nezir, İ. H. Mutlu, F. Aslan, Synthesis and characterization of spray pyrolysis Zinc Oxide microrods, *Thin Solid Films* 515 (2007) 3448–3451.
- [114] U. Alver, T. Kılinc, E. Bacaksız, S. Nezir, Temperature dependence of ZnO rods produced by ultrasonic spray pyrolysis method, *Mater. Chem. Phys.* 106 (2007) 227–230.
- [115] E. Sonmez, S. Aydin, M. Yilmaz, M. T. Yurtcan, T. Karacali, M. Ertugrul, Study of Structural and Optical Properties of Zinc Oxide Rods Grown on Glasses by Chemical Spray Pyrolysis, *J. Nanomater.* 2012 (2012) 1–5.
- [116] E. Kärber, T. Raadik, T. Dedova, J. Krustok, A. Mere, V. Mikli, M. Krunks, Photoluminescence of spray pyrolysis deposited ZnO nanorods, *Nanoscale Res. Lett.* 6 (2011) 359.
- [117] R. Mariappan, V. Ponnuswamy, A. C. Bose, A. Chithambararaj, R. Suresh, M. Ragavendar, Structural, optical and electrical characterization of nebulizer-sprayed ZnO nano-rods, *Superlattices Microstruct.* 65 (2014) 184–194.
- [118] M. Krunks, T. Dedova, E. Kärber, V. Mikli, I. Oja Acik, M. Grossberg, A. Mere, Growth and electrical properties of ZnO nanorod arrays prepared by chemical spray pyrolysis, *Physica B* 404 (2009) 4422–4425.
- [119] M. Tomakin, Structural and optical properties of ZnO and Al-doped ZnO microrods obtained by spray pyrolysis method using different solvents, *Superlattices Microstruct.* 51 (2012) 372–380.
- [120] T. Dedova, M. Krunks, A. Mere, J. Klauson and O. Volobujeva. Preparation of shape and size-controlled zinc oxide nanostructures by chemical spray pyrolysis technique, *Materials Research Society Symposium Proceedings 957: Warrendale, PA* (2007) 0957–K10–26.
- [121] A. J. Bard, L. R. Faulkner, *Electrochemical methods: fundamentals and applications*, (Eds). D. Harris, E. Swain, C. Robey, E. Aiello, 2nd edition, New York: John Wiley and Sons, Inc. (2001) 9–23.

- [122] A. Ray, Electrodeposition of Thin Films for low-cost solar cells, Chapter 7, In: Electroplating of Nanostructures. (Ed.) M. Aliofkhazraei, In Tech (2015).
- [123] R. K. Pandey, S. N. Sahu, S. Chandra, Handbook of Semiconductor Electrodeposition, New York: M. Dekker (1996).
- [124] G. Jiangfeng, D. Zhaoming, D. Qingping, X. Yuan, Z. Weihu, Controlled Synthesis of ZnO Nanostructures by Electrodeposition Method, *J. Nanomater.* 2010 (2010) 1–6.
- [125] F. Xu, Y. Lu, L. Xia, Y. Xie, M. Dai, Y. Liu, Seed layer-free electrodeposition of well-aligned ZnO submicron rod arrays via simple aqueous electrolyte, *Mater. Res. Bull.* 44 (2009) 1700–1708.
- [126] X.-D. Gao, F. Peng, X.-M. Li, W.-D. Yu, J.-J. Qiu, Growth of highly oriented ZnO films by two-step electrodeposition technique, *J. Mater. Sci.* 42 (2007) 9638–9644.
- [127] C.-T. Hsieh, S.-Y. Yang, J.-L. Gu, Y.-R. Jiang, Influence of growth parameters on texture of ZnO nanorods by using electrochemical deposition at low temperatures, *Solid State Ionics* 209–210 (2012) 43–50.
- [128] J. Elias, R. Tena-Zaera, C. Lévy-Clément. Effects of the Chemical Nature of the Anions on the electrodeposition of ZnO Nanowire Arrays, *J. Phys. Chem. C* 112 (2008) 5736–5741.
- [129] O. Lupan, T. Pauporté, L. Chow, B. Viana, F. Pelle, L. K. Ono, B. R. Cuenya, H. Heinrich, Effects of annealing on properties of ZnO thin films prepared by 65 electrochemical deposition in chloride medium, *Appl. Surf. Sci.* 256 (2010) 1895–1807.
- [130] M. Li, J. Zhai, H. Liu, Y. Song, L. Jiang, D. Zhu. Electrochemical deposition of conductive superhydrophobic Zinc Oxide thin films, *J. Phys. Chem. B* 107 (2003) 9954–9957.
- [131] J. Cembrero, D. Busquets-Mataix, ZnO crystals obtained by electrodeposition: Statistical analysis of most important process variables, *Thin Solid Films* 517 (2009) 2859–2864.
- [132] T. Pauporté, G. Bataille, L. Joulaud, F. J. Vermersch, Well-aligned ZnO nanowire arrays prepared by seed-layer-free electrodeposition and their Cassie-Wenzel transition after hydrophobization, *J. Phys. Chem. C* 114 (2010) 194–202.
- [133] H. El Belghiti, T. Pauporté, D. Lincot, Mechanistic study of ZnO nanorod array electrodeposition, *Phys. Status Solidi A* 205 (2008) 2360–2364.
- [134] G. Jiang-Feng, D. Zhao-Ming, W. Zhi-Qiang, Z. Bo, Z. Wei-Hua, Z. Kai-Xiao, L. Ming-Yi, Z. Hao, Z. Jian-Feng, ZnO nanorod arrays with tunable size and field emission properties on an ITO substrate achieved by an electrodeposition method, *Chin. Phys. B* 21 (2012) 06810.
- [135] Y. Lin, J. Yang, X. Zhou, Controlled synthesis of oriented ZnO nanorod arrays by seed-layer-free electrochemical deposition, *Appl. Surf. Sci.* 258 (2011) 1491–1494.
- [136] S. Sun, S. Jiao, K. Zhang, D. Wang, S. Gao, H. Li, J. Wang, Q. Yu, F. Guo, L. Zhao, Nucleation effect and growth mechanism of ZnO nanostructures by electrodeposition from aqueous zinc nitrate baths, *J. Cryst. Growth* 359 (2012) 15–19.

- [137] M. Skompska, K. Zarebska, Electrodeposition of ZnO nanorod arrays on transparent conducting substrates, *Electrochim. Acta* 127 (2014) 467–488.
- [138] M. Guo, C. Yang, M. Zhang, Y. Zhang, T. Ma, X. Wang, X. Wang, Effects of preparing conditions on the electrodeposition of well-aligned ZnO nanorods arrays, *Electrochim. Acta* 53 (2008) 4633–4641.
- [139] A. Goux, T. Pauporté, J. Chivot, D. Lincot, Temperature effects on ZnO electrodeposition, *Electrochim. Acta* 50 (2005) 2239–2248.
- [140] L. Xu, Y. Guo, Q. Liao, J. Zhang, D. Xu, Morphological control of ZnO nanostructures by electrodeposition, *J. Phys. Chem. B* 109 (2005) 13519–13522.
- [141] H. Kim, J. Y. Moon, H. S. Lee, Temperature dependence of the growth of ZnO nanorod arrays by electrochemical deposition, *Electron. Mater. Lett.* 7 (2011) 59–62.
- [142] T. G. Kim, J.-T. Jang, H. Ryu, W.-J. Lee, Impact of first-step potential and time on the vertical growth of ZnO nanorods on ITO substrate by two-step electrochemical deposition, *J. Alloys Compd.* 579 (2013) 558–563.
- [143] T. Pauporté, R. Cortes, M. Froment, B. Beaumont, D. Lincot, Electrocrystallization of Epitaxial Zinc Oxide onto Gallium Nitride, *Chem. Mater.* 14 (2002) 4702–4708.
- [144] A. E. Rakhshani, Optical and electrical characterization of well-aligned ZnO rods electrodeposited on stainless steel foil, *Appl. Phys. A* 92 (2008) 303–308.
- [145] M. H. Wong, A. Berenov, X. Qi, M. J. Kappers, Z. H. Barber, B. Illy, Z. Lockman, M. P. Ryan, J. L. MacManus-Driscoll, Electrochemical growth of ZnO nano-rods on polycrystalline Zn foil, *Nanotechnology* 14 (2003) 968–973.
- [146] S. Peulon, D. Lincot, Cathodic Electrodeposition from Aqueous Solution of Dense or Open-Structured Zinc Oxide Films, *Adv. Mater.* 8 (1996) 166–170.
- [147] M. Izaki, T. Omi, Transparent zinc oxide films prepared by electrochemical reaction, *Appl. Phys. Lett.* 68 (1996) 2439.
- [148] B. Canava, D. Lincot, Nucleation effects on structural and optical properties of electrodeposited zinc oxide on tin oxide, *J. Appl. Electrochem.* 30 (2000) 711–716.
- [149] J. Cembrero, A. Elmanouni, B. Hartiti, M. Mollar, B. Mari, Nanocolumnar ZnO films for photovoltaic applications, *Thin Solid Films* 451–452 (2004) 198–202.
- [150] J. Elias, R. Tena-Zaera, C. Lévy-Clément, Electrodeposition of ZnO nanowires with controlled dimensions for photovoltaic applications: Role of buffer layer, *Thin Solid Films* 515 (2007) 8553–8557.
- [151] H. Kim, J. Young Moon, H. S. Lee, Growth of ZnO nanorods on various substrates by electrodeposition, *Electron. Mater. Lett.* 5 (2009) 135–138.
- [152] S. Sun, S. Jiao, K. Zhang, D. Wang, H. Li, S. Gao, J. Wang, Q. Yu, F. Guo, L. Zhao, S. Su, Morphology and properties of ZnO nanostructures by electrochemical deposition: effect of the substrate treatment, *J. Mater. Sci. – Mater. Electron.* 24 (2013) 85–88.
- [153] C.-T. Hsieh, S.-Y. Yang, J.-Y. Lin, Electrochemical deposition and superhydrophobic behavior of ZnO nanorod arrays, *Thin Solid Films* 518 (2010) 4884–4889.

- [154] M. Wang, C. Xing, K. Cao, L. Meng, Ji. Liu, Alignment-controlled hydrothermal growth of well-aligned ZnO nanorod arrays, *J. Phys. Chem. Solids* 75 (2014) 808–817.
- [155] L. E. Greene, M. Law, D. H. Tan, M. Montano, J. Goldberger, G. Somorjai, P. Yang, General Route to Vertical ZnO Nanowire Arrays Using Textured ZnO Seeds, *Nano Lett.* 5 (2005) 1231–1236.
- [156] Z. Liu, J. Ya, L. E, Effects of substrates and seed layers on solution growing ZnO nanorods, *J. Solid State Electrochem.* 14 (2010) 957–963.
- [157] J. Elias, R. Tena-Zaera, C. Lévy-Clément, Effect of the Chemical Nature of the Anions on the Electrodeposition of ZnO Nanowire Arrays, *J. Phys. Chem. C* 112 (2008) 5736–5741.
- [158] M. R. Khajavi, D. J. Blackwood, G. Cabanero, R. Tena-Zaera, New insight into growth mechanism of ZnO nanowires electrodeposited from nitrate-based solutions, *Electrochim. Acta* 69 (2012) 181–189.
- [159] Z. Liu, L. E, J. Ya, Y. Xin, Growth of ZnO nanorods by aqueous solution method with electrodeposited ZnO seed layers, *Appl. Surf. Sci.* 255 (2009) 6415–6420.
- [160] N. Orhan, M. C. Baykul, Characterization of size-controlled ZnO nanorods produced by electrochemical deposition technique, *Solid-State Electron.* 78 (2012) 147–150.
- [161] J. Elias, R. Tena-Zaera, G.-Y. Wang, C. Lévy-Clément, Conversion of ZnO Nanowires into Nanotubes with Tailored Dimensions, *Chem. Mater.* 20 (2008) 6633–6637.
- [162] H. K. Lee, M. S. Kim, J. S. Yu, Effect of AZO seed layer on electrochemical growth and optical properties of ZnO nanorod arrays on ITO glass, *Nanotechnology* 22 (2011) 445602.
- [163] S. Peulon, D. Lincot, Mechanistic study of cathodic electrodeposition of Zinc Oxide and Zinc Hydroxychloride films from oxygenated aqueous Zinc Chloride solutions, *J. Electrochem. Soc.* 145 (1998) 864–874.
- [164] F. Xu, Y. Lu, L. Xia, Y. Xie, M. Dai, Y. Liu, Seed layer-free electrodeposition of well-aligned ZnO submicron rod arrays via a simple aqueous electrolyte, *Mater. Res. Bull.* 44 (2009) 1700–1708.
- [165] C. Badre, T. Pauporté, M. Turmine, P. Dubot, D. Lincot, Water-repellent ZnO nanowires films obtained by octadecylsilane self-assembled monolayers, *Physica E* 40 (2008) 2454–2456.
- [166] C. Badre, P. Dubot, D. Lincot, T. Pauporté, M. Turmine, Effects of nanorod structure and conformation of fatty acid self-assembled layers on superhydrophobicity of zinc oxide surface, *J. Colloid Interface Sci.* 316 (2007) 233–237.
- [167] C. Badre, T. Pauporté, M. Turmine, D. Lincot, A ZnO nanowire array film with stable highly water-repellent properties, *Nanotechnology* 18 (2007) 365705.
- [168] G. He, K. Wang, The super hydrophobicity of ZnO nanorods fabricated by electrochemical deposition method, *Appl. Surf. Sci.* 257 (2011) 6590–6594.
- [169] J. Steinhäuser, Low pressure chemical vapor deposited zinc oxide for silicon thin film solar cells (2009) 1–162.

- [170] J. Rodríguez, D. Onna, L. Sánchez, M. C. Marchi, R. Candal, S. Ponce, S. A. Bilmes, The role of seeding in the morphology and wettability of ZnO nanorods films on different substrates, *Appl. Surf. Sci.* 279 (2013) 197–203.
- [171] H. Luo, J. Ma, P. Wang, J. Bai, G. Jing, Two-step wetting transition on ZnO rods arrays, *Appl. Surf. Sci.* 347 (2015) 868–874.
- [172] C. Mondal, M. Ganguly, A. K. Sinha, J. Pal, T. Pal, Fabrication of a ZnO nanocolumnar thin film on a glass slide and its reversible switching from a superhydrophobic to a superhydrophilic state, *RSC Adv.* 3 (2013) 5937–5944.
- [173] D. Pradhan, K.T. Leung, Vertical growth of two-dimensional zinc oxide nanostructures on ITO-coated glass: effects of deposition temperature and deposition time, *J. Phys. Chem. C* 112 (2008) 1357–1364.
- [174] E. McCafferty, J. P. Wightman, Determination of the concentration of surfacehydroxyl groups on metal oxide films by a quantitative XPS method, *Surf. Interface Anal.* 26 (1998) 549–564.
- [175] L. Grzadziel, M. Krzywiecki, Ambience-related adsorbates on CuPc surface—photoemission and thermal desorption spectroscopy studies for control of organic electronics degradation processes, *Synth. Met.* 210 (2015) 141–147.
- [176] E. De la Rosa, S. Sepúlveda-Guzman, B. Reeja-Jayan, A. Torres, P. Salas, N. Elizondo, M. Jose Yacaman, Controlling the growth and luminescenceproperties of well-Faceted ZnO nanorods, *J. Phys. Chem. C* 111 (2007) 8489–8495.
- [177] H. Hu, H.-F. Ji, Y. Sun, The effect of oxygen vacancies on water wettability of a ZnO surface, *Phys. Chem. Chem. Phys.* 15 (2013) 16557–16565.
- [178] N. Sakai, A. Fujishima, T. Watanabe, K. Hashimoto, Quantitative evaluation of the photoinduced hydrophilic conversion properties of TiO₂ thin film surfaces by the reciprocal of contact angle, *J. Phys. Chem. B* 107 (2003) 1028–1035.
- [179] Y. Liu, W. Chen, S. Wei, W. Gao, TiO₂/ZnO nanocomposite, ZnO/ZnO bi-level nanostructure and ZnO rod arrays: microstructure and time-affected wettability change in ambient conditions, *RSC Adv.* 4 (2014) 30658–30665.
- [180] Z. Li, Y. Wang, A. Kozbial, G. Shenoy, F. Zhou, R. McGinley, P. Ireland, B. Morganstein, A. Kunkel, S. P. Surwade, L. Li, H. Liu, Effect of airborne contaminants on the wettability of supported graphene and graphite, *Nat. Mater.* 12 (2013) 925–931.
- [181] C. P. Marshall, A. O. Marshall, The potential of Raman spectroscopy for the analysis of diagenetically transformed carotenoids, *Philos. Trans. R. Soc. A* 368 (2010) 3137–3144.

Acknowledgements

I would like to express my sincerest gratitude to my supervisors Dr. Tatjana Dedova, Prof. Malle Krunks and Dr. Ilona Oja Acik for their guidance, support and motivation throughout the years of my doctoral study.

I am very thankful to the co-authors and colleagues at the Department of Materials and Environmental Technology. I want to sincerely thank Dr. Deniss Klauson for the assistance with the photocatalytic characterisation of the layers, Dr. Valdek Mikli for the SEM and AFM measurements, Dr. Olga Volobujeva for SEM measurements and Dr. Mati Danilson for XPS measurements.

I am also sincerely grateful to the members of Laboratory of Thin Film Chemical Technologies for helpful discussions and continuous support.

I would like to acknowledge Estonian Ministry of Education and Research under the project IUT 19-4, TUT base financing project B24, European Regional Development Fund through the projects TK114 (Centre of Excellence: “Mesosystems: Theory and Applications”), TK141 (Centre of Excellence: “Advanced materials and high-technology devices for sustainable energetics, sensorics and nanoelectronics”), AR12118 (Efficient plasmonic absorbers for solar cells), Archimedes Foundation (Kristjan Jaak scholarship), European Regional Development Fund (Dora plus program), and ASTRA “TUT Institutional Development Programme for 2016-2022” Graduate School of Functional Materials and Technologies (2014-2020.4.01.16-0032).

My warmest thanks to my family and friends for their encouragement and support.

Abstract

ZnO nanostructured layers by wet chemical methods: growth, surface properties, photocatalytic capability

The interest in the synthesis of low-dimensional nanostructured ZnO materials raised by their successful application in optoelectronic devices such as solar cells, optical sensors, gas sensors, and light emitters. During the last few decades, ZnO has emerged as an outstanding material for environmental applications as a photocatalyst material applicable for water treatment from organic pollutants. For that reason, the development of strategies to synthesize ZnO nanostructured layers with tailored geometries and suitable surface properties by low-cost deposition methods like spray pyrolysis (SP) or electrodeposition (ED) has emerged as a challenge. To our best knowledge, studies on the photocatalytic properties of ZnO rods obtained by both ED and SP methods are very scarce, and the influence of the surface properties of these samples on photocatalytic activity has not been studied so far.

The aim of this thesis was to study the influence of the substrate and seed layer properties on the morphology of ZnO crystals deposited by SP and ED methods and evaluate the photocatalytic activity of the SP and ED ZnO nanostructured layers in terms of different morphological and surface chemical properties.

The thesis is based on four publications and comprises literature overview, experimental, and results and discussions sections. The literature overview includes chapters describing wet chemical methods, with an emphasis on SP and ED, scientific papers overview on the properties and other studies of SP and ED ZnO nanostructured layers, and widely used applications of the ZnO layers, with an accent towards photocatalysis. The experimental section presents the details of the experimental process and characterisation methods. The last chapter is divided into three sections that contain the experimental results, discussion, and conclusions based on the main results.

The first section is divided into two subsections. The first subsection introduces the deposition of ZnO rod-shaped crystals by SP on commercial FTO/glass ($\text{SnO}_2:\text{F}$) substrates with different FTO layer morphologies. The relationship between the FTO layer morphological properties and ZnO rod formation is investigated. Samples were characterized using SEM, AFM, and XRD methods. It was found that the ZnO crystal shape and dimensions depend on the surface roughness and grain size values of the substrates. It has been shown that FTO/glass, with RMS values for FTO in the range 7 – 9 nm and grain sizes in the range 30 – 50 nm, yielded elongated hexagonal ZnO rod-like crystals ($L \sim 800 - 1400$ nm, $D \sim 250 - 300$ nm). The FTO/glass substrates with a FTO layer of higher roughness (≥ 12 nm) and grain size (≥ 80 nm) are not suitable for the growth of elongated ZnO rod-like crystals.

The second subsection presents a study on the deposition of ZnO rod-shaped layers by the ED method on various sprayed seed layers (TiO_2 , ZnO, ZnO:In) and focuses on the investigation of the relationship between the seed layer properties and ZnO crystal morphologies. The samples were characterized by means of SEM and XRD methods. The influence of the morphology and conductivity of the seed layers on the dimensions of the ZnO rod-shaped crystals obtained by ED was established. Hexagonal ZnO crystals were obtained on the TiO_2 and ZnO:In seed layers with relatively smooth morphologies. Undoped ZnO underlays with surfaces composed of grains with different sizes and shapes induce the growth of short ($D \sim 150 - 300$ nm, $L \sim 150$ nm) and compactly standing ZnO

crystals. An electrically more conductive layer such as ITO or ZnO:In induces the growth of ZnO rods with larger dimensions ($D \sim 200$ nm, $L \sim 700$ nm), compared to the less conductive seed layers like TiO_2 , where the ZnO rods obtained were smaller ($D \sim 60$ nm, $L \sim 350$ nm).

The second section is dedicated to the evaluation of the photocatalytic activity of sprayed ZnO nanostructured layers with different morphologies (nanoneedles, rods, pyramids, and hierarchical structures) and a comparison of the photocatalytic activity of ZnO with that of the commercial catalyst P25 TiO_2 . To evaluate the photocatalytic activity, the ZnO nanostructured layers were investigated through the photocatalytic oxidation of methyl-tert-butyl ether (MTBE), humic acid (HA), N, N-dimethyl p-nitrosoaniline (RNO), and prednisolone (PNL). Independent of the morphology, the sprayed ZnO nanostructured layers were effective for the photocatalytic oxidation of the MTBE pollutant. The highest photocatalytic oxidation efficiency of MTBE was achieved by hierarchical pyramid-shaped SP ZnO nanostructures ($518 \text{ mg O}_2 \text{ W}^{-1} \text{ h}^{-1}$ after 2 h), indicating that a ZnO structure with increased surface area is beneficial for the degradation of such types of pollutants. The highest photocatalytic oxidation efficiency of the RNO pollutant was achieved after 6 h by the ZnO rod layer sample ($44.7 \text{ mgW}^{-1} \text{ h}^{-1}$). SP ZnO nanostructures were not efficient in degrading the HA and PLN pollutants.

The last section presents a comparative study on the surface properties of ZnO rod layers obtained by SP at 550°C , and ED at 80°C . In order to exclude the influence of surface area on photocatalytic performance, ZnO rod layers with similar morphologies and surface areas were deposited by both the methods. The samples were studied using XPS, SEM, XRD, Raman, and water contact angle (CA) measurements, and the photocatalytic oxidation of doxycycline. It was found that different chemical compositions of the surfaces (amount of hydroxyl, carbon-containing groups, oxygen vacancies) of the as-deposited, two-month-stored, and heat-treated SP and ED ZnO rods determine their wettability and photocatalytic properties.

The as-ED ZnO rod layers showed the highest relative amount of hydroxyl groups on their surface ($[\text{OH}]/[\text{Zn-O}] \sim 1.2 \text{ at.}/\text{at.}\%$), and consequently, the highest photocatalytic activity among the studied samples: 85 % of the initial amount of doxycycline degraded after 4 h. A high amount of hydroxyl groups on the surface of the as-deposited ED ZnO rod layers also makes it highly hydrophilic ($\text{CA} \sim 3^\circ$). The impact of hydroxyl groups on two-month-stored ZnO rod layers is completely shaded by the increased amount of carbon-containing groups. As a result, CA increases (SP rods $\text{CA} \sim 50^\circ$, ED rods $\text{CA} \sim 120^\circ$) and the photocatalytic efficiency drops from 48 % to 30 % (after 4 h) for the SP rods, and from 85 % to 30 % (after 4 h) for the ED rods. The amount of carbon-containing groups on the surface of two-month-stored ED rod layers is six times higher compared to that on aged SP rods. The heat-treatment of the ZnO rod layers at 400°C during 30 min restores their initial wettability (SP rods $\text{CA} \sim 9^\circ$, ED rods $\text{CA} \sim 3^\circ$), however, the photocatalytic activity of the heat-treated ED rod layers shows only a moderate improvement (45 %/4 h) compared to that of the aged ED ZnO rod layers (30 %/4 h), not reaching the initial efficiency of the as-deposited ED ZnO samples (85%/4 h). The photocatalytic activity of the SP heat-treated ZnO rod layers was improved (60 %/4 h) compared to the photocatalytic performance of the aged SP rods (30 %/4 h) or as-deposited SP rods (48 %/4 h).

The results presented in this thesis are of practical importance in synthesizing rod-like ZnO nanostructures by low-cost methods such as SP and ED. The obtained ZnO nanostructured layers have the photocatalytic capability to degrade various water

pollutants as efficiently as, or more efficiently than the commercial P25 TiO₂ slurry, eliminating the problem of separation and recovery of the powder photocatalyst after treatment. The efficiency of photocatalytic activity, however, depends on the surface chemical composition, which is different for the SP and ED rods, and also depend on the sample freshness or treatment conditions.

Lühikokkuvõte

ZnO nanostruktuursed kihid vedeliksadestuse meetoditel: kasvatamine, pinnaomadused, fotokatalüütiline võimekus

ZnO nanostruktuurseid materjale on edukalt rakendatud optoelektronika seadistes, nagu päikesepatareid, optilised- ja gaasandureid, valgusdioode jne. Viimastel aastakümnetel on hakatud ZnO kasutama ka keskkonnakaitselistes rakendustes, sh fotokatalüütilise materjalina vee puhastamiseks orgaanilistest saasteainetest. Kontrollitud geomeetria ja pinnaomadustega ZnO nanostruktuursete kihtide sünteesi areng odavate sadestamismeetoditega nagu pihustuspürolüüs (SP) või elektrokeemiline sadestamine (ED) on praeguseks sihipõhine strateegia. ED ja SP-meetodil sadestatud ZnO nanovarrastest koosnevate kihtide fotokatalüütilisi omadusi on väga vähe uuritud, puuduvad ka uuringuid kihtide pinnaomaduste mõjust fotokatalüütilisele võimekusele.

Antud töö eesmärkideks oli uurida aluste ja aluskihtide omaduste mõju SP ja ED meetoditel sadestatud ZnO kristallide morfoloogiale ning hinnata nende nanostruktuursete kihtide fotokatalüütilist võimekust sõltuvalt kihtide morfoloogiast ja pinna keemilistest omadustest.

Dokoritöö põhineb neljal publitseeritud teadusartiklil ja koosneb kirjandusülevaadest, eksperimentaalsest osast, tulemustest ning arutelust. Kirjanduse ülevaates kirjeldatakse keemilisi vedeliksadestusmeetodeid, põhirõhk on pihustuspürolüüsil ja elektrokeemilisel sadestamisel. Antakse ülevaade SP ja ED meetoditel kasvatatud ZnO nanostruktuursete kihtide omadustest ja uuringutest, ZnO kihtide kasutusalaadest, rõhutades fotokatalüüsi omadusi. Eksperimentaalses osas on esitatud eksperimentaalsed andmed ja karakteriseerimismeetodid. Viimane peatükk on jaotatud kolme ossa ja sisaldab peamisi eksperimentaalseid tulemusi ja arutelu.

Esimene osa jaguneb kaheks alapeatükiks. Esimeses alapeatükis käsitletakse ZnO vardakujuliste kristallide kasvatamist SP meetodil FTO-ga ($\text{SnO}_2\text{:F}$) kaetud klaasalustele. Uuritakse FTO kihi morfoloogia mõju ZnO varraste kujunemisele. Kihte iseloomustati SEM, AFM ja XRD meetoditega. Leiti, et ZnO kristallide kuju ja mõõtmed sõltuvad aluspinna karedusest ja terade suurusest. Leiti, et FTO mille RMS väärtused on vahemikus 7 – 9 nm ja tera suurused vahemikus 30-50 nm lubavad kasvatada kuusnurkse kujuga ZnO piklikke kristallid ($L \sim 800 - 1\,400$ nm, $D \sim 250 - 300$ nm). FTO/klaas alused FTO kihi kõrgema karedusega (≥ 12 nm) ja tera suurusega (≥ 80 nm) ei sobi piklikke ZnO-vardakujuliste kristallide kasvatamiseks.

Teises alapeatükis esitatakse uuringu tulemused ED-meetodil ZnO nanovarrastest koosnevate kihtide kasvatamise kohta erinevatele aluskihtidele (TiO_2 , ZnO, ZnO:In). Siin rõhutatakse aluskihi omaduste ja ZnO kristallide morfoloogia seost. Kihte iseloomustati SEM ja XRD meetoditega. Leiti, et aluskihi morfoloogia ja juhtivus mõjutavad ZnO vardakujuliste kristallide mõõtmeid. Suhteliselt sileda morfoloogiaga TiO_2 ja ZnO:In aluskihtide peal kasvasid piklikud vardakujulised ZnO kristallid, kuid ZnO aluskihi peale, mis koosneb erineva suuruste ja kujuga teradest, kasvasid lühikesed ($D \sim 150 - 300$ nm, $L \sim 150$ nm) ZnO kristallid. Elektriliselt juhtivad kihid nagu ITO ($\text{In}_2\text{O}_3\text{:Sn}$) ja ZnO:In võimaldavad kasvatada suuremaid ZnO kristalle ($D \sim 200$ nm, $L \sim 700$ nm) kui väiksema elektrijuhtivusega TiO_2 aluskiht, kus saadud ZnO vardad olid peenemad ja lühemad ($D \sim 60$ nm, $L \sim 350$ nm).

Teine osa on pühendatud erinevate morfoloogiatega (nanonõeldad, vardad, püramiidid ja hierarhilised struktuurid) pihustussadestatud ZnO nanostruktuursete

kihtide fotokatalüütilise võimekuse hindamisele ning võimekuse võrdlusele kaubandusliku fotokatalüsaatoriga P25 TiO₂. Fotokatalüütilise võimekuse hindamiseks mõõdeti ZnO nanostruktuursete kihtide võimekust lagundada vees lahustunud metüül-tert-butüületrit (MTBE), huumushape (HA), N, N-dimetüül-p-nitrosoaniliini (RNO) ja prednisolooni (PNL). Sõltumata morfoloogiast olid SP ZnO nanostruktuursete kihid efektiivsed lagundama MTBE-d, kusjuures kõrgeim fotokatalüütilise oksüdatsiooni efektiivsus (518 mg O₂ W⁻¹ h⁻¹ pärast 2 tundi) saavutati SP ZnO nanostruktuuride puhul, mis koosnesid hierarhilise püramiidi kujulistest kristallidest. RNO lagundamisel saavutati kõrgeim fotokatalüütilise oksüdatsiooni efektiivsus 6 tunni pärast (44,7 mgW⁻¹ h⁻¹) ZnO kihtide puhul, mis koosnesid vardakujulistest kristallidest.

Doktoritöö kolmandas osas esitatakse võrdlusuuring SP ja ED meetoditel kasvatatud ZnO nanovarrastest koosnevate kihtide pinnaomaduste kohta. Vardad saadi SP meetodil 550 °C juures, ja ED sadestamisel 80 °C juures. Selleks, et välistada pindala mõju kasvatati mõlema meetodiga sarnase morfoloogiaga ja pindalaga ZnO-varrastest koosnevad kihid. Kihte uuriti XPS, SEM, XRD, Ramani ja vee kontaktnurga (CA) mõõtmiste ja doksütsükliini fotokatalüütilise oksüdatsiooni abil. Leiti, et pindade keemiline koostis (hüdroksüülrühma ja süsinikku sisaldavate rühmade hulk, hapniku vakantsid) äsjasadestatud kihtidele ning kahe kuu vanustele ning kuumutatud kihtidele määrab SP ja ED ZnO kihtide märgumise ja fotokatalüütilise võimekuse).

Äsjasadestatud ED ZnO vardakihtid näitasid pinnal kõrgeimat hüdroksüülrühmade suhtelist kogust ([OH]/[Zn-O] ~ 1.2 at.%/at.%) ja tulemusena ka suurimat fotokatalüütilise lagundamise efektiivsust uuritud proovide hulgast: 85 % doksütsükliini esialgsest kogusest lagunes 4 tunni jooksul. Kõrge hüdroksüülrühmade sisaldus värskest sadestatud ED ZnO pinnakihtis muudab selle pinna superhüdrofiilseks (CA ~ 3 °). Vananenud objektide pinna peal leiti suures koguses süsinikku sisaldavaid rühmi ning seetõttu hüdroksüülrühmade mõju vähenes. Selle tulemusena kasvasid ka CA väärtused (SP varraste CA ~ 50 °, ED varraste CA ~ 120 °) ja fotokatalüütiline võimekus vähenes SP-varrastel 48 %-st 30 %-ni (pärast 4 tundi) ja ED-varrastel 85 %-st 30 %-ni (pärast 4 tundi). Süsinikku sisaldavate rühmade kogus kaks kuud vanade ED varraste pinnal on kuus korda suurem võrreldes vananenud SP varrastega. ZnO kihtide järelkuumutamine temperatuuril 400 °C 30 minuti jooksul taastab ZnO kihtidel esialgse märguvuse taseme (SP kihid: CA ~ 9 °, ED kihid: CA ~ 3°), kuid see ei kajastu fotokatalüütilise võimekuse tesemes. Näiteks, järelkuumutatud ED varraste kihtide fotokatalüütiline võimekus näitab vaid osalist paranemist (45 %/4 h), võrreldes vananenud ED ZnO kihtidega (30 %/4 h), ning ei taasta oma esialgset värske kihi võimekust (85 %/4 h). SP ZnO järelkuumutatud vardakihtide fotokatalüütiline võimekus paranes (60 %/4 h) võrreldes vananenud SP varrastega (30 %/4 h).

Doktoritöös esitatud tulemused omavad praktilist tähtsust uut tüüpi fotokatalüütiliste katete valmistamisel odavate meetoditega nagu SP ja ED. Saadud ZnO kihid omavad fotokatalüütilist võimekust lagundada erinevaid saasteaineid vees sama hästi või paremini kui klassikaline TiO₂ nanopulbriline fotokatalüsaator. Tänu sellele, et ZnO nanostruktuurid on kasvatatud alusele on nad immobiilsed ja ei kujuta ohtu keskkonnale.

Appendix 1

Publication I

T. Dedova, O. Volobujeva, M. Krunks, V. Mikli, **I. Gromyko**, A. Katerski, A. Mere. Growth of ZnO rods on FTO electrodes by spray pyrolysis. *IOP Conf. Ser.: Mater. Sci. Eng.* 49 (2013) 012001.

Growth of ZnO rods on FTO electrodes by spray pyrolysis

Tatjana Dedova¹, Olga Volobujeva¹, Malle Krunks¹, Valdek Mikli², Inga Gromyko¹, Atanas Katerski¹, Arvo Mere¹

¹Department of Materials Science, Tallinn University of Technology, Estonia,

²Centre for Materials Research, Tallinn University of Technology, Estonia

E-mail: tatjana.dedova@ttu.ee

Abstract. ZnO layers comprising rods were deposited by chemical spray pyrolysis (CSP) method at 520 °C on different FTO (SnO₂:F)/glass substrates using zinc chloride aqueous solutions. Substrates were purchased from different manufactures and differ by morphology, grain size and roughness of FTO electrode. FTO/glass substrates and ZnO layers grown on them were characterised with the help of XRD, AFM, high resolution SEM, EDX methods. The relationship between nanorod formation and substrate properties was studied. It was found that substrate roughness and grain size influence the ZnO rods formation. Deposition of rods (d=300 nm, L=1.4 µm) was successful on the FTO layers with grain sizes around 30-50 nm and roughness below 10 nm, whereas large-grained FTO (grain size > 130 nm) resulted in thick, low-aspect ratio crystals with diameter around 400 nm and length of about 400 nm.

Keywords: FTO, substrate, morphology, ZnO rod, spray pyrolysis, nanostructured layers, haze factor,

1. Introduction

ZnO nanostructured layers have been the research focus in recent years because of their potential applications in various nanodevices [1-5]. Key challenges in ZnO nanorod growth for device application are controlled growth using simple and inexpensive growth methods. ZnO nanorods can be produced by diverse methods, as summarized in numerous review articles [1, 2]. Among them, spray pyrolysis, presented in this study, is simple and low-cost method to produce large area thin films and nanostructured layers including ZnO nanorods [6-8].

Particular significance in nanorods growth has a substrate and its preparation. In many studies to contribute the rods growth or improve their vertical alignment a seed layer (ZnO nanoparticles) is required prior to the deposition of the ZnO nanorods [1, 9, 10]. However, for some applications (emitting diodes, solar cells), it is required to grow ZnO nanorod directly on a transparent conductive oxide [11, 12]. There are some reports on the direct deposition of ZnO rods onto Indium Tin Oxide (ITO) substrates [11, 13, 14]. However, due to the scarcity of indium search for alternative transparent conductive oxide (TCO) materials has been a topic of an active research. Such a good alternative could be fluorine-doped tin dioxide FTO, however, very little studies were reported on growth of ZnO rods on FTO substrates up to now [12, 15-17]. As FTO might have different morphologies depending on the manufacturer and preparation method, therefore it is important to find out a correlation between initial morphology of the substrate and final morphology of the grown layers.



In this study, we present a systematic study on ZnO rods on FTO substrates with different morphology. The morphology, structural and optical properties of the substrates are studied by means of high resolution SEM, AFM and UV-VIS techniques.

2. Experimental

ZnO layers were deposited using pneumatic spray pyrolysis method, described in details earlier [6, 7, 13, 16, 18]. To grow ZnO layers, 50 ml of 0.05 mol/l aqueous solution of ZnCl₂ (Fluka) (pH=5) was sprayed over the FTO (SnO₂:F) substrate surface at T_{sub}=520 °C. The solution spraying rate and carrier gas (compressed air) flow rate were 2.4 ml/min and 8 l/min, respectively. The variety of FTO substrates (further referred in a text as FTO-1, FTO-2, FTO-3, FTO-4, FTO-5) purchased from different manufactures was used in this study. All substrates undergone standard cleaning procedure: firstly in soap solution, then in isopropyl alcohol cleaning in ultrasonic bath for 1 minute and finally, treatment during 1 minute in concentrated H₂SO₄ (T_{ca} ~40 °C). The samples were rinsed with deionised water after each cleaning step.

The morphology of the FTO substrates and ZnO layers were studied by a high resolution SEM on a Zeiss HR FESEM Ultra 55 apparatus at an accelerating voltage of 1.7 kV. Structural characterization of the FTO substrates was carried out on a Rigaku Ultima IV diffractometer using Cu K α radiation ($\lambda=1.5406\text{\AA}$, 40 kV at 40 mA). Surface topographies of the FTO substrates were studied by AFM using the NT-DT Solver47 Prosystem operated in a "semi-contact" (tapping) mode. The root mean square (RMS) and average roughness (Sa) values were taken on AFM from area of $2\times 2\mu\text{m}^2$. The diffuse (T_{diff.}) and total (T_{tot.}) transmittance spectra were measured in the wavelength range of 200–2500 nm on a Jasco 670-V UV-VIS-NIR spectrophotometer equipped with an integrating sphere. Haze factor (HF) values were determined as $HF=T_{diff}/T_{tot}$.

3. Results and discussion

Figure 1 presents SEM and AFM images of FTO surface and of corresponding ZnO layers grown on them at similar growth conditions. The morphological parameters obtained from SEM and AFM studies for FTO and dimensions of ZnO crystals are summarized in Table 1.

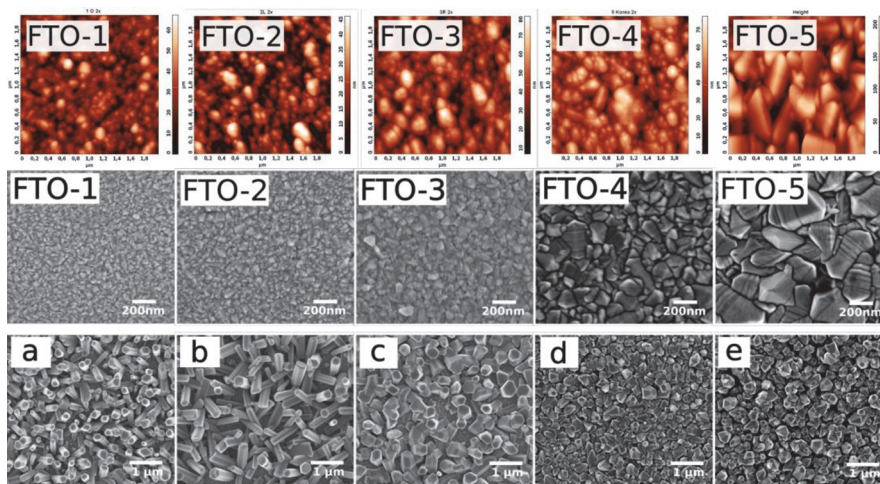


Figure 1. Influence of FTO substrate morphology on the formation of ZnO rods grown by spray pyrolysis. Upper row: AFM images of the substrates FTO-1 up to FTO-5; middle row: SEM images of the same substrates; bottom row: SEM images of ZnO rods grown on these substrates (a, b, c, d, e correspond to FTO-1, 2, 3, 4 and 5, respectively).

As it can be seen from Fig.1 and Table 1, the substrates mainly differ by grain and crystallite size, roughness and grain shape. Elongated ZnO rods ($L=800-1400$ nm) were formed only on FTO -1 and 2 which have low roughness ($RMS=7-9$ nm) and smaller grains (ca. 30-50 nm). The FTOs with higher roughness ≥ 12 nm (FTO-3, 4 and 5) resulted in low aspect ratio ca. 1, fat ZnO crystals. FTO-5 and 6 differ from others by large and pyramidal shaped grains. It should be mentioned here, that ZnO crystals on FTO-4 and 5 are tightly standing next to each other. This could be explained by high number of nucleation centres on FTO-5 and 6 substrates. The step-like texture of FTO facets (clearly seen on SEM of FTO-5) might be a good platform for preferable sites for ZnO nucleation. High amount of ZnO nuclei lead to further coalescence of the crystals and formation of closely standing to each other thick low-aspect ratio rods.

Table 1. Root mean square roughness (RMS), average roughness (Sa), average grain and crystallite size of FTO substrates and dimensions of ZnO crystals grown on them.

FTO No.	Properties of FTO substrates				Dimensions of ZnO crystals		
	RMS, nm (AFM)	Sa, nm (AFM)	Average grain size, nm (SEM)	Crystallite size, nm (XRD)	L, nm	D, nm	Aspect Ratio, L/D
FTO-1	7	6	30	12	800	250	3
FTO-2	9	7	50	13	1400	300	4.5
FTO-3	12	10	80	15	600	500	1
FTO-4	15	12	130	17	300	200	1
FTO-5	36	30	250	40	300	300	1

Haze factor values presented in Figure 2 are in a good correspondence with AFM and SEM studies. The rougher FTO substrate is, the higher is light scattering and haze factor in the visible spectral region. Thus, haze factor measurements might be a handy and fast tool to estimate the surface roughness of the substrate and its suitability for growth of the ZnO rods. According to EDS study, the elemental composition of the FTO substrates (not presented here) is similar and, therefore impurity coming out from the substrate does not affect the rods formation in our case. According to the XRD patterns presented in Fig. 3, SnO_2 crystallites in FTO-5 are orientated along (110) plane parallel to the substrate, while in FTO-1 – FTO-4 the crystallites are preferably grown along (200) plane parallel to the substrate. Thus, the orientation of the crystallites in the substrate doesn't have strong influence on the formation of the rods. Thus, the main factor influencing the ZnO rods formation in our case is FTO roughness. Obtained result is in a good correlation with that reported for ZnO rods growth on GaN substrate by MOCVD [19] and ZnO seed layers by solution growth [20], where ZnO rod growth was favoured using relatively smooth substrates.

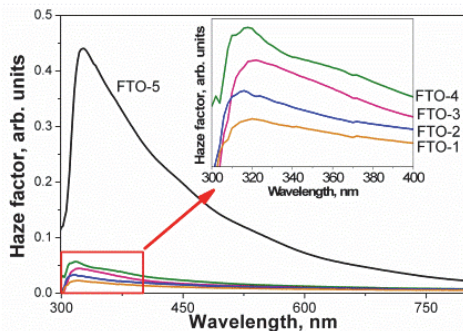


Figure 2. Haze factor spectra of FTO substrates.

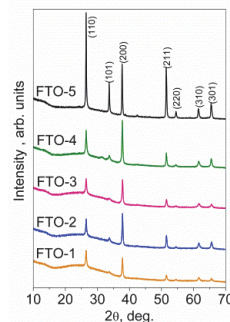


Figure 3. XRD patterns of FTO substrates.

4. Conclusions.

Herein we present a systematic study on ZnO rods growth by spray pyrolysis depending on the FTO substrates morphology. Depending on the manufacture, FTO surface morphology differs by roughness, grain size and shape, and crystallite orientation. Haze factor calculated from optical transmittance spectra measurements is a handy and fast tool for rough estimation of the surface roughness of the substrate and its suitability for growth of the ZnO rods. It was shown that rods formation is strongly affected by roughness and grain sizes of the FTO substrates. It was found that elongated ZnO rods (L=1400 nm, d=300 nm) can be produced on FTO with small roughness (ca. 8 nm) and grain sizes ca. 30-50 nm. FTO RMS roughness values higher than 12 resulted in thick ZnO crystals with low aspect ratio.

Acknowledgement.

This work is financially supported by the Estonian Ministry of Education and Research (SF0140092s08 and IUT19-4), Estonian Science Foundation (ETF8509) and European Regional Development Fund (Centre of Excellence "Mesosystems: Theory and Applications" TK114, 3.2.0101.11-0029 and project "Efficient plasmonic absorbers for solar cells" 3.2.1101.12-0023).

References:

- [1] Yi G-C, Wang C, Park W I 2005 *Semicond. Sci. Technol.* **20** 22
- [2] Weintraub B, Zhou Z, Li Y, Deng Y 2010 *Nanoscale* **2** 1573
- [3] Yin Z, Wu S, Zhou X, Huang X, Zhang Q, Boey F, Zhang H 2010 *Small* **6** 307
- [4] Acik Oja I, Katerski A, Mere A, Aarik J, Aidla A, Dedova T, Krunks M 2009 *Thin Solid Films* **517** 2443
- [5] Belaidi A, Dittrich Th, Kieven D, Tornow J, Schwarzburg K, Kunst M, Allsop N, Lux-Steiner M-Ch, Gavrilov S 2009 *Sol. Energy Mater. Sol. Cells* **93** 1033
- [6] Dedova T, Krunks M, Volobujeva O, Oja I 2005 *Phys. Status Solidi C* **2** 1161
- [7] Dedova T, Klauson J, Badre C, Pauporté Th, Nisumaa R, Mere A, Volobujeva O, Krunks M 2008 *Phys. Status Solidi A* **205** 2355
- [8] Dedova T, Krunks M, Oja Acik I, Klauson D, Volobujeva O and Mere A 2013 *Mater. Chem. Phys.* **141** 69
- [9] Kim D C, Hyun Kong B, Cho H K 2008 *J. Mater. Sci.–Mater. Electron.* **19** 760
- [10] Yin Y T, Que W X, Kam C H 2010 *J. Sol–gel Sci. Technol.* **53** 605
- [11] Lee H K, Kim M S, Yu J S 2011 *Nanotechnology* **22** 445602
- [12] Masuda Y, Kato K 2009 *Cryst. Growth Des.* **9** 3083
- [13] Dedova T, Krunks M, Grossberg M, Volobujeva O, Oja Acik I 2007 *Superlattice Microstr.* **42** 444
- [14] Krunks M, Dedova T, Kärber E, Mikli V, Oja Acik I, Grossberg M, Mere A 2009 *Phys. B Condens. Matter* **404** 4422
- [15] Pauporté Th, Bataille G, Joulaud L, Vermersch F J 2010 *J. Phys. Chem. C* **114** 194
- [16] Dedova T, Volobujeva O, Klauson J, Mere A, Krunks M 2007 *Nanoscale Res. Lett.* **2** 391
- [17] Lee J H 2010 *Adv. Mat. Res.* **123-125** 715
- [18] Dedova T, Oja Acik I, Krunks M, Mikli V, Volobujeva O, Mere A 2012 *Thin Solid Films* **520** 4650
- [19] Park S-H, Seo S-Y, Kim S-H, Han S-W 2006 *Appl. Phys. Lett.* **88** 251903
- [20] Lee Y-J, Sounart T L, Scrymgeour D A, Voigt J A, Hsu J W P 2007 *J. Cryst. Growth* **304** 80

Publication II

I. Gromyko, T. Dedova, M. Krunk, V. Syritski, A. Mere, V. Mikli, T. Unt, I. Oja Acik. ZnO nanorods grown electrochemically on different metal oxide underlays. *IOP Conf. Ser.: Mater. Sci. Eng.* 77 (2015) 012012.

ZnO Nanorods Grown Electrochemically on Different Metal Oxide Underlays

I Gromyko, T Dedova, M Krunks, V Syritski, A Mere, V Mikli, T Unt and I Oja Acik

Department of Material Science, Tallinn University of Technology, Ehitajate tee 5, 19086 Tallinn, Estonia

E-mail: inga.gromyko@gmail.com

Abstract. In this study we present results on electrochemically grown ZnO nanorods on different metal oxide underlays, such as ZnO seed layers with different morphologies, ZnS and TiO₂ compact thin films produced by spray pyrolysis on transparent conductive oxide (TCO) substrates. Also in this work we present results on ZnO nanorods directly deposited on some chosen TCO substrates. The relationship between nanorod formation and substrate properties were studied. All ZnO nanorod layers were grown electrochemically using ZnCl₂ aqueous solutions ($c=0.2$ mmol/L) at the bath temperature of 80 °C during one hour. The structural properties and morphology of metal oxide underlays and ZnO nanorods grown on them were studied by scanning electron microscopy (SEM), x-ray diffraction spectroscopy (XRD). Depending on the substrate morphology, ZnO rods with different dimension, orientation, shape and density were obtained. For instance, larger rods ($d\sim 200$ nm, $l\sim 700$ nm) were obtained on substrates, such as ITO/glass, FTO/glass and ZnO:In/ITO/glass. Smaller rods ($d\sim 60$ nm, $l\sim 350$ nm) were obtained on smooth, uniform and fine-grained underlays, such as ZnS and TiO₂.

1. Introduction

Zinc oxide (ZnO) is an n-type II-VI semiconductor with a direct band gap (3.37 eV) and large exciton binding energy of 60 meV [1-2]. ZnO has attracted research interest in recent years due to its potential applications in various nanodevices such as lasers and light emitting diodes [3], gas sensors [1, 4], field emission devices [1, 4] and solar cells [4, 5]. For hybrid organic/inorganic solar cells with “absorber layer/ZnO nanorod/blocking layer/TCO (transparent conductive oxide)” structure, it is highly important to synthesize ZnO nanorod/blocking layer/TCO structures. In order to increase the solar cell performance, it is desired to obtain high aspect ratio (l/d , where l – length and d – diameter) conductive ZnO nanorods. Among various deposition techniques, electrodeposition is a promising approach for growing ZnO nanorods, because it is simple, low-cost, low temperature and easily scalable to large-area deposition [6-7].

Morphology of the substrate has a particular significance in nanorods growth. A seed layer (usually ZnO thin film) is required prior to the electrodeposition of the ZnO nanorods to contribute the rods growth or improve their vertical alignment [1, 8, 9]. For some applications (emitting diodes, solar cells), it is required to grow ZnO nanorod directly on a transparent conductive oxide [10-11]. In this paper, we present a study on the growth of ZnO nanorods by electrodeposition on various substrates: 1) commercially available indium tin oxide (ITO) and fluorine doped tin oxide (FTO) coated glass substrates, 2) set of ZnO seed layers with various morphologies prepared by spray pyrolysis onto ITO/glass substrates and 3) ZnS and TiO₂ thin films deposited by spray pyrolysis on ITO/glass



substrates. Herein we study relationship between the initial morphology of the substrate and final morphology of the ZnO nanorod layer. The morphology and structural properties of the substrates and ZnO nanorods deposited on them, respectively, are studied by means of high resolution scanning electron microscopy (SEM) and X-ray diffraction (XRD) techniques.

2. Experimental

2.1. Synthesis details

Prior the deposition, ITO and FTO covered glass substrates were washed thoroughly with soap, ethanol and sulphuric acid. The samples were rinsed with deionised water after each cleaning step. On some chosen ITO/glass and FTO/glass substrates, the ZnO nanorods were deposited directly onto the substrate. Commercially available ITO/glass substrates have been chosen for the deposition of metal oxide underlays such as ZnO seed layers, ZnS and TiO₂ thin films prepared by using spray pyrolysis method as described in details earlier [12-13]. Electrodeposition of ZnO nanorods was carried out potentiostatically in a three-electrode glass cell, where the TCO/glass was used as a working electrode, while a silver/silver chloride/3M KCl (Ag/AgCl/KCl) and a platinum (Pt) wire were used as reference and counter electrodes, respectively.

Solution of 0.2 mmol ZnCl₂ (Sigma-Aldrich), and 0.1 M KCl in amount of 50 ml was utilized as a supporting electrolyte. The growth temperature was kept at 80 °C using a temperature controlled circulating bath. Deposition time was fixed to 1 hour. Electrochemical deposition was done under -1.0 V potential, vs the reference electrode using the Radiometer Analytical potentiostat PGP201.

2.2. Characterization

The morphology of the substrates was studied by the high resolution scanning electron microscope Zeiss EVO-MA15 at the operating voltage of 10 kV. The crystal structure of the nanorods was characterized by using X-ray diffraction on a Rigaku Ultima IV diffractometer using CuK α radiation ($\lambda=1.5406\text{\AA}$, 40 kV at 40 mA). Crystals density was evaluated from the SEM surface images, from area of 6.2 $\mu\text{m}\times 4.7\ \mu\text{m}$.

3. Results and Discussion

3.1. Deposition of ZnO rods on TCO electrodes

In this study two different types of conducting electrodes were used: commercially available ITO and FTO coated glass substrates. The SEM images of TCO electrodes are shown in figure 1a (from ITO/glass) and in figure 1c (from FTO/glass). Corresponding morphologies of the electrodeposited ZnO layers directly grown on ITO and FTO electrodes are presented in figures 1b and 1d, respectively. As can be seen from the figures, the final shape of the ZnO nanorods differs depending on the substrate morphology. In case of ITO/glass, the rods are thinner ($d\sim 170\ \text{nm}$, $l\sim 700\ \text{nm}$) and show higher density ($\sim 7.4\times 10^8\ \text{cryst./cm}^2$) than those grown on FTO/glass ($d\sim 300\ \text{nm}$, $l\sim 600\ \text{nm}$, density $\sim 6.5\times 10^8\ \text{cryst./cm}^2$). Such difference can be explained by the difference in the morphology of the substrate. Higher density of the grains on the FTO electrode (Figure 1c) provoke large amount of nuclei that can further coalescence and promote the lateral growth of the crystal. Similar behaviour has

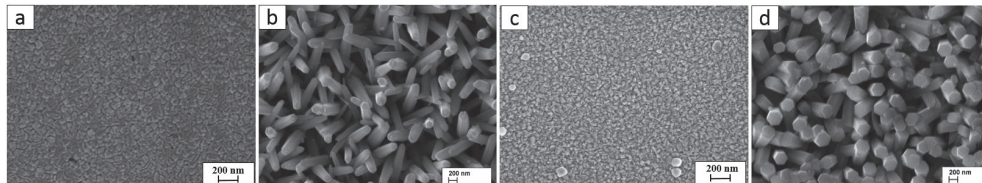


Figure 1. SEM images of: a) ITO/glass substrate, b) ZnO nanorods grown onto ITO/glass, c) FTO/glass substrate, d) ZnO nanorods grown onto FTO/glass.

already been reported for spray pyrolysis deposited ZnO nanorods on ITO/glass and FTO/glass substrates [14–15]. The resistivity of the substrates might be also a reason of such difference in final shape of the ZnO crystals. In our case, the ITO has lower resistivity ($\rho \sim 15\text{--}20 \Omega\cdot\text{cm}$) than resistivity of the FTO substrate ($\rho \sim 150 \Omega\cdot\text{cm}$). It was reported earlier by Kim et al., that conductive substrates greatly affect on the structural and optical properties of ZnO nanorods [16].

3.2. Deposition of ZnO nanorods on ZnO seed layers obtained by spray pyrolysis

In previous studies on ZnO thin films by spray pyrolysis [17–19], it was shown that temperature, concentration of the precursor solution (zinc acetate), dopant type and amount are the most important technological parameters that influence the morphology of the film. Here we prepared ZnO seed layers by spray pyrolysis on ITO/glass substrates using different technological parameters mentioned above. The morphology of ZnO seed layers are shown in figures 2a, 2c, 2e and 2g. The SEM images of ZnO nanostructures grown on those seed layers are presented in figures 2b, 2d, 2f and 2h, respectively.

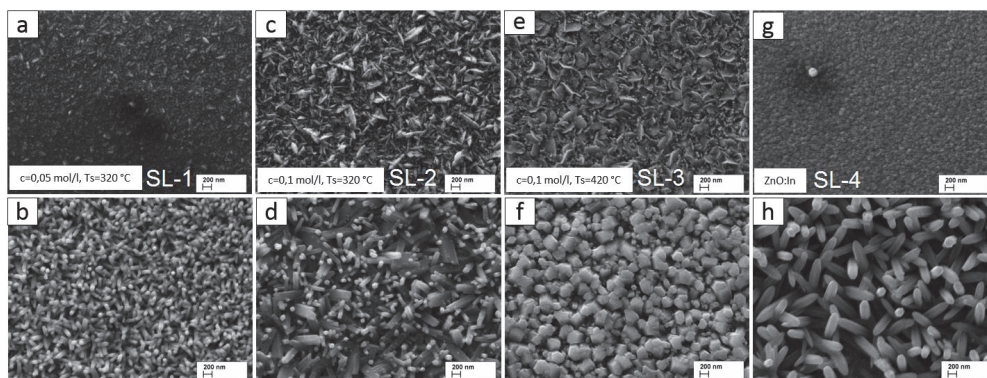


Figure 2. SEM images of: a) ZnO seed layer SL-1 grown by spray of zinc acetate solution with $c=0.05 \text{ mol/L}$ at $T_s=320 \text{ }^\circ\text{C}$; b) ZnO nanorods on seed layer SL-1; c) ZnO seed layer SL-2 grown by spray of zinc acetate solution with $c=0.1 \text{ mol/L}$ at $T_s=320 \text{ }^\circ\text{C}$; d) ZnO nanorods on seed layer SL-2; e) ZnO seed layer SL-3 grown by spray of zinc acetate solution with $c=0.1 \text{ mol/L}$ at $T_s=420 \text{ }^\circ\text{C}$; f) ZnO nanorods on seed layer SL-3; g) ZnO seed layer doped with In (3 at.%) SL-4 grown by spray of zinc acetate solution with $c=0.2 \text{ mol/L}$ at $T_s=440 \text{ }^\circ\text{C}$, (ZnO:In); h) ZnO nanorods on seed layer SL-4.

Seed layer SL-1 is compact and flat, composed of densely packed fine grains. As a result, ZnO nanorods grown on SL-1 have a diameter of 80 nm and length of ca. 270 nm, and show uniform dense coverage (figure 2b). SL-2 seed layer from solution with higher concentration at the same temperature have highly structured surface composed of the flake-like grains with different sizes (figure 2c). Because of such nonuniformity in the dimensions of the grains on this substrate, the sizes of the ZnO rods vary greatly. ZnO nanorod layers compose of smaller crystals ($d \sim 80 \text{ nm}$) as well as of much larger crystals ($d \sim 350 \text{ nm}$) with length of ca. 300 nm (figure 2d). Seed layer SL-3 is also composed of grains with different shapes including platelets and nanoneedles (figure 2e). The ZnO nanostructures grown on this seed layer are mixture of fat and thin compactly standing ZnO crystals ($d \sim 150\text{--}300 \text{ nm}$, $l \sim 150 \text{ nm}$) (figure 2f). The ZnO nanorods have been deposited also onto ZnO:In seed layer. SEM image for SL-4 seed layer is presented in figure 2g and for the resultant ZnO nanorod crystals in figure 2h. Rods have uniform dimensions ($d \sim 200 \text{ nm}$, $l \sim 700 \text{ nm}$) comparable to those grown on bare ITO/glass layer. Rods grown on ZnO:In are markedly larger than those grown on undoped ZnO layers, that might be explained with difference in conductivity of ZnO:In and ZnO films [20–21].

XRD patterns of ZnO seed layers and of samples with ZnO nanorod grown on those seed layers are presented in figure 3. All the samples show the reflections at 2θ of 31.73° , 34.36° , 36.21° and 62.75° corresponding to the (100), (002), (101) and (103) planes of ZnO (PDF 01-080-0074) [20].

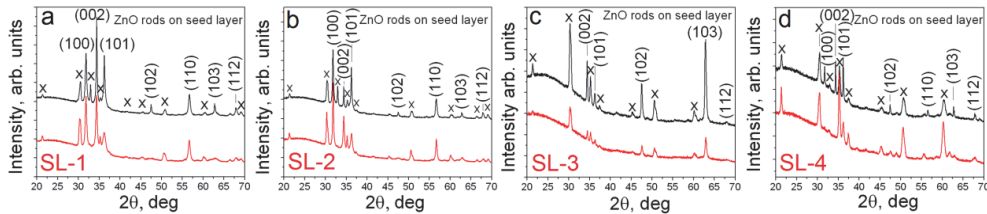


Figure 3. XRD patterns of the nanorods grown on different ZnO seed layers: a) SL-1; b) SL-2; c) SL-3; d) SL-4; x – reflections from ITO/glass substrate.

For the SL-1 seed layer, the $I_{(002)}/I_{(100)} \sim 1$ and $I_{(002)}/I_{(101)} \sim 4$ (figure 3a). As in ZnO powder reference [20] the $I_{(002)}/I_{(100)} \sim 0.7$ and $I_{(002)}/I_{(101)} \sim 0.4$, thus the crystallites in SL-1 film are orientated along the (002) plane parallel to the substrate. The $I_{(100)}/I_{(002)} \sim 1.9$ is characteristic of the SL-2 ZnO seed layer, in ZnO powder $I_{(100)}/I_{(002)} \sim 1.4$, thus the orientation is along the (100) plane (figure 3b). For the SL-3 ZnO seed layer the $I_{(103)}/I_{(002)} \sim 2$, in ZnO powder $I_{(103)}/I_{(002)} \sim 0.7$, thus the crystallites are orientated along the (103) plane (figure 3c). According to XRD pattern of ZnO:In film (figure 3d), the intensity of the (002) reflection is negligible and the intensity of the (101) is the strongest, the crystallites do not have preferred orientation. Observed result is in a good correspondence with the results of earlier studies [21]. Therefore, according to the XRD patterns presented in figure 3, all the ZnO underlays show different crystallographic orientations. Herein are presented intensities ratios of resultant ZnO nanostructured layers: $I_{(002)}/I_{(101)} \sim 1.6$, $I_{(100)}/I_{(101)} \sim 1.2$, $I_{(103)}/I_{(002)} \sim 2.2$, $I_{(002)}/I_{(101)} \sim 1$ (figures 3a, b, c, d, respectively). Comparing them with the ZnO powder references [20] where the $I_{(002)}/I_{(101)} \sim 0.4$, $I_{(100)}/I_{(101)} \sim 0.56$, $I_{(103)}/I_{(002)} \sim 0.7$, $I_{(002)}/I_{(101)} \sim 0.4$ it seems that for all resultant ZnO nanostructured layers intensities ratios changed. Orientation along the (002) plane is characteristic of all electrodeposited ZnO layers except of ZnO rods on seed layer SL-2 (figure 3b). It could be that differences in seed layer thicknesses (SL-2 is deposited from more concentrated solution than SL-1 and thus SL-2 layer is probably thicker [15, 22]) or surface morphologies (compare figures 2a and 2c) are responsible for such kind behavior. XRD study shows that the ZnO rods grow preferably along the (002) plane parallel to the substrate independent of the orientation of corresponding ZnO seed layer.

3.3. Deposition of ZnO nanorods on ZnS and TiO₂ underlays grown by spray on ITO/glass substrates
For some purposes (dye-synthesized solar cell etc.) it is important to have a less conductive thin barrier layer between TCO and ZnO nanorods, therefore it is important to find out technological parameters in order to grow nanorods on such types of the substrate. Here we prepared ZnS and TiO₂ thin films by spray pyrolysis using knowledge of the earlier studies on ZnS [23] and TiO₂ films deposition by spray [24]. Both ZnS and TiO₂ films have smooth morphologies according to SEM images (figures 4a and 4c). Both substrates resulted in very uniform and dense coverage of well-shaped hexagonal ZnO nanorods. The dimension of the rods grown onto ZnS are slightly larger ($d \sim 150$ nm, $l \sim 450$ nm), than those grown on TiO₂, ($d \sim 60$ nm and $l \sim 370$ nm). The difference in rods dimensions could be explained by different surface roughness on ZnS and TiO₂ underlays.

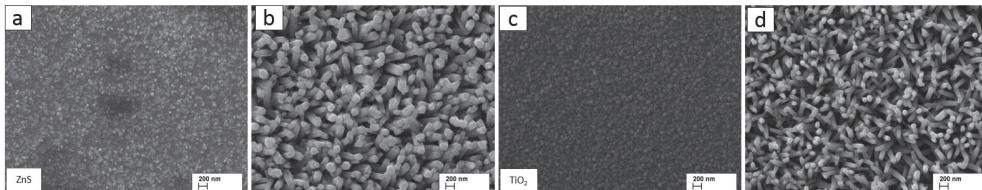


Figure 4. SEM images of the a) ZnS underlay; b) ZnO nanorods deposited on underlay (a); c) TiO₂ underlay; d) ZnO nanorods deposited on underlay (c).

4. Conclusions

Herein we presented a study on the growth of ZnO nanorods by electrodeposition on various substrates: commercially available ITO, FTO substrates on glass, metal oxide underlays such as ZnO seed layers, ZnS and TiO₂ thin films prepared by using spray pyrolysis. The underlays with highly structured surface composed of grains with different sizes provoke the growth of ZnO crystals with different sizes and shape. ZnO rods were grown on smooth, flat, uniform and fine-grained substrates, such as ITO, FTO, ZnS and TiO₂ thin films, ZnO seed layer obtained at 320 °C and c=0.05 mol/L and indium-doped ZnO seed layer. The conductivity of the substrates might also affect the shape of resultant ZnO crystals. Electrically more conductive substrates- such as ITO, FTO and indium-doped ZnO seed layer provoke the growth of ZnO rods with larger dimensions. Thus, dimensions, shape and density of the rods depends strongly on the properties of the substrate or seed layer used, the orientation of the seed layer has minor effect.

5. Acknowledgements

This work is financially supported by the Estonian Ministry of Education and Research (IUT 19-4), TUT base financing project B24 and European Regional Development Fund through the projects: Centre of Excellence “Mesosystems: Theory and Applications” (MESO) TK114, 3.2.0101.11-0029 and project “Efficient plasmonic absorbers for solar cells” 3.2.1101.12-0023 and the Estonian Research Council grant PUT150.

References

- [1] Yi G-C, Wang C and Park W I 2005 *Semicond. Sci. Technol.* **20** 22
- [2] Wang Z L 2004 *J. Phys.: Condens. Matter* **16** 829
- [3] Choi Y-S, Kang J-W, Hwang D-K and Park S-J 2010 *IEEE Trans. Electr. Dev.* **57** 26
- [4] Weintraub B, Zhou B, Li Y and Deng Y 2010 *Nanoscale* **2** 1573
- [5] Yin Z, Wu S, Zhou X, Huang X, Zhang Q, Boey F and Zhang H 2010 *Small* **6** 307
- [6] Pauporte T, Bataille G, Joulaud L and Vermersch F J 2010 *J. Phys. Chem. C* **114** 194
- [7] Kim H, Moon J Y and Lee H S 2011 *Electron. Mater. Lett.* **7** 59–62
- [8] Kim D C, Kong B H and Cho H K 2008 *J. Mater. Sci. Mater. Electron.* **19** 760
- [9] Yin Y T, Que W X and Kam C H 2010 *J. Sol-Gel Sci. Technol.* **53** 605
- [10] Lee H K, Kim M S and Yu J S 2011 *Nanotechnology* **22** 445602
- [11] Masysda Y and Kato K 2009 *Cryst. Growth Des.* **9** 3083
- [12] Dedova T, Krunks M, Oja Acik I, Klauson D, Volobujeva O and Mere A 2013 *Mater. Chem. Phys.* **141** 69
- [13] Krunks M, Dedova T and Oja Acik I 2006 *Thin Solid Films* **515** 1157
- [14] Dedova T, Oja Acik I, Krunks M, Mikli V and Volobujeva O 2012 *Thin Solid Films* **520** 4650
- [15] Dedova T, Volobujeva O, Krunks M, Mikli V, Gromyko I, Katerski A and Mere A 2013 Growth of Zinc Oxide Rods on FTO Electrodes by Spray Pyrolysis *Int. Conf. on Functional Materials and Nanotechnologies (Tartu, Estonia, 21–24 April 2013)* IOP Conf. Series: Mater. Sci. Eng. vol 49 (Bristol: IOP Publishing) pp. 1–4
- [16] Kim H, Moon J Y and Lee H S 2009 *Electron. Mater. Lett.* **5** 135
- [17] Krunks M and Mellikov E 1995 *Thin Solid Films* **270** 33
- [18] Dedova T, Klauson J, Badre C, Pauporte Th, Nisumaa R, Mere A, Volobujeva O and Krunks M 2008 *Phys. Status Solidi A* **205** 2355
- [19] Kriisa M, Karber E, Krunks M, Mikli V, Unt T, Kuk M and Mere A 2014 *Thin Solid Films* **555** 87
- [20] International Centre for Diffraction Data (ICDD), PDF-2 Release 2008
- [21] Kriisa M, Krunks M, Karber E, Kuk M, Mikli V and Mere A 2013 *J. Nanomater.* **2013** 1
- [22] Shinde V R, Gujar T P and Lokhande C D 2006 *Sensors and Actuators B: Chemical* **120** 551
- [23] Dedova T, Krunks M, Gromyko I, Mikli V, Sildos I and Unt T 2014 *Phys. Status Solidi A* **211** 514
- [24] Oja Acik I, Junolainen A, Mikli V, Danilson M and Krunks M 2009 *Appl. Surf. Sci.* **256** 1391

Publication III

D. Klauson, **I. Gromyko**, T. Dedova, N. Pronina, M. Krichevskaya, O. Budarnaja, I. Oja Acik, O. Volobujeva, I. Sildos, K. Utt. Study of photocatalytic activity of zinc oxide nanoneedles, nanorods, pyramids and hierarchical structures obtained by spray pyrolysis. *Mater. Sci. Semicond. Process* 31 (2015) 315–324.



Study on photocatalytic activity of ZnO nanoneedles, nanorods, pyramids and hierarchical structures obtained by spray pyrolysis method



Deniss Klauson^{a,*}, Inga Gromyko^b, Tatjana Dedova^b, Natalja Pronina^a, Marina Krichevskaya^a, Olga Budarnaja^a, Ilona Oja Acik^b, Olga Volobujeva^b, Ilmo Sildos^c, Kathriin Utt^c

^a Department of Chemical Engineering, Tallinn University of Technology, Ehitajate tee 5, 19086 Tallinn, Estonia

^b Department of Materials Science, Tallinn University of Technology, Ehitajate tee 5, 19086 Tallinn, Estonia

^c University of Tartu, Institute of Physics, Riia 142, 51014 Tartu, Estonia

ARTICLE INFO

Available online 24 December 2014

Keywords:

Zinc oxide
Hierarchical
Spray pyrolysis
Photocatalytic activity

ABSTRACT

In this research, ZnO nanostructured layers with various morphology, i.e. nanoneedles, nanorods, pyramid shaped ZnO crystals, and hierarchical structures of ZnO deposited on nanorods and pyramid shaped crystals, were synthesised by pneumatic spray pyrolysis method. Hierarchical structures, a dense network of well-ordered platelets covering the side facets of the rod-like and pyramid shaped ZnO crystals, were obtained by spraying Zn (Ac)₂ solution over the surface of pre-grown ZnO crystals at deposition temperature of 330 °C within 5 min. All ZnO layers have been characterised by scanning electron microscopy (SEM), X-ray diffraction spectroscopy (XRD), absorbance of ultraviolet and visible light (UV–vis), surface wettability measurements and photoluminescence (PL). Photocatalytic activity of the layers was evaluated by means of photocatalytic oxidation activity (PCO) of several organic pollutants, namely, methyl-tert-butyl ether (MTBE), humic acid (HA), N,N-dimethyl p-nitrosoaniline (RNO), and prednisolone (PNL); the results were compared to the performance of well-established commercial photocatalyst, P25 titanium dioxide (Evonik). MTBE was the most efficiently degradable compound by all objects, while RNO was effectively degraded by plain structures only. In HA photocatalysis, needle-like ZnO as the most efficient material; PNL was the least degradable by ZnO layers. In the degradation of MTBE, RNO and HA, ZnO objects have shown activity comparable to or highly exceeding that of P25 TiO₂. The explanation of the differences in ZnO objects' photoactivity is proposed to be the different character of oxidising species produced by the ZnO objects, and different interactions of these with the degradation substrates, based on the relative amount of surface defects, surface morphology and hydroxylation of the ZnO structures' surface.

© 2014 Elsevier Ltd. All rights reserved.

1. Introduction

The interest in the preparation of ZnO nanostructures such as nanowires, nanorods, hierarchical structures of ZnO is continuously growing due to the wide potential of their applications in optoelectronic devices, gas sensors, or

* Corresponding author. Tel.: +372 620 2851; fax: +372 620 2856.

E-mail address: deniss.klauson@ttu.ee (D. Klauson).

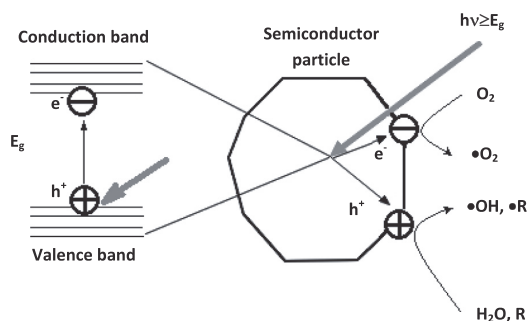


Fig. 1. Schematic representation of photocatalytic oxidation working principle: $h\nu$ stands for electromagnetic radiation, E_g for band gap, e^- for electron and h^+ for hole.

photocatalysis for degradation of environmentally hazardous pollutants. For photocatalysis ZnO has been attracted great interest due to its low cost, low-toxicity, abundance, and ease of preparation of ZnO with various morphologies.

Up to now there are many reports on efficient photocatalytic activity of ZnO nanorods and hierarchical structures deposited by electrodeposition, chemical bath, solvothermal method [1,2].

In addition to these techniques, spray pyrolysis is a very simple and relatively low-cost processing method for preparing plain and nanostructured layers with precise composition control, precise stoichiometry, high crystallinity and purity of the materials [3–5]. In spite of many reports on photocatalytic activity of the ZnO layers it is still a great challenge to produce photocatalytically active ZnO with new morphologies by inexpensive and well controllable techniques and study their photocatalytic properties with respect to the growth conditions.

Herein, we present a study on synthesis and photocatalytic performance of spray-deposited ZnO nanostructured layers with various morphology, namely, nanoneedles, rods, hierarchical structures grown on the rods, pyramid shaped crystals, and hierarchical structures grown on the pyramid shaped crystals.

Literature data on various ZnO objects (including hierarchical ones) synthesis and activity testing is plentiful, but it deals mostly with dyes as degradation substrates, such as methyl orange (MO) [2,6,7], methylene blue (MB) [8–10], rezaurin [11], rhodamine B (RhB) [1], etc., in mg L^{-1} scale, with degradation rates ranging from 40% to 100%; some notable exceptions are the works dealing with degradation of actual pollutants, such as 2,4-dichlorophenoxyacetic acid (2,4-D) [12], estrone [13] and 4-chlorophenol (4-CP) [14]; as a rule, only one degradation substrate is used in such works. The authors' approach, on the other hand, lies within assessment of their objects' photocatalytic activity by degrading several organic pollutant types with different structure, giving a more detailed insight on their abilities.

In order to assess the photoactivity of ZnO layers, the authors chose aqueous photocatalytic oxidation of several organic compounds with different structure. Photocatalytic oxidation is a phenomenon based on the creation of

excitons by the subjection of the semiconductor material to electromagnetic radiation the quanta of which possess equal or higher energy to that of the semiconductor's band gap. With the existence of suitable charge carrier traps (e.g. oxygen vacancies, surface defects, sharp edges, etc.), positively charged holes produce hydroxyl radicals from water molecules, or can directly abstract pollutant molecules' electrons. At the same time, conduction band electrons reduce suitable electron acceptors (e.g. dissolved oxygen). This way, the defects on irradiated semiconductor material are a source of reactive oxygen species (ROS). Besides the relative abundance of defects, their availability to the aqueous pollutant (governed both geometrically and hydrodynamically by the surface morphology) and chemical composition of the surface (hydroxylated surfaces produce hydroxyl radicals, while non-hydroxylated ones produce less potent oxidising species) are the primary factors influencing the photocatalytic oxidation efficiency. The mechanism of photocatalysis is schematically represented in Fig. 1.

The following compounds were chosen to evaluate the photocatalytic activity of ZnO objects in this study: methyl-tert-butyl ether (MTBE, CAS 1634-04-4), humic acid sodium salt (HA, CAS 68131-04-4), N,N-dimethyl p-nitrosoaniline (RNO, CAS 138-89-6) and prednisolone (PNL, CAS 50-24-8). An aliphatic and relatively non-polar MTBE is perhaps best known as a fuel additive, used worldwide, although banned for some time in the United States; it is non-biodegradable and hard to remove from water by conventional means, and a suspected carcinogen [15–18]. RNO is an aromatic compound, which has also seen the application in measuring the number of hydroxyl radicals in various advanced oxidation processes (AOPs), including photocatalysis, due to RNO decolouration upon stoichiometric reaction of its molecule with OH-radical [19]. Humic acid was chosen as a representative of a wider compound class, humic substances (HS), the product of plant matter decay, that have various polycyclic, aromatic and heteroatom-containing functional groups; besides the coloration of water, HS, being radical scavengers and thus hardly affected by common water treatment methods, are easily bonded with heavy metals and other toxics [20], being able to effectively transport them through drinking water treatment stages [21]. Upon HS-containing water chlorination, they serve as a source of carcinogenic trihalomethanes [22,23]. Finally, PNL is a widely used glucocorticoid anti-inflammatory agent, and as such is a very common emerging micropollutant [24]. The substances' structural formulae can be seen in Fig. 2.

The aim of this study was the synthesis and investigation of hierarchical ZnO objects, possessing different morphology and surface properties, and thorough and representative investigation of their photoactivity by their action on several substrates with different chemical structure and properties. Such an approach will no doubt give an objective view on the new materials and their abilities in the light of their possible applications. This should give an insight on the characteristics of an "ideal" photocatalytic material in terms of its structure and properties, and, consequently, on the conditions of synthesis which would provide such a material.

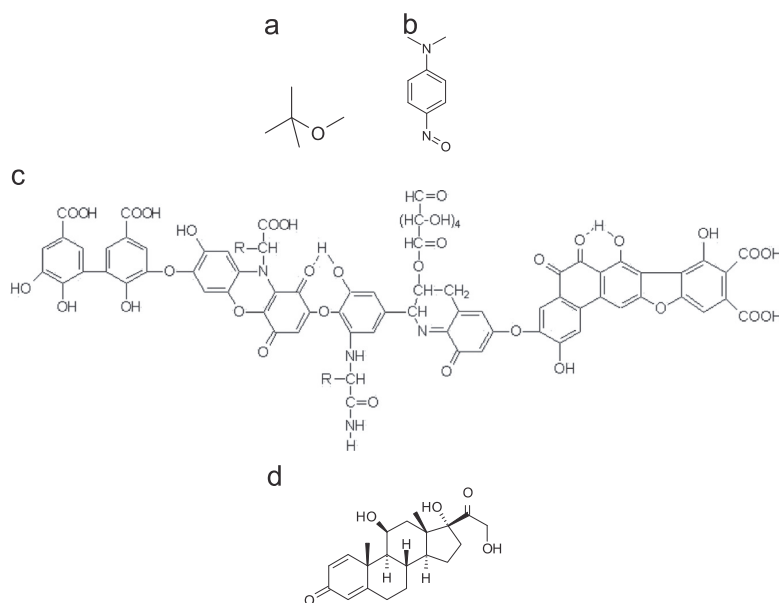


Fig. 2. Structural formulae of substrates used in this study to test the photocatalytic activity of ZnO samples: (a) methyl-tert-butyl ether (MTBE); (b) N,N-dimethyl p-nitrosoaniline (RNO); (c) hypothetical molecule of humic substances (HS) and (d) prednisolone (PNL).

2. Materials and methods

2.1. Synthesis of ZnO layers

In this study, ZnO nanostructured layers with different morphology, such as nanoneedles (S-1), nanorods (S-2), hierarchical structure on nanorods (S-3), truncated pyramid shaped crystals (S-4) and hierarchical structures on those pyramids (S-5) were synthesised by a pneumatic spray pyrolysis method. The preparation details of ZnO layers and illustration of their morphology are summarised in Table 1. The details on the spray pyrolysis deposition and some properties of the ZnO needles, rods and hierarchical structures on the rods can be found in some earlier published studies [25–29]. Sample (S-1) with nanoneedle-like morphology was synthesised by spraying $\text{Zn}(\text{Ac})_2$ solution at $T=330\text{ }^\circ\text{C}$ on glass substrate. Samples S-2, S-3, S-4, S-5 were prepared as follows: first, nanorods or pyramid shaped crystals were prepared by spraying the ZnCl_2 aqueous solution at $T=530\text{ }^\circ\text{C}$ on ITO/glass and SnO_2 /glass substrates, which were mounted side by side to the tin bath. Final morphology depended on the substrate. Nanorod-like crystals were grown on ITO/glass substrate and pyramidal shaped crystals were obtained on SnO_2 /glass substrate. Within one deposition run we prepared 4 samples, 2 samples with nanorod and pyramid morphologies (S-2 and S-3) were taken out of the bath and studied on their photocatalytic activity and 2 others (S-4 and S-5) were left in the bath and proceeded further spray deposition procedure to produce hierarchical structures. In order to produce hierarchical layers, $\text{Zn}(\text{Ac})_2$ aqueous solution was sprayed at $T=330\text{ }^\circ\text{C}$ over those nanorod and pyramid-like samples [27]. In all experiments, independent of the precursor, concentration of precursors was fixed to 0.1 mol L^{-1} and air was used as

carrier gas. The authors' previous studies have shown that under such conditions it is possible to obtain single-crystal ZnO without any traces of chloride ions or organics [30,31].

2.2. Characterisation

The morphology of the layers was studied by a high resolution scanning electron microscope, Zeiss HR FESEM Ultra 55, at an acceleration voltage of 1.5 kV. X-ray diffraction (XRD) patterns were recorded on a Rigaku Ultima IV diffractometer operated at 40 kV and at a 40 mA ($\text{Cu K}\alpha$ radiation, $\lambda=1.5406\text{ \AA}$) using the D/teX Ultra silicon strip detector and a rotating sample holder. The diffuse (R_{diff}) and total (R_{tot}) reflectance spectra were measured in the wavelength range 200–2500 nm on a Jasco 670-UV-vis-NIR spectrophotometer equipped with an integrating sphere. Haze factor values (HF) were determined from $\text{HF}=R_{\text{diff}}/R_{\text{tot}}$. Photoluminescence (PL) was measured at room temperature using the fluorometer Fluoromax-4 at an excitation wavelength of 330 nm (3.76 eV).

Surface wettability of the samples was measured by Rame-Hart Model 260 surface tension metre. Water droplet was placed upon the surface of ZnO objects, filmed with magnifying camera, with contact angle measured by respective software.

Aqueous photocatalytic oxidation experiments were conducted in 200-mL batch reactors with magnetic stirrers, thermostatted at $20\pm 1\text{ }^\circ\text{C}$, and placed under UV-lamps (Philips Actinic 15 W mercury low-pressure lamps, with emission at 365 nm) equipped with reflectors. Irradiance of the lamps used was measured to be around 1.2 mW cm^{-2} by Ocean Optics USB2000+ spectrometer, with the data interpreted by SpectraSuite software. Objects with ZnO layers

Table 1
Synthesis conditions for ZnO samples.

Sample name	Morphology	Preparation details of the samples					
		Substrate	Precursors	C (mol/l)	V sol (ml)	V (ml/min)	T _{gr} (°C)
S-1	Needles	Glass	Zn(Ac) ₂	0.1	75	1.5	330
S-2	Rods	SnO ₂ /glass	ZnCl ₂	0.1	50	2.5	530
S-3	Platelets on side facet of rods, needles on top plane	SnO ₂ /glass	1. ZnCl ₂ 2. Zn(Ac) ₂	0.1 0.1	50 30	2.5 4	530 330
S-4	Pyramid shaped crystals	ITO/glass	ZnCl ₂	0.1	50	2.5	530
S-5	Platelets wounded around the pyramids	ITO/glass	1. ZnCl ₂ 2. Zn(Ac) ₂	0.1 0.1	50 30	2.5 4	530 330

were placed upon larger Pyrex glass plates, submerged into the reactors at constant depth of about 2 cm. The experimental time was chosen to be 2 h in case of MTBE (100 mg L⁻¹) and PNL (10 mg L⁻¹), 6 h in case of RNO (50 mg L⁻¹), and 24 h with HA (25 mg L⁻¹), based on the authors' previous experience [20,32]. For every experiment, two reactors were used: one with ZnO sample, and a reference reactor, without any photocatalyst. Reference reactor is needed to take into account the evaporation of water during the experiments, which results in slight pollutant concentration increase. Photocatalytic experiments were performed at least three times, with parallel experiment deviation being under 5%. While it is generally accepted that ZnO is a material prone to corrosion, i.e. dissolution under acidic and alkaline conditions, in this study the experiments were performed at natural pH of the solutions, i.e. at near-neutral conditions, where ZnO is stable. In order to check this, some of the photocatalytic oxidation experiments were repeated (as described earlier in this section) after the conclusion of the main experimental runs, showing only negligible differences from the results obtained earlier; the latter, together with the visible inspection of the films suggest no

substantial ZnO corrosion. To evaluate the degradation efficiency of MTBE, Chemical Oxygen Demand (COD) was used, as in the authors' previous studies [33]. The concentrations of PNL were determined photometrically as described in [34]. Concentrations of RNO were determined photometrically, by measuring adsorbance at 440 nm. Finally, HA concentrations measurements were conducted as in [20].

The results of these substances' photocatalytic oxidation (PCO) were compared to those obtained with P25 Evonik titanium dioxide, a well-known commercial photocatalyst, applied as slurry, and immobilised upon glass substrate. Photocatalytic performance of ZnO layers was evaluated by PCO efficiency (Eq. 1), showing the amount of pollutant degraded per 1 W h of energy reaching the treated solution surface [35].

$$E = \frac{\Delta c \times V \times 1000}{I \times s \times t} \quad (1)$$

where E is the photocatalytic oxidation efficiency, mg W⁻¹ h⁻¹; Δc is the decrease in the pollutant's concentration, mg L⁻¹, or chemical oxygen demand (COD), mg O₂ L⁻¹; V is

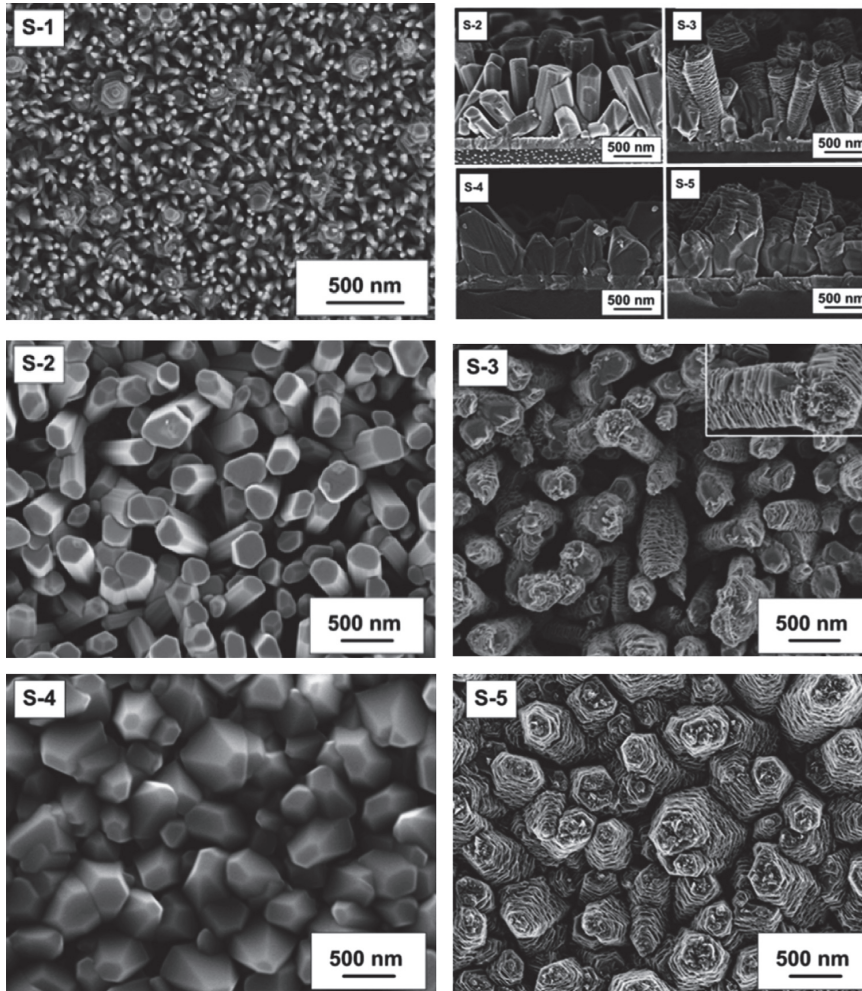


Fig. 3. SEM images of ZnO layers used in the current study: (S-1) nanoneedles; (S-2) rods; (S-3) hierarchical structures on the rods; (S-4) pyramid shaped crystals and (S-5) hierarchical structures on pyramids.

the volume of the treated sample, L ; I is the irradiance, mW cm^{-2} ; s is the irradiated area, cm^2 ; t is the treatment time, h.

As surface reactions preceded by adsorption of the substrates are an important part of PCO in general, the adsorption of the substances under scope was studied at their working concentrations (see above). The experimental setup was similar to that of PCO, with the exception that the reactors were sealed from the atmosphere and closed from the light. The results, expressed in μg of the adsorbed substance per cm^2 of the respective thin film area, were derived from the batch mass balance: the concentration of the substrates was determined before the experiment, and at its end. The duration of adsorption experiments was the same as in case of PCO experiments.

3. Results and discussions

3.1. ZnO layers characterisation

SEM images of the ZnO layers are presented in Fig. 3. Sample S-1 is mainly composed of nanoneedles with diameter of 20 nm and length of 100 nm. This is characteristic morphology of ZnO thin film produced from $\text{Zn}(\text{Ac})_2$ solution at deposition temperatures of 400–450 °C [28]. ZnO rods (S-2) are elongated hexagonally shaped crystals with diameter of 200–300 nm and length of ca. 1 μm . Hierarchical structures (S-3) represent a dense network of platelets wounded around the rod stem with some needles on top of (002) plane of the rod. (002) plane of the rods has highest surface energy and therefore the needles formation is predominantly observed on this plane, as it

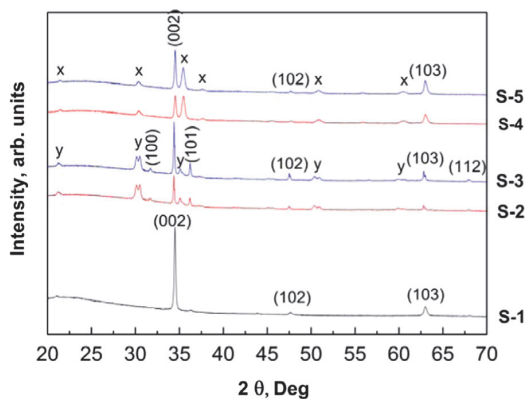


Fig. 4. XRD patterns of the ZnO layers. (S-1) nanoneedles, (S-2) rods on ITO/glass substrate, (S-3) hierarchical structure grown on S-2, (S-4) pyramid shaped crystals on SnO₂/glass and (S-5) hierarchical structure grown on S-4. x is reflections from ITO substrate and y is reflections from SnO₂ substrate.

has been shown in previous study [27]. Truncated pyramidal formed crystals (S-4) were fabricated using SnO₂ substrate that composed of the larger grains compared to ITO surface. The hierarchical structure of ZnO on pyramidal shaped crystals (S-5) is mainly composed of very densely packed platelets and small amount of needles on a top plane of a crystal.

3.2. XRD study

XRD patterns of the layers are presented in Fig. 4. Strong and narrow reflections of (002) plane detected at $2\theta=36.2^\circ$ and weaker reflections of (101), (102), (103), (112) found at $2\theta=36.2^\circ$, 47.5° , 62.9° , 67.9° , respectively, reveal the formation of highly crystalline and strongly c-axis oriented ZnO layers (JSPDS card. No. 80-0074). Both plain crystals (S-2 and S-4) and hierarchical structures (S-3 and S-5) have similar crystallographic orientation along (001) direction. According to the XRD study, the intensity ratios of the main reflections of (002) to (103) planes $I(002)/I(103)$ are slightly higher for hierarchical structures. For example, the $I(002)/I(103)=3.5$ for the hierarchical structure on the rods (S-3) and $I(002)/I(103)=2.6$ for bare rods (S-2); the $I(002)/I(103)=2.8$ for hierarchical structures on pyramidal crystals and 2.4 for bare pyramidal crystals. Both (002) oriented nanoneedles formed on (002) plane of the crystals and platelets perpendicularly winded around the stems of the crystals may contribute the increased (002) plane of hierarchical structures.

3.3. Photoluminescence measurements

The main purpose of PL measurements was to estimate the existence and relative intensities of near band edge (NBE) emission (~ 3.25 eV, 380 nm) and defects related green emission (SA) bands (2.5 eV, 500 nm). Room temperature PL spectra of the ZnO layers are presented in Fig. 5.

NBE emission is usually connected to the excitons and is characteristic for pure high crystalline quality material. The green band is usually attributed to deep level defects within the ZnO crystal such as vacancies and interstitials of oxygen and zinc [36]. As can be seen from PL spectra, ZnO layers produced at higher deposition temperatures around 530°C from ZnCl₂ solution (S-2 and S-4) are less defective, because NBE/SA emission ratios are higher than for the layers produced from Zn(Ac)₂ solution at 330°C . NBE/SA=32 for the rods (S-2), 3.6 for the pyramidal shaped crystals (S-4) and only 0.06 for the needles (S-1). Also after deposition of hierarchical layer on the surface of ZnO rods or pyramidal shaped crystals, the UV emission decreases and green emission becomes more pronounced. The NBE/SA intensities ratios for S-4 sample is 2.3 and for S-5 sample is 0.35.

From point of view of photocatalytic activity, the defect sites, such as oxygen vacancies are favourable adsorption sites and charge carrier traps, and therefore their presence is more desirable. Thus, the increased photocatalytic performance of the layers with hierarchical structures and the needles is expected. However, other parameters, such as adsorption ability, the surface area and its morphology should be also taken into account. In the authors' previous study it was shown that hierarchical layers based on the rods possess ca 4.5 times higher surface areas than bare rods coupled with significantly higher photocatalytic activity in the degradation of doxycycline [28].

3.4. Surface wettability measurements

The contact angle values are presented in Table 2. According to the results obtained, samples S-2 (rods) and S-3 (rods with needles and leaflets) are the most hydrophilic ones, having the smallest contact angle when measured from the inside of the water droplet placed upon the surface of ZnO objects. The least hydrophilic sample, on the other hand, was S-4 (pyramids).

Relative hydrophilicity of the surface, measured through contact angle, should, however, be indirectly linked to the surface hydroxylation, which is in turn responsible for the production of radical species on the photocatalyst surface. If superoxide radical is formed in reaction with conduction band electron scavenged at surface vacancies of the semiconductor crystallites merely in the presence of oxygen, than hydroxyl radicals' formation is contingent on the so-called deep hydroxylation of the surface, coupled with the availability of surface defects. It has been shown on the example of titanium dioxide that the amount of strongly adsorbed water may vary significantly, depending on the crystalline modification of the semiconductor and also on synthesis conditions and surface structure [37]. In the latter case, strong adsorption of water originates from the availability of free surface Ti³⁺ cations, and their amount determines the degree of deep hydroxylation; similarity is inevitable in case of another semiconductor, ZnO. Strong water adsorption may be very different in case of various surface structures, and this way objects having greater amount of surface defects but not properly hydroxylated yield more superoxide radicals or other radical species than hydroxyl ones. However, superoxide radical is known to be

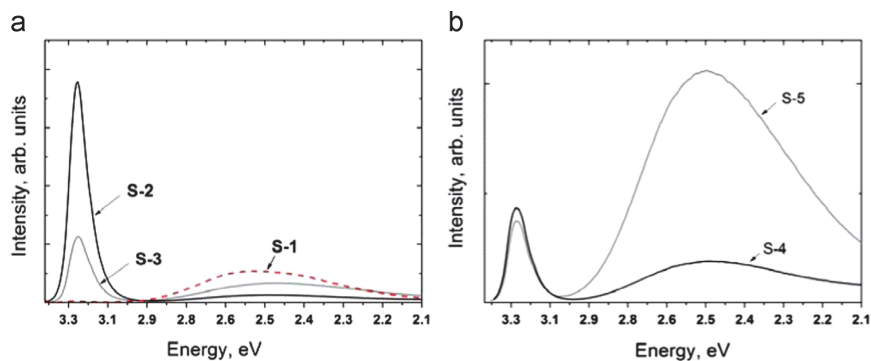


Fig. 5. Room temperature PL spectra of ZnO layers (a) S-1, S-2, S-3 and (b) S-4, S-5.

Table 2
Contact angle values for ZnO samples.

Sample	Contact angle (°)
S-1	14.79 ± 0.09
S-2	8.33 ± 0.14
S-3	13.39 ± 0.08
S-4	36.53 ± 0.25
S-5	23.30 ± 0.08

a much weaker oxidant than hydroxyl radical [38]. This will result in decreased substrate degradation rate and, thus, decreased PCO efficiency. It should be noted here that this characterises not the absolute amount of active species produced, but the amount produced that is readily available and powerful enough for subsequent oxidation reactions, and it can be strongly influenced by the surface morphology of catalytic materials and by structure of organic compounds to be oxidised.

3.5. Adsorption

The results of the substrates' adsorption are presented in Table 3. In general, it can be seen that the adsorption values decrease with the increase in the substances' molar mass and dimensions, showing evidence of relatively strong molecule geometry influence on adsorption. The adsorption of MTBE is relatively high, with hierarchical structures giving the best results (S-3, plates on rods, and S-5, plates on pyramids), followed by plain rods (S-2), whereas the adsorption results on needles and plain pyramids are comparable. The connexion of MTBE adsorption to surface hydrophilicity is not well pronounced due to relatively hydrophobic nature of MTBE molecule, which is however well miscible in water. With RNO, the highest adsorption results were observed with rods (S-2), which is the most hydrophilic object. Some adsorption was observed with S-4 and S-5 (more hydrophobic objects), with S-5, being hierarchical structure, providing higher results. HA and PNL, even larger molecules, were adsorbed only on S-1 (needles), among the degradation substrates used in this study, larger molecules appear to adsorb better on plain structures.

Table 3
Adsorption results of the substances under scope on ZnO layers; initial concentrations of the substrates: MTBE (100 mg L⁻¹), RNO (50 mg L⁻¹), HA (25 mg L⁻¹), and PNL (25 mg L⁻¹).

Sample	q (μg cm ⁻²)			
	MTBE	RNO	HA	PNL
S1	318	0	8	3
S2	709	61	0	0
S3	2049	0	0	0
S4	329	2	0	0
S5	1384	8	0	0

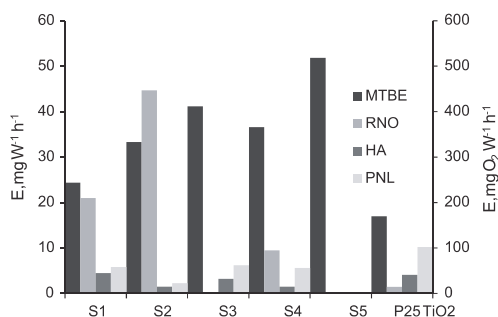


Fig. 6. Results of MTBE, RNO, HA and PNL photocatalytic oxidation by ZnO layers (S1–S5) compared to P25 Evonik TiO₂ (MTBE is TiO₂ slurry, 1 g L⁻¹, others are TiO₂ deposited upon plate, 0.6 mg cm⁻²).

3.6. Photocatalytic activity characterisation

3.6.1. MTBE

Fig. 6 shows the results obtained in MTBE PCO with ZnO layers, compared to those of P25 Evonik (slurry). It can be seen that the highest MTBE PCO efficiency (518 mg O₂ W⁻¹ h⁻¹) was exhibited by sample S-5 (pyramids and needles), followed S-3 (rods and needles), S-4 (pyramids), S-2 (rods) and S-1 (needles). Even the least effectively working object, S-1 (needles), still showed PCO efficiency superior to that of P25 in slurry (244 and 170 mg O₂ W⁻¹ h⁻¹ respectively). It can be seen that although the best results here were obtained with the hierarchical structures, which are supposed to have more

surface defects that may act as charge carrier traps and active sites, and possess far greater surface area, the performance of plain structures (rods and pyramids) was quite comparable to that of the hierarchical structures (rods with needles and leaflets). However, trying to synthesize catalysts with increased surface area should not be the main goal: it should always be kept in mind that greater surface area does not automatically result in increased adsorption, or greater photocatalytic activity, as it was noted both by the authors in the earlier studies [33,39] and by other researchers [40,41].

In terms of the ZnO samples' hydrophilicity, it can be seen that MTBE degrades well with both more or less hydrophilic photocatalysts, although in general less hydrophilic samples showed the best performance. This can be explained by the fact that MTBE molecule is relatively hydrophobic, although this effect is not pronounced to such a degree where the performance of more hydrophilic objects would be negligible.

When compared to the MTBE adsorption results, it can be seen that in general higher adsorption of MTBE results in higher PCO efficiency. However, S-5 showed ca. 20% higher efficiency than S-3, which had nearly two times higher adsorption of MTBE. This could be explained by a greater radical species production by S-5, as radicals production and adsorption capacity are likely not closely connected.

When taking into account the PL results, one can see that S-5, which has the highest defect content relatively to other ZnO samples, indeed has the highest efficiency in MTBE degradation.

To sum up, the production of reactive oxygen species (ROS) at the ZnO surface defects, initiated the UV-irradiation of the ZnO objects' surfaces, appears to be sufficient for the efficient MTBE degradation. In case of MTBE, it appears to be the quantity of various ROS (as opposed to their composition) is enough to provide highly efficient degradation results (far surpassing those of P25 titanium dioxide); adsorption as the prerequisite of photocatalysis does not seem to be of very high importance consequently, it can be stated that radical oxidation is predominant in MTBE photocatalytic decomposition.

3.6.2. RNO

In case of RNO, PCO efficiency generally declined from S-1 to S-5; the results were significantly higher compared to P25 Evonik titanium dioxide ($1.45 \text{ mg W}^{-1} \text{ h}^{-1}$ for P25 and 44.7 for S-2). The results can be seen in Fig. 6.

In this instance, rods (S-2), a simple structure, showed the best results as well, followed by needles (S-1) pyramids (S-4); hierarchical structures, i.e. pyramids with needles and leaflets (S-5) and rods in combination with needles (S-3) showed no RNO degradation within the limits of analytical precision. This can be explained by the fact that unlike MTBE and HA, RNO is readily oxidised only by hydroxyl radicals, but does not react with superoxide radicals or other peroxy compounds [34,42]. If the surface defects under UV irradiation tend to produce peroxy radicals, RNO degradation rate will decrease.

From the hydrodynamic point of view, leaflets and needles, protruding from the surface of rods or pyramids, may hinder RNO molecules from reaching the main body

of ZnO particles, as laminary liquid layer is created in spaces between those close-lying structures. This, in turn, should hinder RNO molecules' movement in the vicinity of the ZnO surface by mass transfer, originating from solution agitation, supplanting it with far slower diffusion process. This will result in the decrease of the overall PCO efficiency. At the same time, numerous sharp edges and tips of needles and leaflets, when protruding into the turbulent core of the moving liquid, serve as local turbulence sources.

In case of RNO, the increase of PCO efficiency results from the increased amount of hydroxyl radicals produced by the photocatalyst surface that (or the vicinity of which) can be readily reached by RNO molecules; this way, the relative degradation rate of RNO by various ZnO samples shows their hydroxyl radical production ability in relative terms. Two most hydrophilic samples – S-2 and S-1 – showed the best performance in RNO PCO; interestingly, third most hydrophilic object – S-3 – showed no detectable RNO degradation, whereas some amount of RNO was degraded by the least hydrophilic object (S-4) as well. This can be explained by the surface geometry obstacles.

The adsorption results of RNO (see Table 3) show that although higher adsorption in case of S-2 (rods) could be connected with higher PCO efficiency, then e.g. S-1 (needles), which showed relatively good PCO efficiency exhibited no adsorption, and on the contrary, S-5 (pyramids with leaflets and needles) shows no RNO oxidation, although its adsorption there is four times higher than in case of S-4 (pyramids). As RNO is degraded by hydroxyl radicals, it may be assumed that in case of the hierarchical structures, the needles and leaflets could be producing various peroxy radicals, as opposed to hydroxyl radicals production by the plain structures; however, these are the needles and leaflets where the adsorption of RNO is likely to take place due to hydrodynamic and geometry obstacles described above, or at least where RNO molecules can get sufficiently close to the ZnO surface, into what we may call radical mist, i.e. the zone where radical species formed on the catalyst surface exist during their lifetime. When compared to PL results, it can be seen that in case of RNO the best PCO performance was provided by object with the highest exciton content, i.e. S-2.

To conclude with RNO PCO, it can be stated that its results show the comparative hydroxyl radical production ability by the ZnO objects (at least the production of OH-radicals available for RNO degradation), and it was shown in most cases to be significantly higher than that of P25 TiO₂.

3.6.3. Humic acid

With humic acid, the results obtained with several of ZnO objects showed performance comparable or inferior to P25: while P25 immobilised on glass substrate showed $4.1 \text{ mg W}^{-1} \text{ h}^{-1}$, the result of S-2 (rods) and S-4 (pyramids) was $1.5 \text{ mg W}^{-1} \text{ h}^{-1}$, and that of S-1 (needles) was $4.5 \text{ mg W}^{-1} \text{ h}^{-1}$, while object S-5 (pyramids with leaflets and needles) showed no HA degradation. The results can be seen in Fig. 6.

HA has been reported in the literature to be a radical scavenger, this way, it can react to certain extent with different radical types, but the majority of HA's degradation

should originate from surface reactions of pre-adsorbed molecules, when possible. As in case of RNO, sample S-5 (pyramids with needles and leaflets), that supposedly produces small amounts of hydroxyl radicals vs. peroxy radicals, showed no detectable HA degradation. Sample S-3 (rods and needles), having the same radical production issues, on the other hand, showed performance second to needle structure (S-1) only. Thus, from HA PCO performance it can be seen that from ZnO objects it is oxidised best by needle-containing structures that have also shown their ability to produce hydroxyl radicals. The best performance of S-1 should likely be also attributed to this object's ability to adsorb certain amounts of HA. But on the whole, as the adsorption on the surface of ZnO objects is poor, their PCO performance was also mediocre.

It appears that HA PCO can be connected to the relative amount of the ZnO objects' surface defects and adsorption: S-1, providing both adsorption of HA and relatively high defect amount, is most efficient in HA degradation. It is followed by S-3, where no adsorption of HA could be experimentally determined, but where there is still sufficient number of defects, that can produce radicals, which, in the vicinity of the photocatalyst surface, can degrade HA.

3.6.4. PNL

With PNL, several experiments with ZnO layers were made, showing results inferior to that of P25 titanium dioxide (6.2 at best with S-3 compared to $10.2 \text{ mg W}^{-1} \text{ h}^{-1}$). While S-5 showed no detectable PNL degradation, the results of S-1, S-3 and S-4 were comparable, but still inferior to those of P25 (see Fig. 6). These results bear a certain similarity to the case of HA, suggesting similarities in degradation mechanism: indeed, PNL was also shown to be more sensitive towards oxidation on photocatalyst surface [34].

3.6.5. Comparison

When comparing the action of ZnO samples towards the substances under scope, it can be seen that objects S-4 and S-5 seem to have less hydroxylated surface, resulting in smaller production of OH-radicals, and, consequently, no or low observable RNO degradation, whereas other objects appear to produce hydroxyl radicals (i.e. reachable by the substrates to be degraded) in the relative amount described by the descending row S-2 > S-1 > S-4; S-3, which has relatively hydrophilic surface and should thus produce more hydroxyl radicals, showed no observable RNO degradation likely due to surface geometry obstacles (total radicals production vs. the amount of radicals readily available for reactions). On the other hand, MTBE, although recalcitrant towards conventional oxidation methods, was shown earlier to yield well to PCO with various photocatalysts [33,39], which had different surface properties, including hydrophobicity [39], although in the earlier studies more hydrophilic catalysts showed in general better performance; this way, it can be concluded that MTBE oxidises well with various radical species. With HA and RNO, oxidised mostly by surface reactions upon adsorption, or at least in the closest vicinity of the photocatalyst surface, greater surface area coupled with the ability of the surface to produce radical species results in greater PCO efficiency, as it was seen in case of needle-containing structures. Generally, with the

increase of molecule size, plain structures seem to be more favoured in both adsorption and photocatalytic activity, allowing to suggest greater obstacles in larger molecules (among the investigated ones) adsorption on the hierarchical objects. The availability of both surface defects and excitons seem to produce favourable conditions for PCO, depending on the substrate: if MTBE, HA and RNO were better degraded with photocatalysts possessing greater relative abundance of surface defects (serving as charge carrier traps and thus improving overall PCO performance), then in case of RNO object with the highest relative exciton content (together with highest hydrophilicity, meaning better OH-radical production) has shown the best performance. It must be noted that the different properties of the photocatalytic materials discussed here do not influence PCO performance in a discrete manner, but should be viewed as an interdependent complex, together with the properties of degradation substrates.

To sum up, the activity of the photocatalysts towards various substrates depends on a combination of several factors, some of them interconnected; the most important (and perhaps equally important) of these are: (a) oxidant production ability, dependent on semiconductor defects, such as oxygen vacancies, and surface hydroxylation: this accounts for the total possible oxidant production, whereas surface morphology regulates the amount of oxidants available for surface reaction; (b) hydrodynamic aspects, which should be viewed together with surface morphology, and which regulate the amount of oxidants readily available for substrate degradation in the vicinity of the photocatalyst surface; (c) the ability of photocatalyst to adsorb degradation substrates, which depends on both structure characteristics and morphology; greater surface area does not immediately result in greater adsorption, whereas increased adsorption does not mean increased degradation rate: it is adsorption at or in the closest vicinity of oxidant-producing sites that will result in improved photocatalytic oxidation results. A photocatalyst with unselective performance should have highly hydroxylated surface (enabling the production of more potent hydroxyl radicals) and neutral surface; surface area should be sufficiently high to provide good adsorption at the oxidant-producing sites (surface defects), and at the same time be able to provide as little as possible hydrodynamic obstacles for the transfer of both substrate molecules and radical oxidants in the vicinity of the photocatalyst surface. Judging from the available results, needle-containing structures seem to combine the abovementioned qualities to the highest extent among the objects studied in this research.

4. Conclusions

In this research, five ZnO layers with both plain (3) and hierarchical (2) structure were synthesised; their properties were investigated using XRD and SEM, and their activity assessed by aqueous photocatalytic oxidation (PCO) of four organic substrates with different structure: methyl-tert-butyl ether (TBE), humic acid (HA), N,N-dimethyl p-nitrosoaniline (RNO), and prednisolone (PNL). The results obtained with ZnO object were compared to those of P25 Evonik TiO₂. Different trends observed in the substrates' PCO were explained by the differences in the objects' surface morphology, relative

production of various radical species, and different properties of the substrates.

It was found that the degradation ability (PCO) of ZnO layers differed significantly depending on the degradation substrate. MTBE was the most efficiently degradable compound by ZnO layers irrespective of their initial morphology. Hierarchical layers either grown on the rod or pyramidal shaped crystals showed at least three times better performance compared to P25. Oppositely to MTBE, RNO was effectively degraded by plain structures, namely needles, plain rods or pyramid-shaped crystals without any detectable degradation by hierarchical structures: the performance bare rods exceeded that of TiO₂ (P25) 45 times. In case of humic acid (HA), ZnO with needle-like morphology is most efficient sample showing very similar degradation ability to P25 TiO₂. PNL was the least degradable by ZnO layers. The degradation ability is at least two times lower than that of P25.

The observed differences were explained by the different character of oxidising species produced by the ZnO objects, and different interactions of these with the substances under scope. This, in turn, depends on the relative amount of surface defects, surface morphology and hydroxylation of the ZnO structures' surface. Among the structures analysed in this study, needle-containing ZnO objects appear to possess a combination of these qualities. As a result, this is a material with efficient and at the same times the least selective performance towards different substrates in this study. This allows suggesting that objects with similar morphology, surface properties and structure should be given a more detailed study as both highly efficient and potentially universal photocatalysts, overcoming one of the main obstacles in successful photocatalytic oxidation implementation at a wider scale, i.e. the selective performance of the process towards different compounds. A determination of the photocatalyst properties optimisation direction, thus provided, is tied to the respective synthesis conditions, the optimisation of which, as a final outcome, would result in the creation of the desired ideal or near-ideal photocatalyst, having highly efficient and non-selective performance.

Acknowledgements

The authors would like to express their gratitude to Dr. Natalja Savest for surface wettability measurements. This authors would like to thank the Estonian Ministry of Education and Research institutional research funding projects IUT1-7 and IUT19-4, Estonian Science Foundation Grants (GUS10, G8978), European Regional Development Fund through the projects: Centre of Excellence "Mesosystems: Theory and Applications" (MESO) TK114, 3.2.0101.11-0029, project "Efficient plasmonic absorbers for solar cells" 3.2.1101.12-0023 and US Civilian Research and Development Foundation Grant ESC2-2974-TL-09 for the financial support of this research.

References

- [1] Z.Z. Han, L. Liao, Y.T. Wu, H.B. Pan, S.F. Shen, J.Z. Chen, J. Hazard. Mater. 217 (2012) 100–106.
- [2] F. Lu, W.P. Cai, Y.G. Zhang, Adv. Funct. Mater. 18 (2008) 1047–1056.
- [3] D. Perednis, L.J. Gauckler, J. Electroceram. 14 (2005) 103–111.
- [4] T. Dedova, M. Krunk, O. Volobujeva, I. Oja, Phys. Status Solidi C 2 (2005) 1161–1166.
- [5] M. Okuya, K. Nakade, S. Kaneko, Sol. Energy Mater. Sol. Cells 70 (2002) 425–435.
- [6] W.-W. Wang, Y.-J. Zhu, L.-X. Yang, Adv. Funct. Mater. 17 (2007) 59–64.
- [7] S. Ma, R. Li, C. Lv, W. Xu, X. Gou, J. Hazard. Mater. 192 (2011) 730–740.
- [8] L. Sun, D. Zhao, Z. Song, C. Shan, Z. Zhang, B. Li, D. Shen, J. Colloid Interface Sci. 363 (2011) 175–181.
- [9] P. Amornpitoksuk, S. Suwanboon, S. Sangkanu, A. Sukhoom, N. Muensit, Superlattice Microstruct. 51 (2012) 103–113.
- [10] Y. Cui, C. Wang, G. Liu, H. Yang, S. Wu, T. Wang, Mater. Lett. 65 (2011) 2284–2286.
- [11] R. Mohan, K. Krishnamoorthy, S.-J. Kim, Solid State Commun. 152 (2012) 375–380.
- [12] S.-M. Lam, J.-C. Sin, A.Z. Abdullah, A.R. Mohamed, J. Mol. Catal. A 370 (2013) 123–131.
- [13] Y. Liu, J. Han, W. Qiu, W. Gao, Appl. Surf. Sci. 263 (2012) 389–396.
- [14] Y. Wang, X. Li, N. Wang, X. Quan, Y. Chen, Separation Purif. Technol. 62 (2008) 727–732.
- [15] C.K. Yeh, J.T. Novak, Water Environ. Res. 66 (1994) 744–752.
- [16] A. Safarzadeh-Amiri, Water Res. 35 (2001) 3706–3714.
- [17] P.C. Johnson, Environ. Sci. Technol. 32 (1998) 276–281.
- [18] X.R. Xu, Z.Y. Zhao, X.Y. Li, J.D. Gu, Chemosphere 55 (2004) 73–79.
- [19] M.E. Simonsen, J. Muff, L.R. Bennedsen, K.P. Kowalski, E.G. Sogaard, J. Photochem. Photobiol. A 216 (2010) 244–249.
- [20] E. Portjanskaja, K. Stepanova, D. Klauson, S. Preis, Catal. Today 144 (2009) 26–30.
- [21] S.E. Manahan, Environmental Chemistry, 6th ed. CRC Press/Lewis Publishers, New York, 1994.
- [22] B.R. Eiggins, F.L. Palmer, J.A. Byrne, Water Res. 31 (1997) 1223–1226.
- [23] G.S. Wang, C.H. Liao, F.J. Wu, Chemosphere 42 (2001) 379–387.
- [24] H. Chang, J.Y. Hu, B. Shao, Environ. Sci. Technol. 41 (2007) 3462–3468.
- [25] T. Dedova, I.O. Acik, M. Krunk, V. Mikli, O. Volobujeva, A. Mere, Thin Solid Films 520 (2012) 4650–4653.
- [26] M. Krunk, T. Dedova, E. Karber, V. Mikli, I.O. Acik, M. Grossberg, A. Mere, Physica B 404 (2009) 4422–4425.
- [27] T. Dedova, M. Krunk, I.O. Acik, D. Klauson, O. Volobujeva, A. Mere, Mater. Chem. Phys. 141 (2013) 69–75.
- [28] T. Dedova, J. Klauson, C. Badre, T. Pauporte, R. Nisumaa, A. Mere, O. Volobujeva, M. Krunk, Phys. Stat. Solidi A 205 (2008) 2355–2359.
- [29] T. Dedova, O. Volobujeva, J. Klauson, A. Mere, M. Krunk, Nanoscale Res. Lett. 2 (2007) 391–396.
- [30] T. Dedova, M. Krunk, I. Gromyko, V. Mikli, I. Sildos, K. Utt, T. Unt, Phys. Status Solidi A 211 (2014) 514–521.
- [31] M. Krunk, T. Dedova, I. Oja Acik, Thin Solid Films 515 (2006) 1157–1160.
- [32] M. Krichevskaya, A. Kachina, T. Malygina, S. Preis, J. Kallas, Int. J. Photoenergy 5 (2003) 81–86.
- [33] D. Klauson, E. Portjanskaja, O. Budarnaja, M. Krichevskaya, S. Preis, Catal. Commun. 11 (2010) 715–720.
- [34] D. Klauson, J. Piinik-Sudareva, N. Pronina, O. Budarnaja, M. Krichevskaya, A. Kaekinen, K. Juganson, S. Preis, Cent. Eur. J. Chem. 11 (2013) 1620–1633.
- [35] S. Preis, M. Krichevskaya, Y. Terentyeva, A. Moiseev, J. Kallas, J. AOTS 5 (2002) 77–84.
- [36] E. Kaerber, T. Raadik, T. Dedova, J. Krustok, A. Mere, V. Mikli, M. Krunk, Nanoscale Res. Lett. 6 (2011).
- [37] J.T. Carneiro, T.J. Savenije, J.A. Moulijn, G. Mul, J. Phys. Chem. C 115 (2011) 2211–2217.
- [38] B. Sun, M. Sato, J.S. Clements, J. Electrostat. 39 (1997) 189–202.
- [39] D. Klauson, E. Portjanskaja, S. Preis, Environ. Chem. Lett. 6 (2008) 35–39.
- [40] A.G. Agrios, P. Pichat, J. Photochem. Photobiol. A 180 (2006) 130–135.
- [41] R. Enriquez, A.G. Agrios, P. Pichat, Catal. Today 120 (2007) 196–202.
- [42] W. Bors, C. Michel, M. Saran, Eur. J. Biochem. 95 (1979) 627.

Publication IV

I. Gromyko, M. Krunk T. Dedova, A. Katerski, D. Klauson, I. Oja Acik, Surface properties of sprayed and electrodeposited ZnO rod layers. *Appl. Surf. Sci.* 405 (2017) 521–528.



Contents lists available at ScienceDirect

Applied Surface Science

journal homepage: www.elsevier.com/locate/apsusc

Full Length Article

Surface properties of sprayed and electrodeposited ZnO rod layers



I. Gromyko, M. Krunk, T. Dedova*, A. Katerski, D. Klauson, I. Oja Acik

Department of Materials and Environmental Technology, Tallinn University of Technology, Ehitajate tee 5, 19086 Tallinn, Estonia

ARTICLE INFO

Article history:

Received 17 August 2016
 Received in revised form 30 January 2017
 Accepted 9 February 2017
 Available online 13 February 2017

Keywords:

ZnO rods
 Chemical spray pyrolysis
 Electrodeposition
 XPS
 Wettability
 Photocatalytic oxidation

ABSTRACT

Herein we present a comparative study on as-deposited, two-month-stored, and heat-treated ZnO rods obtained by spray pyrolysis (SP) at 550 °C, and electrodeposition (ED) at 80 °C. The aim of the study is to establish the reason for different behaviour of wettability and photocatalytic activity (PA) of SP and ED rods. Samples were studied using XPS, SEM, XRD, Raman, contact angle (CA) measurements and photocatalytic oxidation of doxycycline.

Wettability and PA are mainly controlled by surface composition rather than by morphology. The relative amount of hydroxyl groups on the surface of as-deposited ED rods is four times higher compared to as-deposited SP rods. Opposite to SP rods, ED rods contain oxygen vacancy defects (Vo). Therefore, as-deposited ED rods are superhydrophilic (CA ~ 3°) and show highest PA among studied samples, being three times higher compared to SP rods (removing of 75% of doxycycline after 30 min). It was revealed that as-deposited ED rods are inclined to faster contamination. The amount of C=C groups on the surface of aged ED rods is six times higher compared to aged SP rods. Stored ED samples become hydrophobic (CA ~ 120°) and PA decreases sharply while SP rods remain hydrophilic (CA ~ 50°), being more resistive to the contamination.

© 2017 Elsevier B.V. All rights reserved.

1. Introduction

ZnO is one of the most important n-type semiconducting material with a wide band gap (3.37 eV) and a large exciton binding energy of 60 meV at room temperature [1]. Due to its superior inherent properties and other benefits including non-toxicity, low cost, high electronic conductivity, and ease of fabrication with a diversity of nanostructures ZnO has already found numerous applications in optoelectronic devices, such as solar cells [2], light-emitting diodes [3], gas sensors [4]. Due to controllable and peculiar wetting properties, great attention has recently been devoted to the ZnO for the development of photocatalytic, self-cleaning, antifogging coatings [5–7]. Also ZnO nanomaterials have gained enormous interest in biomedical applications, such as biomedical imaging, drug delivery, gene delivery, and biosensing [8].

According to the literature, wettability may depend on both the geometry and the chemical composition of the surface [9,10], these in turn depend on deposition method and growth conditions. A number of techniques for the deposition of ZnO nanostructures have been reported, including hydrothermal growth [11], chem-

ical bath deposition [12], chemical vapor deposition [13], chemical spray pyrolysis (SP) [14], electrodeposition (ED) [15]. The various deposition methods listed here have their own individual advantages and disadvantages.

For this study we have chosen SP and ED methods for a number of reasons. Both methods are technologically attractive, being fast, simple, and low-cost techniques, capable of being scaled up for producing large area coatings. In both cases ZnO rods are obtained from similar precursor, ZnCl₂. SP rods are obtained by spray of the solution onto preheated substrates; growth temperatures 500 °C and above are used [14,16]. ED rods deposition is usually performed at significantly lower temperatures around 80 °C in an aqueous solution [15,17]. Wetting properties of SP ZnO layers have yet to be studied in detail [18], whereas wettability of electrodeposited ZnO rods is studied to a certain extent [10,15,19–21].

Our systematic study on wettability of ZnO rods revealed the difference in wettability of ZnO ED and SP rods after deposition and within storage time. Technological details for preparation of ZnO nanostructures with desired morphology by these two methods are studied well. Therefore, we obtained ZnO nanostructures with similar surface morphology and surface area and studied the influence of the surface chemical composition on wettability and photocatalytic activity.

* Corresponding author.

E-mail address: tatjana.dedova@ttu.ee (T. Dedova).

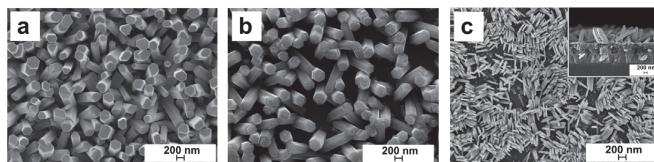


Fig. 1. SEM micrographs of (a) SP ZnO rods on ITO/glass substrate (A-type), (b) ED ZnO rods on ITO/glass substrate (B-type), (c) ED ZnO rods on TiO₂/ITO/glass substrate (C-type), the inset shows the corresponding SEM cross-section micrograph.

Table 1
Summary of dimensional parameters (Length-L, Diameter-D, nm), density of crystals, surface area of ZnO rods and preferred orientation of crystallites for ZnO rod layers.

Sample	Dimensions		Density of crystals, pcs/cm ²	Surface area, cm ² /cm ²	Preferred crystallographic orientation
	L, nm	D, nm			
SP (A-type)	750	300	6.25E+08	~4	(002)
ED (B-type)	950	350	3.44E+08	~4	(002)
ED (C-type)	450	70	1.75E+09	~2	(101)

Here we present a complex study containing full overview on the SP and ED layer properties. The aims of this work are: 1) to gain a deeper understanding of as-deposited, aged, and heat-treated SP and ED rod layers properties including surface chemical composition, wettability, morphology, crystallinity 2) to define the major factors that determine the wettability and photocatalytic performance of the ZnO rods layers. The relationship between wettability, surface composition and photocatalytic activity of as-deposited, aged, and heat-treated samples is established.

2. Experimental

2.1. Samples preparation

In this study we investigate three types of the ZnO rod samples: A – sprayed on ITO/glass substrate, B – electrochemically deposited on ITO/glass substrate, C – electrochemically deposited on TiO₂/ITO/glass substrate. ITO/glass substrates with ITO thickness of 150 nm were purchased from Zentrum Sonnenenergie and Wasserstoff Forschung (ZSW). Each sample was studied right after the deposition (as-deposited), then, after two weeks and again after two months of storage in plastic boxes in the dark at room temperature. To study the reversibility of ZnO rod layers from hydrophobic to the initial superhydrophilic stage, two-month-aged samples were annealed at 400 °C for 30 min in the air.

Previous studies have described SP set-up for ZnO rods deposition in detail [16]. 50 mL of aqueous solution of ZnCl₂ (Sigma Aldrich) with a concentration of 0.05 M was sprayed onto the heated substrates. The ZnO growth temperature was maintained at 550 °C. The solution spray rate and carrier gas (compressed air) flow rate were 2.4 mL/min and 8 L/min, respectively.

ED ZnO rods deposition has been performed in accordance with previous studies [15,17]. ED was carried out in a three-electrode glass cell: the ITO/glass and TiO₂/ITO/glass were used as a working electrode, the Ag/AgCl 3 M KCl and the platinum wire were used as reference and counter electrodes, respectively. ZnO ED rods were grown from 0.2 mM aqueous solution of ZnCl₂ together with 0.1 M KCl solution saturated with O₂ under –1.0 V potential using Radiometer Analytical potentiostat PGP201. The growth temperature was kept at 80 °C. Deposition time was fixed to 45 min.

In order to deposit ZnO rod on TiO₂/ITO substrates, TiO₂ seed layer was prepared by SP method using the spray solution containing titanium (IV) isopropoxide, acetylacetone and ethanol. Deposition was carried out at a substrate temperature of 450 °C employing 1–125 spray pulses (1 s spray and 30s pause) [22].

2.2. Characterization

The surface morphology of the ZnO layers was examined using a high resolution scanning electron microscope (SEM), Zeiss HR FESEM Ultra 55, at an acceleration voltage of 1.5 kV. To calculate and compare the surface areas of SP and ED rods, high resolution SEM micrographs were used. Dimensions of the crystals, their average open surface area were calculated from 3 intentionally chosen places of SEM image (plane and cross-sectional views) from area of 2 × 2 μm². The surface area of one ZnO crystal was calculated according to the cylinder surface area (CSA) formula excluding one bottom surface, $CSA = \pi r^2 + 2\pi rh$. The density of the crystals has been counted from 10 × 10 μm² area.

X-ray diffraction (XRD) patterns were recorded on a Rigaku Ultima IV diffractometer operated at 40 kV and at 40 mA (CuKα radiation, λ = 1.5406 Å) using the D/teX Ultra silicon strip detector and a rotating sample holder. ZnO XRD reflections were indexed according to JSPDS card no. 80-0074. The wettability of the films was evaluated by the water contact angle (CA) measurements on a DSA 25 (KRÜSS Instrument) at room temperature, using the sessile drop fitting method. At least three spots per substrate were averaged. X-ray photoelectron spectroscopy (XPS) study was performed on the Kratos Analytical AXIS ULTRA DLD spectrometer fitted with the monochromatic Al Kα X-rays source and the achromatic Mg Kα/Al Kα dual anode X-ray source. All the spectra have been charge-corrected by taking C1s peak (BE = 285.0 eV) as reference. Raman spectra of the films were recorded at room temperature on a Horiba's Lab Ram HR800 spectrometer using laser line at 532 nm that was focused on the sample with spot diameter of 200 μm.

Photocatalytic activity of ZnO samples was measured through the photocatalytic oxidation (PCO) of doxycycline (DC) (initial concentration 25 mg L⁻¹). These experiments were carried out in a 20-mL batch reactor equipped with a 2.7 W UVA-LED (LZ1-UV00, LED Engin Inc.), providing radiation at 365 ± 5 nm with the irradiance intensity of 7.5 mW cm⁻², measured by Ocean Optics UV-VIS-ES-2000+ radiometer equipped with cosine corrector. The reactor was thermostatted at 20 ± 0.5 °C by cooling water jacket. ZnO sample area was 2.5 cm². The experimental time was chosen to be 4 h in accordance to the earlier studies [14,23].

3. Results and discussion

3.1. Morphology and structural properties

In this study we have chosen three types of ZnO rod samples: A, B and C (details are given in the experimental part). Samples A and

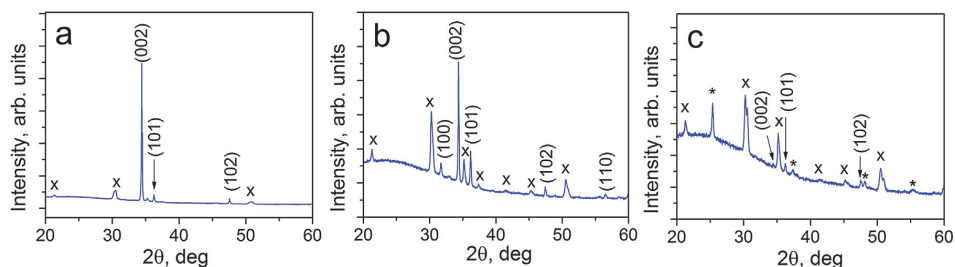


Fig. 2. XRD patterns of (a) SP ZnO rods on ITO substrate (A-type), (b) ED ZnO rods on ITO substrate (B-type), (c) ED ZnO rods on TiO₂/ITO substrate (C-type); x-ITO, *-TiO₂.

Table 2

Contact angle values of as-deposited, aged (stored in plastic boxes), and annealed ZnO rods.

Sample	As-deposited	Two-week-aged	Two-month-aged	Annealed
SP (A-type)	CA ~ 12° 	CA ~ 40° 	CA ~ 50° 	CA ~ 9° 
ED (B-type)	CA ~ 3° 	CA ~ 112° 	CA ~ 120° 	CA ~ 3° 
ED (C-type)	CA ~ 5° 	CA ~ 104° 	CA ~ 111° 	CA ~ 7° 

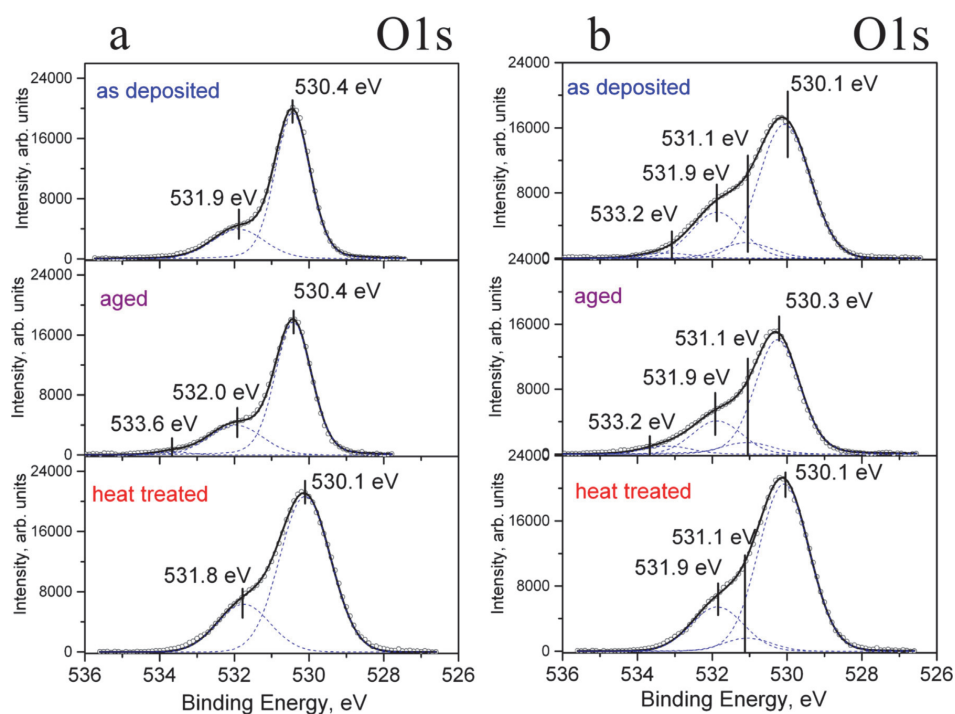


Fig. 3. XPS spectra of as-deposited, aged, and heat-treated at 400 °C in air ZnO rod samples in the binding energy region of O1s; (a) SP rods (A-type) and (b) ED rods (B-type).

B (Fig. 1a, b) have similar morphology, where elongated hexagonal rod-like ZnO crystals are perpendicularly attached to the substrate. A and B both have nearly similar surface areas of ca. 4 cm²/cm². Sample C (Fig. 1c) differs in morphology compared to A and B, C

is composed of randomly distributed ZnO rods tilted towards the substrate.

The dimensions, density of the crystals on a substrate, surface area and preferable crystallographic orientation of the ZnO rods are summarized in Table 1.

Fig. 2 shows the XRD patterns of all three types of ZnO rod layers studied here. The most intensely sharp (002) reflection peak at $2\theta = 34.39^\circ$ of A and B rods reveals high crystallinity and strong c-axis orientation of both SP and ED rods deposited on ITO/glass substrate. Intensity ratio of XRD peaks, $I_{(002)}/I_{(101)}$, is 24.5 for A-rods and 3.5 for B-rods, indicating that the SP deposited rods have much stronger c-axis orientation compared to ED rods. In contrast to A and B, preferred crystallographic orientation of C-type ZnO rods is along the (101) plane, parallel to the substrate, the (002) reflection peak, at $2\theta = 34.39^\circ$, is barely visible in the XRD pattern of sample C. XRD study is in a good correspondence with SEM images, where it is clearly seen that A and B rods are only slightly tilted and positioned almost vertically on the substrate, whereas C rods are nearly parallel to the substrate surface (according to SEM cross-section image shown as inset in Fig. 1c, tilting angle of C-rods is ca. 45°).

3.2. Wettability

Surface wettability of the ZnO rod layers was investigated by measuring the static water contact angle (CA). Table 2 summarizes the average water CAs values together with the droplet photos of the as-deposited, two-week and two-month-stored in plastic boxes and annealed at 400°C rods of A, B and C-type.

According to the results, as-sprayed ZnO rods are hydrophilic in nature with CA of ca. 12° . These values are close to earlier reported for as-deposited ZnO nanostructured layers (CA of $11\text{--}13^\circ$) produced by spray from zinc acetate solutions [18].

Both electrochemically as-grown ZnO rod samples B and C are superhydrophilic ($CA \leq 5\text{--}10^\circ$ [13]) showing contact angle values of 3° and 5° , respectively. These data are in a good correspondence with Th. Pauporté's studies, where superhydrophilic behavior of electrodeposited ZnO rods (CA of ca. 2° or less) was reported [15,20]. The contact angles of B and C are nearly similar in spite of such a significant difference in crystals orientation and size. This means that in our study the surface geometry (crystals orientation, shape, "exposed" planes, distribution) has a minor effect on the surface wetting properties. There are number of studies in the literature that support this observation. For example, K. Yadav et al. [24] reported that morphology of the nanostructures does not play a significant role in their wetting behaviour, but the defects in the material may control the wettability. They reported that CA of the oxygen-rich, oxygen-deficient and highly oxygen-deficient In_2O_3 nanowires with similar morphology was 8° , 134° and 168° , respectively [24].

Further, after keeping the samples in a plastic box for two weeks the difference in wetting behaviour of ED and SP deposited rods becomes more pronounced (Table 2). ED rods independent of the crystals orientation showed a hydrophobic nature having a contact angle of 112° and 104° for samples B and C, respectively. In a contrast, the SP rod sample had smaller CA change from 12° to 40° after two weeks of storage in a plastic box. Longer storage time (two months) in a plastic box did not change the wetting behaviour of the SP and ED rods noticeably. CA of SP rods has increased up to 50° and CA of ED rods has also increased slightly, up to 120° and 111° for samples B and C, respectively. Thus, SP rods remained hydrophilic even after two months of storage time. Similarly to ED rods, the wettability of hydrothermally grown rods have been reported to change from superhydrophilic ($CA \sim 0^\circ$) to superhydrophobic ($CA \sim 150^\circ$) upon storage during 20 days in the dark [25].

Reverse hydrophilic behaviour for all studied types of the rods was detected after heat treatment of the samples at 400°C for 30 min in air (Table 2). The water CAs decreased so remarkably that ZnO rods surface turned back to highly hydrophilic stage. Again, CA of SP rods has shown slightly higher values ($CA \sim 9^\circ$) compared to

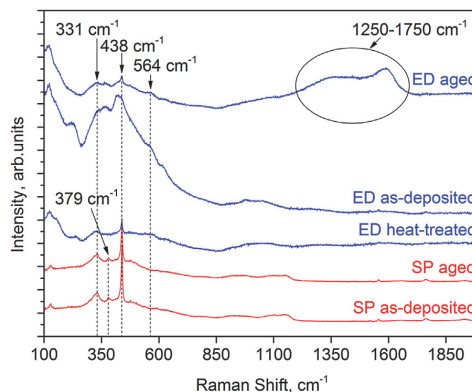


Fig. 4. Raman spectra of as-deposited, aged, and heat-treated ED and SP ZnO rod layers. Raman peaks located at 438 cm^{-1} and 379 cm^{-1} are attributed to the E_2 (high) and A_1 (TO) Raman modes of wurtzite phase of ZnO, respectively [35].

ED ZnO rods ($CA \sim 3^\circ$). Obtained values of heated samples are very close to the CA values of as-deposited ones. Reversibility of the wetting properties from hydrophobic to hydrophilic state is very common feature for ZnO rods obtained by solution methods after heating [13,26] or UV illumination [27].

3.3. XPS study

The surface composition of as-deposited, aged and heat-treated SP (A-type) and ED grown rods (B-type) was investigated by XPS analysis. Herein the O1s and C1s core level spectra are presented only. Those spectra are of greatest interest for the evaluation of chemical composition, presence and nature of defects, and degree of surface contamination.

3.3.1. O1s core level spectra

Fig. 3 represents the O1s core level spectra of as-deposited, aged and heat-treated ZnO rods samples obtained by spray (a) and electrodeposition (b).

The asymmetric O1s core level peaks were deconvoluted using Lorentzian-Gaussian (function pseudo-Voigt) fitting analysis.

In the O1s core level spectra of as-deposited SP ZnO rods samples the peaks observed at binding energy (BE) values of $530.4 \pm 0.3\text{ eV}$ and $531.9 \pm 0.1\text{ eV}$ are ascribed to the Me-O bond [28] and to the surface hydroxyl ($-\text{OH}$) groups [29], respectively. The Me-O bond in our case originates from two oxides: ZnO and $\text{In}_2\text{O}_3:\text{Sn}$ (ITO). In order to calculate the atomic concentration of single Zn-O component, In-O part coming from the ITO substrate was deducted from the Me-O peak area. Atomic concentrations of all the components (Zn-O, Vo, $-\text{OH}$, H_2O) found in O1s core level spectrum of SP and ED ZnO rod samples were calculated from integrated areas of the O1s spectrum using Scofield's cross-sections. Atomic ratios of the components, $\text{OH}/\text{Zn-O}$ and $\text{Vo}/\text{Zn-O}$, are summarized in Table 3.

Relative amount of hydroxyl groups remains almost similar during all modification steps for SP rods (See Table 3). On the spectrum of the aged SP ZnO rods sample a low intensity peak at BE of 533.6 eV was found. This peak is usually assigned to the oxygen bonds with carbon, C-O and C=O or H_2O , and disappears from the O1s spectra of heat-treated SP rods (Fig. 3a) [30,31].

In the O1s core level spectrum of as-deposited ED ZnO rods sample, the peaks at BE of $530.1 \pm 0.2\text{ eV}$ is ascribed to Me-O [28], at 531.1 eV to the oxygen deficient region i.e. oxygen vacancies (Vo) [1,32,33,34], at 531.9 eV to the surface hydroxyl groups [29], and

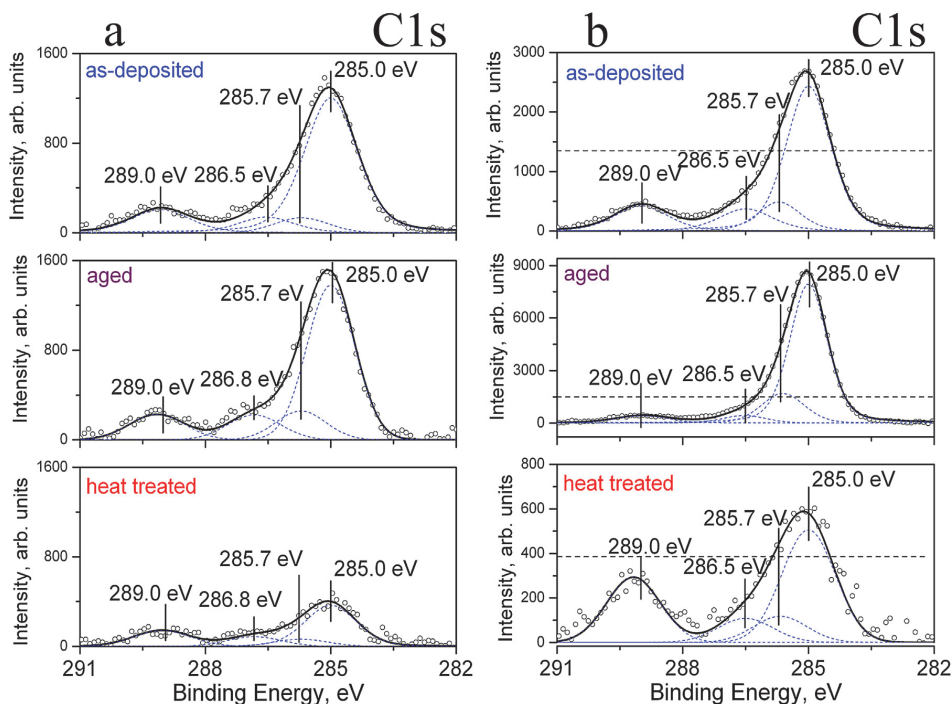


Fig. 5. XPS spectra of as-deposited, aged, and heat-treated at 400C in air ZnO rod samples in the C1s binding energy region, (a) SP rods (A-type) and (b) ED rods (B-type). Note: Scale is different. Dashed lines on ED C1s spectra correspond to the peak maximum of analogue SP rods.

Table 3

XPS analysis data (atomic ratios of the OH/Zn-O and Vo/Zn-O) obtained from the O1s core level peaks.

	SP (A-type)			ED (B-type)		
	As-dep.	Two-month-aged	Annealed	As-dep.	Two-month-aged	Annealed
[OH]/[Zn-O], arb.units (at%/at%)	0.3	0.3	0.4	1.2	0.7	0.8
[Vo]/[Zn-O] arb.units (at%/at%)	–	–	–	0.4	0.3	0.2

the peak at BE of 533.2 ± 0.4 eV is associated with the C–O, C=O and H₂O species [30,31].

The main difference in the O1s spectra of SP and ED samples is the presence of a peak at BE of 531.1 eV in the case of ED rods independent of storage or treatment and an absence of this peak in the spectrum of SP rod samples (Fig. 3, Table 3).

PL and Raman studies provide additional confirmation about the defect nature of ED rods. Raman spectra of SP and ED rods are presented in Fig. 4. In addition to the main Raman modes at 331, 379 and 438 cm⁻¹ characteristic of both SP and ED samples, a wide band centred at 564 cm⁻¹ could be detected on Raman spectra of ED rods only. Raman shift located in the region of 560–580 cm⁻¹ is associated with the oxygen vacancy defect, Vo [35–37].

According to the PL spectra presented by different authors earlier [38], ED rods usually exhibit broad self-activated (SA) emission band at around 500 nm associated with oxygen vacancy defects, and weak near band edge (NBE) emission peak ($I_{NBE}/I_{SA} \sim 2$). In contrast to ED rods, SP rods show weak SA emission band and possess intense NBE band, the evidence of high crystalline quality ($I_{NBE}/I_{SA} = 30$ [35]). Thus, according to the PL and Raman data, the ED rods probably contain oxygen vacancy defects, and the O1s

core level peak at BE of 531.1 eV is likely associated with the oxygen vacancies, while SP rods have higher crystalline quality without those defects.

It has been reported in the literature that the oxygen vacancy defects possess enhanced adsorption energy and subsequently high capability to bind the hydroxyl groups [39,40]. That kind of interdependency between oxygen vacancies and hydroxyl groups on a surface is characteristic of ED rods, namely, the higher amount of Vo leads to the higher amount of OH on the sample surface (Table 3). For example, [Vo]/[Zn-O] = 0.4 and [OH]/[Zn-O] = 1.2 are characteristic of as-deposited ED rods; [Vo]/[Zn-O] = 0.2 and [OH]/[Zn-O] = 0.8 are characteristic of annealed ED rods.

In fact, XPS O1s spectra show that the relative difference of hydroxyl groups (RD_{OH}) for ED ZnO rods is four times higher compared to SP ZnO rods. RD_{OH} on the surface of ED and SP as-deposited rods was evaluated according to the following Eq. (1).

$$RD_{OH} \left(\frac{ED_{as-dep.}}{SP_{as-dep.}} \right) = \frac{\left(\frac{C_{Zn-OH}}{C_{Zn-O}} \right)_{ED}}{\left(\frac{C_{Zn-OH}}{C_{Zn-O}} \right)_{SP}} = \frac{1.2}{0.3} = 4.0 \quad (1)$$

It is also commonly accepted that in ED process the Zn(OH) $_n$ species are formed in the solution as an intermediate product prior to the dehydration of Zn(OH) $_n$ to ZnO [28]. In contrary to ED rods, the SP rods are fabricated at high temperature and relative amount of hydroxyl groups is expected to be lower (Table 3).

Results on XPS studies are in good correlation with the wettability studies showing that higher amount of hydroxyl groups contributes to higher hydrophilicity for as-deposited samples. According to the wettability studies, the CA for as-deposited SP rods (CA $\sim 12^\circ$) is higher than CA of as-deposited ED rods (CA $\sim 3^\circ$) (Table 2).

However, it seems that wettability cannot be directly connected to the amount of hydroxyl groups of aged samples. For example, relative amount of hydroxyl groups for aged ED sample is ca. two times higher than aged SP sample has (Table 3), but CA is 120° and 50° for aged ED and SP rods, respectively. Also, as-grown and aged SP rods have similar relative amount of hydroxyl group (Table 3), but CA values are higher for aged sample (Table 2). We assume that hydroxyl groups in aged samples are not active anymore, being inactivated by carbon species during storage. This assumption is strongly supported by the fact that CA values of both ED and SP samples drop down after thermal treatment, and the surfaces become hydrophilic, although no significant change is detected in relative amount of hydroxyl groups (Table 3). Thus, the relative amount of hydroxyl groups affects the wettability of as-deposited ZnO rods but not of aged samples.

3.3.2. C1s core level spectra

Fig. 5 represents the C1s core level spectra of as-deposited, aged, and heat-treated ZnO rods samples obtained by spray (a) and electrodeposition (b). The C1s core level spectra of SP and ED rods are resolved into four main peaks with BE of 285.0 eV, 285.7 eV, 286.5 ± 0.3 eV and 289.0 eV corresponding to the C=C, C–C/C–H, C–O–C/C–O and COOH/C=O, respectively [41].

Furthermore, we are focusing our discussion on hydrocarbon species (C=C, C–C/C–H) as these are more dominant over oxygen containing organics (C–O–C/C–O, COOH/C=O).

A common source of such unintentional contamination is the presence of hydrocarbons in ambient air. The concentrations of volatile organic compounds (VOCs; for example, alkanes, alkenes, aromatics and alcohols) in air are typically in the ppb to ppm range. Many surfaces are known to adsorb hydrocarbon from ambient air, including metals, TiO $_2$, SiO $_2$, etc. Such hydrocarbon adsorption decreases the surface energy of the substrate and increases its hydrophobicity, which is reflected as an increase of their CA [42].

The intensity of the C=C peak of two-month-aged ED sample is about three times higher than that of as-deposited ED sample (Table 4). At the same time the aging almost does not affect the intensity of the C=C peak of SP sample although some increase in C–O peak with BE at 286.8 eV could be observed (Fig. 5). In addition, Raman spectra of aged ED rods show broad bands in the region of 1250–1750 cm $^{-1}$ (Fig. 4), usually assigned to the C–C, C–H species [43]. Raman spectra of as-deposited ED rods and SP rods both do not exhibit any shift in that region. Consequently, XPS and Raman studies both confirm that as-deposited ED rods have higher inclination to be contaminated with carbon species compared to SP rods.

Those results are in a good accordance with the water contact angle measurements as SP rods remain hydrophilic even after two months of storage time (CA $\sim 50^\circ$), whereas ED rods turned from superhydrophilic to hydrophobic, CA increased from 3° to 120° upon aging. In agreement with Y. Liu et al. [44] and our XPS results, wettability alteration of ZnO rod layers from hydrophilic to hydrophobic state is associated with the adsorption of organic contaminants.

After thermal treatment the intensity of the C=C peak of ED sample decreases more than ten times and more than three times

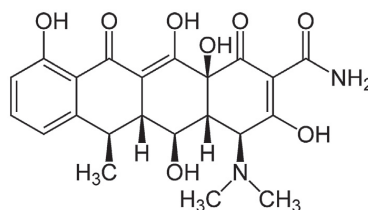


Fig. 6. Doxycycline molecule structure [23].

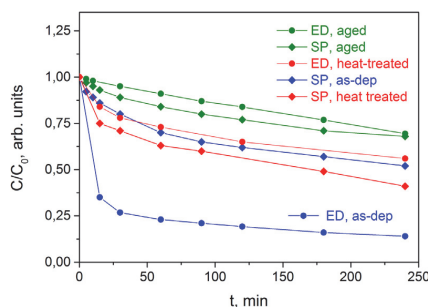


Fig. 7. Decrease of doxycycline normalised concentration in-time.

for the SP sample compared to the correspondent aged sample (Table 4). Additionally, the Raman spectrum of annealed after aging ED rods (Fig. 4) demonstrates that broadened peak in the region of 1250–1750 cm $^{-1}$ corresponding to C–C, C–H species, present in the spectrum of aged ED sample, disappears after heat treatment. Both annealed samples show reversible wettability behaviour, CA values dropped back down to the initial values independent of the ZnO rods type mainly due to the efficient removal organic contaminants from the sample surface upon annealing.

Thus, according to the wettability, XPS and Raman study, as-deposited ED rods contain higher amount of hydroxyl groups and Vo defects on a surface and, therefore, they are inclined to the faster and easier contamination by organic species from air and plastic boxes.

3.4. Photocatalytic activity of as-deposited, aged, and heat-treated samples

Photocatalytic activity of as-deposited, aged, and heat-treated (after two month aging) samples was studied using the removal of a tetracycline group antibiotic, doxycycline. Doxycycline molecule structure is presented in Fig. 6. The decrease of doxycycline normalised concentration within time is presented in Fig. 7.

According to Fig. 7, as-deposited ED rods have shown the highest photocatalytic activity among all the studied samples: ca. 75% of the initial amount of doxycycline was removed already after 30 min, with ca. 85% removal observed after the experimental time of 4 h under the influence of as-deposited ED rod sample. However, aging reduced the performance of the ED rods drastically: only 30% of the initial doxycycline was removed. The observed low photocatalytic activity of aged ED rods is caused by surface contamination of the sample. The surface of the aged rods is highly hydrophobic (CA $\sim 120^\circ$) being contaminated by airborne hydrocarbon species (XPS study) that can decrease doxycycline adsorption on the ZnO rods, and more importantly those hydrocarbons will be the primary targets for produced oxidants, leaving less of these for doxycycline.

Opposite to ED rods, photocatalytic activity of SP rods does not change markedly with aging of the samples. After the experimental

Table 4
Intensities (*I*) of C=C peaks at BE = 285 eV from C1s core level spectra for ZnO samples.

SP (A-type)			ED (B-type)		
As-dep. 1400	Two-month-aged 1500	Annealed 400	As-dep. 2700	Two-month-aged 9000	Annealed 600

time of 4 h, as-deposited SP rods removed ca. 50% of doxycycline, while the aged ones were able to remove ca. 30%. This is an additional complementation that the surface properties of SP rods do not change significantly.

Photocatalytic activity of ED rods is ca. three times higher than as-deposited SP rods. According to the wettability, XPS and Raman studies, as-deposited ED rods contain higher amount of hydroxyl groups and Vo defects on a surface. It is well-known in the literature that oxygen vacancies and hydroxyl groups make the surface hydrophilic or superhydrophilic and facilitate the trapping of photoinduced electrons and holes, thus enhancing the photocatalytic degradation process [29]. However, they may also effectively serve as adsorption sites for the airborne contaminants, most likely the VOCs, which leads to the long-term reduction of the ED rods' photocatalytic activity, observed in this study.

In order to study whether the PA activity of aged samples can be restored after heat treatment, aged ED and SP samples were annealed and corresponding PA tests were performed (Fig. 7). PA activity of annealed ED samples has slightly improved compared to aged ED sample (69 and 56% of doxycycline removed, respectively), but the original activity of the as-deposited samples was not restored. This result is in a correspondence with the XPS study, that shows that relative amount of OH groups and vacancies on a surface of annealed ED sample is still lower than that on as-deposited sample (Table 3). On the other hand, the annealing of aged SP rods was able to restore their PA to the level of as-deposited sample: 60% of the initial doxycycline was removed. Thus, according to the results obtained in this study, the reversibility in wettability was not accompanied by similar reversibility in photocatalytic activity of SP and ED ZnO rods.

4. Conclusions

In this work we have studied and compared the wettability, surface composition and photocatalytic activity of as-deposited, two-month-aged, and heat-treated electrodeposited (ED) and spray pyrolysed (SP) ZnO rods.

Our study is an instalment confirmation that the surface composition, namely, the amount of hydroxyl groups on a surface determine the wettability and photocatalytic properties of as-deposited samples making the surfaces hydrophilic and photocatalytically active. Opposite to as-deposited ZnO rods, impact of hydroxyl groups of aged samples is completely shaded by onsetting airborne hydrocarbon contamination within the storage time. Hydrocarbons onsetting on the surface make the surface of the aged ED rods hydrophobic and photocatalytically less active.

According to the XPS analysis, as-deposited ED ZnO rods samples contain four times higher amount of hydroxyl groups and defects such as oxygen vacancies, compared to analogue SP rods. Such surface composition makes the as-deposited ED rods highly hydrophilic (CA ~ 3°) and photocatalytically active. Ca. 75% of doxycycline, has been removed by as-deposited ED rods already after 30 min of treatment. However, as-deposited ED rods are inclined to become quickly contaminated from contact with the air and already after two weeks ED samples become hydrophobic with CA of 112°, and photocatalytic performance drops down four times.

ZnO spray deposited rods have good crystalline quality according to the XRD and Raman studies. However, the low number of hydroxide groups and absence of oxygen vacancy defects reduces

the photocatalytic performance of as-deposited SP ZnO rods. The photocatalytic activity of as-deposited SP ZnO rods is ca. three times lower than that of as-deposited ED rods (20% of doxycycline was removed after 30 min). However, the rate at which contaminants accumulate on a surface of SP rods is slower compared to ED, even after two months of storage the samples didn't change wettability significantly, the CA is 50° instead of 12° and photocatalytic performance is about 1.5 times lower for the two-month-aged spray rods compared to as-deposited ones.

The annealing of the rods restore the PA activity of SP rods and show only moderate improvement in case of ED rods. Consequently, significance of usage of the as-deposited layers for further manipulations or potential applications such as photocatalysis cannot be underestimated.

Acknowledgements

Dr. M. Danilson is thanked for recording the XPS spectra. Dr. V. Mikli is thanked for recording the SEM images.

This work is financially supported by the Estonian Ministry of Education and Research institutional research funding projects IUT 19-4 and IUT 1-7, European Regional Development Fund through the project: TK 141, Centre of Excellence: Advanced materials and high-technology devices for energy recuperation systems.

References

- [1] X. Zhang, J. Qin, Y. Xue, P. Yu, B. Zhang, L. Wang, R. Liu, Effect of Aspect Ratio and Surface Defects on the Photocatalytic Activity of ZnO Rods, *Sci. Rep.* 4 (2014) 4596.
- [2] M. Krunks, E. Karber, A. Katerski, K. Otto, I. Oja Acik, T. Dedova, A. Mere, Extremely thin absorber layer solar cells on zinc oxide rods by chemical spray, *Sol. Energy Mat. Sol. Cells* 94 (2010) 1191–1195.
- [3] S.J. Pearson, F. Ren, *Advances in ZnO-based materials for light emitting diodes*, *Curr. Opin. Chem. Eng.* 3 (2014) 51–55.
- [4] V. Galstyan, E. Comini, C. Baratto, G. Faglia, G. Sberveglieri, Nanostructured ZnO chemical gas sensors, *Ceram. Int.* 41 (2015) 14239–14244.
- [5] D. Klauson, I. Gromyko, T. Dedova, N. Pronina, M. Krichevskaya, O. Budarnaja, I. Oja Acik, O. Volobujeva, I. Sildos, K. Utt, Study on photocatalytic activity of ZnO nanoneedles, rods pyramids and hierarchical structures obtained by spray pyrolysis method, *Mater. Sci. Semicond. Process.* 31 (2015) 315–324.
- [6] S. Patra, S. Sarkar, S.K. Bera, R. Ghosh, G.K. Paul, Hydrophobic self-cleaning surfaces of ZnO thin films synthesized by sol–gel technique, *J. Phys. D: Appl. Phys.* 42 (2009) 075301.
- [7] M. Wen, L. Wang, M. Zhang, L. Jiang, Y. Zheng, Antifogging and icing-delay properties of composite micro- and nanostructured surfaces, *ACS Appl. Mater. Interfaces* 6 (2014) 3963–3968.
- [8] Y. Zhang, T.R. Nayak, H. Hong, W. Cai, Biomedical applications of zinc oxide nanomaterials, *Curr. Mol. Med.* 13 (2013) 1633–1645.
- [9] Y. Zhou, T. Hang, F. Li, M. Li, Anti-wetting Cu/Cr coating with micro-posts array structure fabricated by electrochemical approaches, *Appl. Surf. Sci.* 271 (2013) 369–372.
- [10] M. Li, J. Zhai, H. Liu, Y. Song, L. Jiang, D. Zhu, Electrochemical deposition of conductive superhydrophobic zinc oxide thin films, *J. Phys. Chem. B* 107 (2003) 9954–9957.
- [11] G. Kwak, M. Seol, Y. Tak, K. Yong, Superhydrophobic ZnO nanowire surface: chemical modification and effects of UV irradiation, *J. Phys. Chem. C* 113 (2009) 12085–12089.
- [12] M. Piech, T.L. Sounart, J. Liu, Influence of surface morphology on the wettability of microstructured ZnO-based surfaces, *J. Phys. Chem. C* 112 (2008) 20398–20405.
- [13] H. Luo, J. Ma, P. Wang, J. Bai, G. Jing, Two-step wetting transition on ZnO rods arrays, *Appl. Surf. Sci.* 347 (2015) 868–874.
- [14] T. Dedova, M. Krunks, I. Oja Acik, D. Klauson, O. Volobujeva, A. Mere, Hierarchical nanostructures of ZnO obtained by spray pyrolysis, *Mater. Chem. Phys.* 141 (2013) 69–75.
- [15] C. Badre, T. Pauptoté, M. Turmine, D. Lincot, A ZnO nanowire array film with stable highly water-Repellent properties, *Nanotechnology* 18 (2007) 365705.

- [16] T. Dedova, I. Oja Acik, M. Krunk, V. Mikli, O. Volobujeva, A. Mere, Effect of substrate morphology on the nucleation and growth of ZnO rods prepared by spray pyrolysis, *Thin Solid Films* 520 (2012) 4650–4653.
- [17] I. Gromyko, T. Dedova, M. Krunk, V. Syritski, A. Mere, V. Mikli, T. Unt, I. Oja Acik, ZnO rods grown electrochemically on different metal oxide underlays, *IOP Conf. Ser.: Mater. Sci. Eng.* 77 (2015) 012012.
- [18] T. Dedova, J. Klauson, C. Badre, T. Pauporté, R. Nisumaa, A. Mere, O. Volobujeva, M. Krunk, Chemical spray pyrolysis of zinc oxide nanostructured layers from zinc acetate solutions, *Phys. Stat. Sol. (a)* 205 (2008) 2355–2359.
- [19] T. Pauporté, G. Bataille, L. Joulard, F.J. Vermersch, Well-aligned ZnO nanowire arrays prepared by seed-layer-free electrodeposition and their Cassie-Wenzel transition after hydrophobization, *J. Phys. Chem. C* 114 (2010) 194–202.
- [20] C. Badre, P. Dubot, D. Lincot, T. Pauporté, M. Turmine, Effects of rod structure and conformation of fatty acid self-assembled layers on superhydrophobicity of zinc oxide surface, *J. Colloid Interface Sci.* 316 (2007) 233–237.
- [21] B. Zhang, S. Lu, W. Xu, Y. Cheng, Controllable wettability and morphology of electrodeposited surfaces on zinc substrates, *Appl. Surf. Sci.* 360 (2016) 904–914.
- [22] I. Oja, A. Mere, M. Krunk, C.-H. Solterbeck, M. Es-Souni, Properties of TiO₂ films prepared by the spray pyrolysis method, *Solid State Phenom.* 99–100 (2004) 259–262.
- [23] D. Klauson, A. Poljakova, N. Pronina, M. Krichevskaya, A. Moiseev, T. Dedova, S. Preis, Aqueous photocatalytic oxidation of doxycycline, *J. Adv. Oxid. Technol.* 16 (2013) 234–243.
- [24] K. Yadav, B.R. Mehta, K.V. Lakshmi, S. Bhattacharya, J.P. Singh, Turning the wettability of indium oxide nanowires from superhydrophobic to nearly superhydrophilic: effect of oxygen related defects, *J. Phys. Chem. C* 119 (2015) 16026–16032.
- [25] C. Mondal, M. Ganguly, A.K. Sinha, J. Pal, T. Pal, Fabrication of a ZnO nanocolumnar thin film on a glass slide and its reversible switching from a superhydrophobic to a superhydrophilic state, *RSC Adv.* 3 (2013) 5937–5944.
- [26] R.-D. Sun, A. Nakajima, A. Fujishima, T. Watanabe, K. Hashimoto, Photoinduced surface wettability conversion of ZnO and TiO₂ thin films, *J. Phys. Chem. B* 105 (2001) 1984–1990.
- [27] G. Kenanakis, E. Stratakis, K. Vlachou, D. Vernardou, E. Koudoumas, N. Katsarakis, Light-induced reversible hydrophilicity of ZnO structures grown by aqueous chemical growth, *Appl. Surf. Sci.* 254 (2008) 5695–5699.
- [28] D. Pradhan, K.T. Leung, Vertical growth of two-dimensional zinc oxide nanostructures on ITO-coated glass: effects of deposition temperature and deposition time, *J. Phys. Chem. C* 112 (2008) 1357–1364.
- [29] E. McCafferty, J.P. Wightman, Determination of the concentration of surface hydroxyl groups on metal oxide films by a quantitative XPS method, *Surf. Interface Anal.* 26 (1998) 549–564.
- [30] L. Grządziel, M. Krzywiewicki, Ambience-related adsorbates on Cu₂Pc surface—photoemission and thermal desorption spectroscopy studies for control of organic electronics degradation processes, *Synth. Met.* 210 (2015) 141–147.
- [31] E. De la Rosa, S. Sepúlveda-Guzman, B. Rejea-Jayan, A. Torres, P. Salas, N. Elizondo, M. Jose Yacaman, Controlling the growth and luminescence properties of well-Faceted ZnO nanorods, *J. Phys. Chem C* 111 (2007) 8489–8495.
- [32] J.H. Zheng, Q. Jiang, J.S. Lian, Synthesis and optical properties of flower-Like ZnO rods by thermal evaporation method, *Appl. Surf. Sci.* 257 (2011) 5083–5087.
- [33] C. Mao, L. Fang, H. Zhang, W. Li, F. Wu, G. Qin, H. Ruan, C. Kong, Effect of B doping on optical, electrical properties and defects of ZnO films, *J. Alloys Compd.* 676 (2016) 135–141.
- [34] A. Sahai, N. Goswami, Probing the dominance of interstitial oxygen defects in ZnO nanoparticles through structural and optical characterizations, *Ceram. Int.* 40 (2014) 14569–14578.
- [35] E. Karber, T. Raadik, T. Dedova, J. Krustok, A. Mere, V. Mikli, M. Krunk, Photoluminescence of spray pyrolysis deposited ZnO rods, *Nanoscale Res. Lett.* 6 (2011) 359.
- [36] J.N. Zeng, J.K. Low, Z.M. Ren, T. Liew, Y.F. Lu, Effect of deposition conditions on optical and electrical properties of ZnO films prepared by pulsed laser deposition, *Appl. Surf. Sci.* 197–198 (2002) 362–367.
- [37] K.A. Alim, V.A. Fonoberov, M. Shamsa, A.A. Balandin, Micro-Raman investigation of optical phonons in ZnO nanocrystals, *J. Appl. Phys.* 97 (2005) 124313.
- [38] G. Jiangfeng, D. Zhaoming, D. Qingping, X. Yuan, Z. Weihua, Controlled synthesis of ZnO nanostructures by electrodeposition method, *J. Nanomater.* 2010 (2010) 740628.
- [39] H. Hu, H.-F. Ji, Y. Sun, The effect of oxygen vacancies on water wettability of a ZnO surface, *Phys. Chem. Phys.* 15 (2013) 16557–16565.
- [40] N. Sakai, A. Fujishima, T. Watanabe, K. Hashimoto, Quantitative evaluation of the photoinduced hydrophilic conversion properties of TiO₂ thin film surfaces by the reciprocal of contact angle, *J. Phys. Chem. B* 107 (2003) 1028–1035.
- [41] P. Liu, L. Cao, W. Zhao, Y. Xia, W. Huang, Z. Li, Insights into the superhydrophobicity of metallic surfaces prepared by electrodeposition involving spontaneous adsorption of airborne hydrocarbons, *Appl. Surf. Sci.* 324 (2015) 576–583.
- [42] Z. Li, Y. Wang, A. Kozbial, G. Shenoy, F. Zhou, R. McGinley, P. Ireland, B. Morganstein, A. Kunkel, S.P. Surwade, L. Li, H. Liu, Effect of airborne contaminants on the wettability of supported graphene and graphite, *Nat. Mater.* 12 (2013) 925–931.
- [43] C.P. Marshall, A.O. Marshall, The potential of raman spectroscopy for the analysis of diagenetically transformed carotenoids, *Philos. Trans. R. Soc. A* 368 (2010) 3137–3144.
- [44] Y. Liu, W. Chen, S. Wei, W. Gao, TiO₂/ZnO nanocomposite, ZnO/ZnO bi-level nanostructure and ZnO rod arrays: microstructure and time-affected wettability change in ambient conditions, *RSC Adv.* 4 (2014) 30658–30665.

Appendix 2

Table 1.1 Photocatalytic activities of ZnO photocatalyst toward different ZnO morphologies, preparation method and types of pollutants (MO – Methyl Orange, MB – Methylene Blue, DCB – 1, 2-dichlorobenzene, AO7 – Acid Orange 7, R6G – rhodamine 6G, RB-19 – Reactive Blue 19, DC – doxycycline).

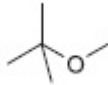
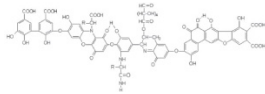
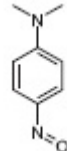
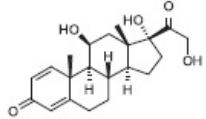
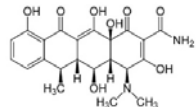
Catalyst	Synthesis method	Pollutant	Photodegradation time	Photodegradation efficiency	Ref.
ZnO flower-like layer 1g	CBD	MO 20 mg l ⁻¹	240 min	2 %	[66]
ZnO nanoparticles 25mg	hydrothermal method	MO 20 mg l ⁻¹	60 min	85 %	[36]
ZnO nanorod layer 25mg			60 min	90 %	
ZnO nanosheet layer 25mg			60 min	100 %	
ZnO hierarchical flower layer 25mg			40 min	100 %	
ZnO nanorods layer 500 mg	thermal decomposition method	MO 3 × 10 ⁻⁵ M	60 min	0.3 %	[67]
		MB 3 × 10 ⁻⁵ M	60 min	2.6 %	
ZnO nanorod layer 10 mg	hydrothermal method	MO 20 mg l ⁻¹	60 min	50 %	[62]
TiO ₂ P25 10 mg	-		60 min	25 %	
ZnO hierarchical flower-like layer 30 mg	aqueous solution route	MO 5.0 × 10 ⁻⁵ M	100 min	99.6 %	[29]
ZnO hierarchical flower-like layer 0.0158 g	thermal decomposition method	MO 10 ⁻⁵ M	100 min	85 %	[37]

ZnO spherical nanostructures 10 mg	hydrothermal method	MO 25 mg l ⁻¹	140 min	98 %	[30]
ZnO flower-like layer 10 mg			140 min	75%	
ZnO nanoparticles 10 mg	Commercial (Aladdin)		140 min	95 %	
ZnO nanowire layer	hydrothermal method	DCB 10 mg l ⁻¹	60 min	95 %	[64]
		MO 20 mg l ⁻¹	60 min	50 %	
TiO ₂ P25	-	DCB 10 mg l ⁻¹	60 min	100 %	
		MO 20 mg l ⁻¹	60 min	100 %	
ZnO nanorod layer	hydrothermal method	MO 5 mg l ⁻¹	60 min	20 %	[68]
ZnO nanorod layer	solution growth	MO 20 mg l ⁻¹	60 min	28 %	[63]
ZnO nanoparticles 160 mg/l	Commercial (Mereck Co.)	AO7 20 mg l ⁻¹	60 min	100 %	[69]
ZnO nanocrystal layer 150 mg/l	precipitation method	Diazinon 20 mg l ⁻¹	60 min	75 %	[70]
ZnO tetrapods 50 mg	evaporating	MO, AO7, MB, R6G 20 mg l ⁻¹	5-10 min	100 %	[33]
ZnO nanoparticles 50 mg	commercial Sigma-Aldrich	MO, AO7, MB, R6G 20 mg l ⁻¹	10-30 min	95-100 %	

ZnO nanoparticles 50 mg	Commercial catalyst 5 types	MB 5 mg l ⁻¹	6-60 and more min	100 %	[71]
ZnO nanorod layers	ED	MO 10 mg l ⁻¹	60 min	13 %	[72]
ZnO nanostructured film	USP	SA 0.1 M	60 min	10-20 %	[73]
ZnO microrod layer	SP	MB 10 ⁻⁵ M	60 min	78 %	[74]
ZnO rod layer	SP	DC 25 mg L ⁻¹	60 min	1 %	[35]
ZnO hierarchical rod layer	SP	DC 25 mg L ⁻¹	60 min	2 %	
ZnO film	SP	MO 10 ⁻⁵ M	60 min	45 %	[75]
ZnO rod layer	CBD	MO 10 mg l ⁻¹	180 min	98.6 %	[76]
ZnO powder 125 mg	Commercial (Nuclear, 99%)	Remazol Black B, Remazol Brilliant Blue R 50 mg l ⁻¹	60 min	100 %	[58]
ZnO powder 0.8 g/l	Commercial (Merck)	RB-19 50 mg l ⁻¹	25 min	100 %	[59]

ZnO powder 2.5 g/l	Commercial (Merck)	Acid brown 14 5.0×10^{-4} M	60 min	62 %	[60]
ZnO powder 1 g/l	Commercial (Merck)	MO 25 mg l ⁻¹	60 min	32 %	[61]
ZnO powder 0.5 g/l		R6G 25 mg l ⁻¹	60 min	29 %	

Table 2.3 Descriptions of micropollutants used in this thesis.

Type of micropollutant	Molecule structure
<p>Methyl-tert-butylether (MTBE) is an aliphatic non-polar non-biodegradable compound, which is hardly removable from water by conventional methods. MTBE is a fuel additive and a suspected carcinogen [III].</p>	
<p>Humic acid (HA) have various polycyclic, aromatic and heteroatom-containing functional groups, hardly affected by common water treatment methods, are easily bonded with heavy metals and other toxics compounds, being able to effectively transport them through drinking water treatment stages [III].</p>	
<p>N,N-dimethyl p-nitrosoaniline (RNO) is an aromatic compound, applied in measuring the number of hydroxyl radicals in various advanced oxidation processes, due to the RNO decolouration upon reaction of its molecule with hydroxyl radical [III].</p>	
<p>Prednisolone (PNL) is a widely used glucocorticoid anti-inflammatory agent, and is a very common emerging micropollutant [III].</p>	
<p>Doxycycline (DC) is one of the most often used semi-synthetic antibiotic in the therapy of human and animal infections [IV].</p>	

Curriculum vitae

Personal data

Name: Inga Gromyko
Date of birth: 24.10.1990
Place of birth: Narva, Estonia
Citizenship: Estonian

Contact data

E-mail: inga.gromyko@gmail.com

Education

2014–2018 Tallinn University of Technology, Chemical and Materials Technology, Doctoral study
2012–2014 Tallinn University of Technology, Faculty of Chemical and Materials Technology, Technology of Materials, Wood Processing, MSc
2009–2012 Tallinn University of Technology Faculty of Chemical and Materials Technology, Technology of Wood and Textile, BSc
1997–2009 Narva Pähklikmäe Gymnasium

Language competence

Russian Native language
Estonian Average
English Average

Training courses, work in other research laboratories, conferences

2016–2018 Graduate school “Functional materials and technologies FMTDK”, Tallinn University of Technology, Estonia
7.05–13.05.2017 Characterization of the photocatalytic properties of ZnO rods, Budapest University of Technology and Economics, Department of Inorganic and Analytical Chemistry, Hungary
27.06–3.07.2016, 28.06–4.07.2015 Studies of perspective Earth abundant materials for solar cells and development of solar cell structures based on them, Grenoble IMEP-LAHC, LMGP, France
24.08–4.09.2015 International Summer University of Energy: Renewable Energies VII: Photovoltaics, Solar Thermal & Wind, Falera, Switzerland
01.07–29.07.2013 IAESTE trainee in Ulsan National Institute of Science and Technology, Interdisciplinary School of Green Energy, South-Korea

Participation in scientific conferences:

22.05–26.05.2017 E-MRS Spring Meeting and Exhibit, Strasbourg, France
27.11–2.12.2016 MRS Fall Meeting & Exhibit, Boston, USA
6.10–9.10.2016 Nanosmat, Aveiro, Portugal
10.06–12.06.2015 EuroNanoForum, Riga, Latvia
10.05–15.05.2015 E-MRS Spring Meeting and Exhibit, Lille, France
5.10–8.10.2015 FM&NT, Vilnius, Lithuania
29.09–2.10.2014 FM&NT, Riga, Latvia

Defended dissertations

2014 Master's Degree: Electrochemical deposition and characterisation of ZnO nanorods, supervisors: Tatjana Dedova, Malle Krunks

Recognition

2014 I prize in National students' research contest on scientific research in the category of master students, natural sciences and engineering

2014 Poster competition award "The most interesting results" at Functional materials and NanoTechnologies (FM&NT) 2014 Conference, Riga, Latvia

Involvement in research projects

1.01.2016–1.03.2023 TK141 Centre of Excellence: "Advanced materials and high-technology devices for sustainable energetics, sensorics and nanoelectronics".

1.01.2014–31.12.2019 IUT19-4 "Thin films and nanomaterials by wet-chemical methods for next-generation photovoltaics".

1.01.2012–31.12.2015 ETF9081 "Absorber layers by chemical spray pyrolysis for nanostructured solar cells".

1.01.2013–31.12.2015 B24 "Metal oxide thin films by wet chemical methods for electronic devices".

1.01.2011–31.12.2015 TK114 Centre of Excellence: "Mesosystems: Theory and Applications".

1.07.2012–31.12.2014 AR12118 "Efficient plasmonic absorbers for solar cells".

1.01.2010–31.12.2013 ETF8509 "Development of ZnO nanorods by chemical spray".

1.01.2008–31.12.2013 SF0140092s08 "Thin film and nanostructured materials by chemical methods".

Supervised dissertations

Jako Siim Eensalu, Master's Degree, 2017, (sup) Malle Krunks; **Inga Gromyko**, Study of ZnO:Al Thin Films Deposited by Chemical Spray, Tallinn University of Technology, School of Engineering, Department of Materials and Environmental Technology.

Ikechukwu Okpara, Master's Degree, 2017, (sup) Tatjana Dedova; **Inga Gromyko**, Deposition and properties of ZnS:Mn thin films and nanostructured layers by spray pyrolysis, Tallinn University of Technology, School of Engineering, Department of Materials and Environmental Technology.

List of publications

1. **I. Gromyko**, T. Dedova, S. Polivtseva, J. Kois, L. Puust, I. Sildos, A. Mere, M. Krunks. Electrodeposited ZnO morphology transformations under the influence of SeO₂ additive: Rods, disks, nanosheets network. *Thin Solid Films* 652 (2018) 10–15.
2. **I. Gromyko**, M. Krunks T. Dedova, A. Katerski, D. Klauson, I. Oja Acik, Surface properties of sprayed and electrodeposited ZnO rod layers. *Appl. Surf. Sci.* 405 (2017) 521–528.

3. R. Parize, A. Katerski, **I. Gromyko**, L. Rapenne, H. Roussel, E. Kärber, E. Appert, M. Krunks, V. Consonni. ZnO/TiO₂/Sb₂S₃ Core–Shell Nanowire Heterostructure for Extremely thin Absorber Solar Cells. *J. Phys. Chem. C* 121 (2017) 9672–9680.
4. J. S. Eensalu, M. Krunks, **I. Gromyko**, A. Katerski, A. Mere. A comparative study on physical properties of Al-doped zinc oxide thin films deposited from zinc acetate and zinc acetylacetonate by spray pyrolysis. *Energetika* 63 (2017) 46–55.
5. **I. Gromyko**, T. Dedova, M. Krunks, V. Syritski, A. Mere, V. Mikli, T. Unt, I. Oja Acik. ZnO nanorods grown electrochemically on different metal oxide underlays. *IOP Conf. Ser.: Mater. Sci. Eng.* 77 (2015) 012012.
6. D. Klauson, **I. Gromyko**, T. Dedova, N. Pronina, M. Krichevskaya, O. Budarnaja, I. Oja Acik, O. Volobujeva, I. Sildos, K. Utt. Study of photocatalytic activity of zinc oxide nanoneedles, nanorods, pyramids and hierarchical structures obtained by spray pyrolysis. *Mater. Sci. Semicond. Process* 31 (2015) 315–324.
7. **I. Gromyko**, I. Oja Acik, M. Krunks, T. Dedova, A. Katerski, A. Mere, V. Mikli, R. Vessart. Surface plasmon resonance in ZnO nanorod arrays caused by gold nanoparticles for solar cell application. *Phys. Status Solidi C* 12 (2015) 1338–1343.
8. T. Dedova, **I. Gromyko**, M. Krunks, V. Mikli, M. Grossberg, I. Sildos, K. Utt, R. Vessart, T. Unt. Spray pyrolysis deposition and characterization of highly c-axis orientated hexagonal ZnS nanorod crystals. *Cryst. Res. Technol.* 50 (2015) 82–95.
9. T. Dedova, M. Krunks, **I. Gromyko**, V. Mikli, I. Sildos, K. Utt, T. Unt. Effect of Zn:S molar ratio in solution on properties of ZnS thin films and formation of ZnS nanorods by spray pyrolysis. *Phys. Status Solidi A* 211 (2014) 514–521.
10. T. Dedova, O. Volobujeva, M. Krunks, V. Mikli, **I. Gromyko**, A. Katerski, A. Mere. Growth of ZnO rods on FTO electrodes by spray pyrolysis. *IOP Conf. Ser.: Mater. Sci. Eng.* 49 (2013) 012001.

Elulookirjeldus

Isikuandmed

Nimi: Inga Gromõko
Sünniaeg: 24.10.1990
Sünnikoht: Narva, Eesti
Kodakondsus: Eesti

Kontaktandmed

E-post: inga.gromyko@gmail.com

Hariduskäik

2014–2018 Tallinna Tehnikaülikool, Keemia- ja materjalitehnoloogia, Doktoriõpe
2012–2014 Tallinna Tehnikaülikool, Keemia- ja materjalitehnoloogia teaduskond, Materjalitehnoloogia, spetsialiseerumine: puidutöötlemine, Magistrikraad
2009–2012 Tallinna Tehnikaülikool, Keemia- ja materjalitehnoloogia teaduskond, Puidu- ja tekstiilitehnoloogia, Bakalaureuse kraad
1997–2009 Narva Pähklimäe Gümnaasium

Keelteoskus

Vene keel Emakeel
Eesti keel Kesktase
Inglise keel Kesktase

Täiendkursused, töö välislaboris, konverentsid

2016–2018 Graduate school “Functional materials and technologies FMTDK”, Tallinn University of Technology, Estonia
7.05–13.05.2017 Characterization of the photocatalytic properties of ZnO rods, Budapest University of Technology and Economics, Department of Inorganic and Analytical Chemistry, Hungary
27.06–3.07.2016, 28.06–4.07.2015 Studies of perspective Earth abundant materials for solar cells and development of solar cell structures based on them, Grenoble IMEP-LAHC, LMGP, France
24.08–4.09.2015 International Summer University of Energy: Renewable Energies VII: Photovoltaics, Solar Thermal & Wind, Falera, Switzerland
01.07–29.07.2013 IAESTE trainee in Ulsan National Institute of Science and Technology, Interdisciplinary School of Green Energy, South-Korea
Osalemise teaduskonverentsidel:
22.05–26.05.2017 E-MRS Spring Meeting and Exhibit, Strasbourg, France
27.11–2.12.2016 MRS Fall Meeting & Exhibit, Boston, USA
6.10–9.10.2016 Nanosmat, Aveiro, Portugal
10.06–12.06.2015 EuroNanoForum, Riga, Latvia
10.05–15.05.2015 E-MRS Spring Meeting and Exhibit, Lille, France
5.10–8.10.2015 FM&NT, Vilnius, Lithuania
29.09–2.10.2014 FM&NT, Riga, Latvia

Kaitstud lõputööd

2014 Tehnikateaduste magistrikraad: ZnO nanovarraste elektrokeemiline sadestamine ja karakteriseerimine, juhendajad: Tatjana Dedova, Malle Krunks

Tunnustused

- 2014 I preemia Eesti üliõpilaste teadustööde konkursil loodusteaduste ja tehnika valdkonnas magistriõppe üliõpilaste astmes
- 2014 Functional materials and NanoTechnologies (FM&NT) Konverents, Riia, Läti, Kõige huvitama postri auhind

Osalemine uurimisprojektides

- 1.01.2016–1.03.2023 TK141 Tippkeskus: "Uudsed materjalid ja kõrgtehnoloogilised seadmed energia salvestamise ja muundamise süsteemidele".
- 1.01.2014–31.12.2019 IUT19-4 "Õhukesed kiled ja nanomaterjalid keemilistel vedeliksadestusmeetoditel uue põlvkonna fotovoltseadistele".
- 1.01.2012–31.12.2015 ETF9081 "Absorberkihid keemilise pihustuspürolüüsi meetodil nanostruktuursetele päikesepatareidele".
- 1.01.2013–31.12.2015 B24 "Keemilistel meetoditel kasvatatud metalli oksiidide õhukesed kiled elektroonikaseadistele".
- 1.01.2011–31.12.2015 TK114 Tippkeskus: "Mesosüsteemide teooria ja rakendused".
- 1.07.2012–31.12.2014 AR12118 "Efektiivsed plasmoonilised absorberid päikesepatareidele".
- 1.01.2010–31.12.2013 ETF8509 " Keemilise pihustuspürolüüsi meetodil kasvatatud ZnO nanovarraste areng".
- 1.01.2008–31.12.2013 SF0140092s08 "Õhukesekilelised ja nanostruktuurset materjalid keemilistel meetoditel".

Juhendatud magistritööd

Jako Siim Eensalu, magistrikraad, 2017, (juh) Malle Krunks; **Inga Gromõko**, Keemilise pihustamise meetoditel sadestatud ZnO:Al õhukeste kilede uurimine, Tallinna Tehnikaülikool, Inseneriteaduskond, Materjali- ja keskkonnatehnoloogia instituut.

Ikechukwu Okpara, magistrikraad, 2017, (juh) Tatjana Dedova; **Inga Gromõko**, Pihustussadestuse meetodil ZnS:Mn õhukeste kilede ning nanostruktuursete kihtide süntees ning omadused, Tallinna Tehnikaülikool, Inseneriteaduskond, Materjali- ja keskkonnatehnoloogia instituut.

Publikatsioonid

1. **I. Gromyko**, T. Dedova, S. Polivtseva, J. Kois, L. Puust, I. Sildos, A. Mere, M. Krunks. Electrodeposited ZnO morphology transformations under the influence of SeO₂ additive: Rods, disks, nanosheets network. *Thin Solid Films* 652 (2018) 10–15.
2. **I. Gromyko**, M. Krunks T. Dedova, A. Katerski, D. Klauson, I. Oja Acik, Surface properties of sprayed and electrodeposited ZnO rod layers. *Appl. Surf. Sci.* 405 (2017) 521–528.

3. R. Parize, A. Katerski, **I. Gromyko**, L. Rapenne, H. Roussel, E. Kärber, E. Appert, M. Krunks, V. Consonni. ZnO/TiO₂/Sb₂S₃ Core–Shell Nanowire Heterostructure for Extremely thin Absorber Solar Cells. *J. Phys. Chem. C* 121 (2017) 9672–9680.
4. J. S. Eensalu, M. Krunks, **I. Gromyko**, A. Katerski, A. Mere. A comparative study on physical properties of Al-doped zinc oxide thin films deposited from zinc acetate and zinc acetylacetonate by spray pyrolysis. *Energetika* 63 (2017) 46–55.
5. **I. Gromyko**, T. Dedova, M. Krunks, V. Syriski, A. Mere, V. Mikli, T. Unt, I. Oja Acik. ZnO nanorods grown electrochemically on different metal oxide underlays. *IOP Conf. Ser.: Mater. Sci. Eng.* 77 (2015) 012012.
6. D. Klauson, **I. Gromyko**, T. Dedova, N. Pronina, M. Krichevskaya, O. Budarnaja, I. Oja Acik, O. Volobujeva, I. Sildos, K. Utt. Study of photocatalytic activity of zinc oxide nanoneedles, nanorods, pyramids and hierarchical structures obtained by spray pyrolysis. *Mater. Sci. Semicond. Process* 31 (2015) 315–324.
7. **I. Gromyko**, I. Oja Acik, M. Krunks, T. Dedova, A. Katerski, A. Mere, V. Mikli, R. Vessart. Surface plasmon resonance in ZnO nanorod arrays caused by gold nanoparticles for solar cell application. *Phys. Status Solidi C* 12 (2015) 1338–1343.
8. T. Dedova, **I. Gromyko**, M. Krunks, V. Mikli, M. Grossberg, I. Sildos, K. Utt, R. Vessart, T. Unt. Spray pyrolysis deposition and characterization of highly c-axis orientated hexagonal ZnS nanorod crystals. *Cryst. Res. Technol.* 50 (2015) 82–95.
9. T. Dedova, M. Krunks, **I. Gromyko**, V. Mikli, I. Sildos, K. Utt, T. Unt. Effect of Zn:S molar ratio in solution on properties of ZnS thin films and formation of ZnS nanorods by spray pyrolysis. *Phys. Status Solidi A* 211 (2014) 514–521.
10. T. Dedova, O. Volobujeva, M. Krunks, V. Mikli, **I. Gromyko**, A. Katerski, A. Mere. Growth of ZnO rods on FTO electrodes by spray pyrolysis. *IOP Conf. Ser.: Mater. Sci. Eng.* 49 (2013) 012001.